Transcriptome-wide Single-cell Analysis of Human Macrophage Heterogeneity

Inaugural-Dissertation
to obtain the academic degree
Doctor rerum naturalium (Dr. rer. nat.)

submitted to the
Department of Biology, Chemistry and Pharmacy of Freie Universität Berlin

by Cornelius Fischer, M. Sc.

April 2017

This dissertation was conducted at the Max Planck Institute for Molecular Genetics Berlin in the workgroup Nutrigenomics and Gene Regulation and at the Genomics platform of the Berlin Institute for Medical Systems Biology at the Max Delbrück Center for Molecular Medicine under the supervision of Dr. Sascha Sauer from April 2012 to April 2017.

First supervisor: Dr. Sascha Sauer
(Max Delbrück Center for Molecular Medicine, Berlin)

Second supervisor: Prof. Dr. Stephan Sigrist
(Freie Universität Berlin)

Date of disputation: 23.10.2017

TO MY GRANDFATHER, LOTHAR EISSMANN.

All truth passes through three stages.

First, it is ridiculed. Second, it is violently opposed.

Third, it is accepted as being self-evident.

– Arthur Schopenhauer

Acknowledgments

I am grateful for the associations I have had over the years that have allowed me to look at different omics fields from different angles at the bench and computationally. Foremost, I would like to thank Dr. Sascha Sauer for the constant support and the opportunities I experienced in sophisticated environments. I would also like to specially thank Prof. Dr. Stephan Sigrist for advising this thesis.

I am most fortunate to have had superior students and colleagues to supply fresh ideas and help. I thank Sophia Bauch and Michael Böttcher for the outstanding support! I thank Maria Metsger for the company entering single-cell genomics and my lab colleagues including Christopher Weidner, Annabell Plauth, Toni Luge and Morten Rousseau. Big thanks to the people at MPI who helped me along the way: Phillip Grote, Frederic Koch and Uta Marchfelder for training and help with FACS; Thorsten Mielke and Beatrix Fauler for microscopy assistance; Norbert Mages, Bernd Timmermann, Sven Klages and the NGS team for help with sequencing and software; Donald Buczek and Sven Püstow and MPI helpdesk for support with IT; Mark Lynch from Fluidigm for training and Margit Stadler, Andreas Dahl and team for hints on C1 issues; Ulrich Stelzl for the robot. Sebastiaan Meijsing for discussion on GR. Finally, I want to thank the Max Planck Society and the Helmholtz Association for the support.

I would also like to express my sincere gratitude to my many friends that make life rich and whole, including my colleagues Alexander Kiefer, Thomas Corwin, Johannes Helmuth and Annita Louloupi. Finally, I thank Barbara for her patience, and my parents, grandparents, as well as my sister and my brother and Michael for the support during my studies.

Contents

List of Figures

List of Tables

Chapter 1

Introduction

Cells rely on evolutionary inherited structural components to respond to a large variety of environmental changes. Imperfect specification and redundancies of biological circuits allow for flexible short-term and long-term evolutionary adaptation to a variety of incoming signals. As a consequence, cellular response to environmental changes is noisy in nature contributing to heterogeneity in gene expression levels across individual cells of genetically homogeneous cell populations (Shalek et al. 2013). Cellular heterogeneity is a phenomenon molecular biologists were for a long time aware of. Understanding the mechanism and higher-level function of single-cell heterogeneity may be the key to understand multi-cellular systems. However, limitation of sensitivity and throughput impeded for a long time the detection of heterogeneity of cells, at least for unbiased analysis of full transcriptomes.

1.1 Cellular diversity in the immune system

Cellular diversity is an important aspect of the immune system. Immune cells derive from the same progenitor cells - the hematopoietic stem cells in the bone marrow. Hematopoietic stem cells can differentiate to cells of more limited potential and finally mature to common lymphoid progenitor cells and myeloid progenitor cells. Lymphoid progenitor cells give rise to the lymphocytes including T cells and B cells. Most of those cells contribute to the slow and specific immune response and

constitute adaptive immunity. Myeloid progenitor cells develop to macrophages, dendritic cells, granulocytes, and mast cells that constitute the rapid and non-specific innate immune response (Janeway et al. 2001). Beside the broad spectrum of different cell types of the immune system, there exists a significant heterogeneity even within specific types of immune cells. Heterogeneity of cell types linked to the adaptive immune response may be intuitive, for example by considering the need of single-cell specific pathogen recognition patterns maintained by antibody diversity (B and T cells). However, it is also apparent that rather unspecific macrophages exist in numerous phenotypical states (Gautier et al. 2012). This makes sense from an evolutionary perspective because the innate immune system is evolutionary older compared to the adaptive immune response. About 95% of all animals do not possess T or B cells (Dzik 2010). Macrophages serve as their primary defense system in a rich environment of pathogens with constantly changing threats (Stoy 2001). Thus, macrophages appear to be heterogeneous to maintain survival under changing environmental conditions and threats.

1.2 Macrophages

Macrophages are key-regulators and effector cells of the immune system, for example in the context of inflammation, and are part of various branches of the immune system. Macrophages originate from circulating peripheral-blood mononuclear cells (PBMCs, monocytes), which migrate into tissue in the steady state or in response to inflammation (Mosser and Edwards 2008). Monocytes develop from common myeloid precursor cells in the bone marrow that give also rise to several other cell types, including neutrophils, eosinophils, basophils, dendritic cells and mast cells. After monocyte maturation, monocytes are released from the bone marrow into the bloodstream. Circulating monocytes then home to different tissues to replenish long-lived tissue-specific macrophages (Mosser and Edwards 2008). Prototypically, as part of the innate immune response, together with eosinophils, neutrophils and natural killer cells, macrophages function as a first level of defense to sense, ingest and eliminate invading microorganisms and other toxic macromolecules by phagocytosis (van Furth et al. 1972). If innate immunity is insufficient to cope

with invading microorganisms, cells of the adaptive immunity (including T and B cells), trigger macrophages in an antigen-specific way. Beside its functions in phagocytosis, macrophages respond to diverse environmental signals and play a crucial role in tissue repair and homeostasis, for example by phagocytic clearance of dying cells (Henson and Hume 2006). Thus, macrophages feature a multiplicity of crucial functions beside pathogen defense, including wound healing and resolution of inflammation, coordinating cell migration, matrix remodeling and angiogenesis, scavenging, elimination of pathogen and tumor cells, clearance of senescent cells, control of tissue cell growth and modulation of the extracellular milieu (Vega and Corbi 2006). As part of the mononuclear phagocyte system macrophages are present in almost every part of the human body. Highly specialized tasks of macrophages depend on external signals from their tissue environments (Davies et al. 2013) and local microenvironments (Stout and Suttles 2004, Gordon and Taylor 2005). Macrophages adapt and respond to these external environmental signals by highly flexible and heterogeneous gene expression programs that thereby orchestrate other cell types and the local macrophage population.

1.2.1 Innate macrophage activation

Innate macrophage activation is induced directly by microbial products via pattern recognition receptors (PRRs), of which the family of Toll-like receptors (TLRs) had been studied most extensively (Akira et al. 2006). TLRs detect distinct evolutionarily conserved structures on pathogens, termed pathogen-associated molecular patterns (PAMPs) (Mogensen 2009). Lipopolysaccharide (LPS), a major determinant of responses to gram-negative microorganisms, is a prototypical PAMP that serves as M1 macrophage signal recognized by TLR4 (Martinez and Gordon 2014, Wang et al. 2014). Mainly two adaptor proteins, MyD88 and TRIF, mediate the signaling downstream of TLR4 upon LPS binding. The LPS response involves coordinated regulation of hundreds of genes and triggers strong gene expression changes towards including expression of pro-inflammatory cytokines (i.e. TNF, IL-1b, IL-6 and IL-8) and chemokines (CCL2, CCL4, CCL5 and CXCL11, Hu and Ivashkiv 2009, Martinez and Gordon 2014). These gene sets are coordinately regulated by dedicated transcription factors with temporal

characteristics including primary response genes (0.5-2 hours after stimulation) and secondary response genes. Transcription factors of the primary (early) response are mainly activated in a protein synthesis-independent manner by TLR signaling (Ramirez-Carrozzi et al. 2009). Primary response genes include nuclear factor of kappa light polypeptide gene enhancer (NF-κB) activator protein 1 (AP-1) and interferon-regulatory factor (IRF) proteins. Feed-forward loops lead to production of TNFα and type I interferons that initiate the secondary response. Secondary (late) response transcription factors are synthesized *de novo* after LPS stimulation to regulate subsequent waves of gene expression over a prolonged period of time with more complex gene expression patterns and changes of chromatin states (Ramirez-Carrozzi et al. 2009, Medzhitov and Horng 2009).

1.2.2 M1-M2 concept

Many macrophage functions appear to be opposing in nature: pro-inflammatory versus anti-inflammatory functions, immunogenic versus tolerogenic activities, and tissue-destructive versus tissue-restorative activities (Stout and Suttles 2004). The concept of classical (M1) versus alternative (M2) macrophage activation phenotypes has become popular (Mills et al. 2000). This M1-M2 concept mimics the T helper cell (Th) nomenclature as M1 and M2 macrophages promote Th1 and Th2 adaptive immunity responses, respectively. Classical macrophage activation (M1) was initially described as antigen-dependent but non-specific response of macrophages upon secondary exposure to microbial products (Mackaness 1962, Martinez and Gordon 2014). Resulting macrophage activity to inhibit infection was linked with T helper 1 (Th1) secreted, activating cytokines such as interferon gamma (IFNγ) and tumor necrosis factor (TNF) as functional external cues for macrophage activation (Nathan et al. 1983). Contrary, alternative macrophage activation (M2) was linked with T helper 2 (Th2) secreted modulating cytokines such as interleukin-4 (IL-4) and interleukin-13 (IL-13) (Stein et al. 1992, Gordon 2003). Upon infection M2 macrophages contribute to resolution of inflammation through high endocytic clearance capacities and trophic factor synthesis, accompanied by reduced pro-inflammatory cytokine secretion (Martinez et al. 2008). Mills and colleagues challenged the dominating view that T cells are required to activate

macrophages towards M1 or M2 (Mills 2012). Accordingly, M1 and M2 macrophage activities exist as a result of transitions from inflammation to healing without T or B cell influence (Mills et al. 2000). Moreover, it was shown that M1 and M2 macrophages would even stimulate T cells toward Th1- or Th2-like activities, respectively. However, macrophage M1 and M2 activity can be elevated by T cell-derived cytokines (Pulendran et al. 1999, Iwasaki and Medzhitov 2010). In general, the M1-M2 concept demonstrated the importance of innate immunity and its link to adaptive immunity in a counterbalanced system in which macrophages represent a central element with potentially intrinsic M1-M2 dichotomy. As a consequence, it appears reasonable to term macrophage activation, that is promoted directly by microbial products as classical innate macrophage activation (classified as M1b). In contrast to this, the traditional term classical macrophage activation (M1a) is induced by IFNγ (Martinez et al. 2008, Mukhopadhyay et al. 2006).

1.2.3 Macrophage diversity

De-regulation of macrophage heterogeneity is implicated in various disorders. Specifically, many diseases exhibit inappropriate M1/M2 macrophage balances that play a role in pathologies, including infectious diseases (El Kasmi et al. 2008), atherosclerosis (Johnson and Newby 2009), cancer (Dvorak 1986, Komohara et al. 2014), allergy (Wills-Karp et al. 2010) and autoimmune disease (Maloy and Powrie 2011, Mills 2012).

In view of recent advances in macrophage research a rethinking of the traditional M1-M2 concept may be required. The M1-M2 concept of macrophage heterogeneity seems to represent a simplified conceptual framework describing a continuum of diverse functional states, of which M1 and M2 states rather represent the extremes of a broad spectrum of possible functional macrophage subsets (Italiani and Boraschi 2014). Especially the classification of different subtypes of M2 macrophages has enormously expanded by applying arrays of specific immune stimulations. Simplified, M2 macrophages can be further subdivided into M2a (triggered by IL-4 or IL-13), M2b (immune complexes in combination with IL-1B or LPS) and M2c (IL-10, TGFbeta or glucocorticoids) subtypes (Mosser and Edwards 2008). Moreover, numerous combinations of different immunoactive regulatory

molecules assayed separately or in combination, all produce distinct and partly overlapping macrophage subsets (Xue et al. 2014). Therefore, a macrophage spectrum model was proposed that included a macrophage classification based on three major functions of macrophages for maintaining homeostasis: host defense, wound healing, and immune regulation (Mosser and Edwards 2008). Plasticity and flexibility are key features of macrophages and of their activation states. It remains controversial to what extent different macrophage states can develop into stable subsets or can undergo phenotypical shifts in response to changing microenvironments (Stout and Suttles 2004, Italiani and Boraschi 2014). It remains speculative if the numerous macrophage subsets are phenotypically distinct to serve various functions in different phases or locations involved in inflammatory reactions. Contrary, macrophage subsets may rather represent intermediate flux states to accomplish complex changes (Mills and Ley 2014). The current controversy is a result of the unsolved mechanisms that might underlie macrophage transitions *in vivo* (Auffray et al. 2007, Nahrendorf et al. 2007). For example, it is not fully understood if identical macrophage cells can shift from one to another functional state in response to microenvironmental signals (Debien et al. 2013, Italiani and Boraschi 2014). Although some examples provide evidence that macrophages can undergo dynamic transitions between different functional states from M1 to M2 (Italiani et al. 2014) or from M2 to M1 (Mylonas et al. 2009, Stout et al. 2005), it is possible that a mixture of M1/M2 phenotypes (Mills 2012, Mills et al. 2000) underlies these conditions or that newly recruited macrophages are confounding those observations *in vivo* (Jenkins et al. 2011). Thus, it is still controversial how to interpret apparent macrophage heterogeneity in the context of time (progressive model of inflammation) and space (different tissues or microenvironments). Moreover, there are discrepancies in observations between human and mouse (Schroder et al. 2012), different mouse strains (Wells et al. 2003) and between observations *in vivo*, *ex vivo* and *in vitro* (Murray et al. 2014).

1.3 Criteria for a simple model system

Conflicting models exist to explain cause and consequences of macrophage heterogeneity. Methodologies of past research were restricted to investigate macrophage heterogeneity with limitations. i) Our understanding of macrophage heterogeneity in terms of different functional macrophage states mostly originated from average population experiments in which the transcriptional state of individual cells is lost. ii) The use of selected stimulations with high doses of different combinations of purified immunoactive signaling molecules (i.e. IL4 to trigger M2 macrophages) hardly reflects the situation in native macrophage microenvironments. iii) Once analyzed at the single-cell level most investigations were biased towards a limited number of marker genes, mostly derived from previous research. Therefore, a promising strategy to shed light on the basis of macrophage heterogeneity is to move away from complicated model systems with average readout. Modulation of macrophage function may be efficiently investigated at hight resolution with a system that is as simple as possible, yet, meeting the following aspects: i) An analysis technique with readouts at the single-cell level for many individual macrophages with genome-wide resolution to identify novel gene modules in an unbiased way. ii) A homogenous macrophage environment with a limited number of clearly defined parameters for macrophage modulation with ideally one single stimulation that leads to native, specific innate macrophage activation. iii) A human model system assayed at a time-point where primary responses instead of secondary response effects can be observed.

1.4 Single-cell mRNA sequencing

In transcriptome analyses with average cell population readouts, it is not feasible to distinguish changes in gene expression from changes in the cellular composition of the population. A particular gene could be measured at a specific expression level, but it is unclear if this expression level is representative for all or only a few cells in the population. Moreover, co-expressed genes at the population level may in fact be mutually exclusively expressed if observed at the level of single

cells. To study single-cell heterogeneity and its biological consequences, researchers have used low-throughput approaches - such as single-cell qPCR (Ståhlberg and Kubista 2014), fluorescent reporters (Han et al. 2014) and RNA fluorescence *in situ* hybridization (FISH) techniques (Raj et al. 2008) - that allow quantification of a limited number of genes in individual cells (Junker and van Oudenaarden 2014). Recent emerging high-throughput single-cell sequencing technologies have enabled high-resolution measurements of genome-wide gene expression in single cells (Tang et al. 2009, Treutlein et al. 2014, Shalek et al. 2014, Kolodziejczyk et al. 2015b, Zeisel et al. 2015, Nagano et al. 2013, Klein et al. 2015), resulting in a growing appreciation for the extent of individual expression variability (Dueck et al. 2016). All studies found that transcriptomes of individual cells, even from seemingly homogenous populations, were highly heterogeneous, opening up new avenues to understand gene regulation. To sequence mRNA from a single cell, two challenges need to be met: i) Isolation of individual cells and ii) Amplification of minute amounts of mRNA from a cell for next generation sequencing library construction.

1.4.1 Single-cell isolation

Capturing single cells quickly and accurately with high efficiency is one of the main challenges of single-cell sequencing (Kolodziejczyk et al. 2015a). Several techniques exist to accomplish single-cell capturing: Fluorescence activated cell sorting (FACS), laser capture microdissection (LCM), manual cell picking via micromanipulators, and microfluidics techniques. FACS, and microfluidics-based techniques allow for random capturing of single cells from cell suspensions, whereas LCM and micromanipulator-based techniques allow targeted retrieval of individual cells directly from the tissue. Although time consuming and low throughput, both techniques are suited to capture single cells from samples with few cells of interest (i.e. Yan et al. 2013). In most cases, microfluidics workflows include both cell capturing to individual reaction spaces and subsequent processing of material for library preparation for next generation sequencing. FACS-based cell capturing to individual wells of microtiter plates is popular and flexible due to considerable throughput and speed (Gross et al. 2015). Enrichment of particular cells of interest

is possible using fluorescent tagging. A major drawback of using microtiter plates is that, unlike microfluidic methods, reactions often cannot be downscaled to nanolitre volumes using traditional liquid handling robotics (i.e. Beckman Coulter BioMek) or manual liquid handling (Kolodziejczyk et al. 2015a). However, acoustic dispensing liquid handlers (i.e. Labcyte Echo 525) are becoming available leading to significant cost reduction by down-scaling to 500 nl reaction volumes without sacrificing data quality (Sackmann et al. 2016, Agrawal et al. 2016). Moreover, commercial assays are being launched that enable high throughput and low-volume microtiter plates-based single-cell library preparation (BD Precise Assays).

Recent developments in microfluidic technology have enabled new methods for capturing and processing of single cells with high throughput and low reaction volumes (Kimmerling et al. 2016). Mature techniques are for example integrated fluidics circuits (Fluidigm C1 method Pollen et al. 2014), microdroplet-based methods (inDrop (Klein et al. 2015), Drop-seq (Macosko et al. 2015) and Chromium (Zheng et al. 2017)). Moreover, random seeding methods have been developed (CytoSeq, Fan et al. 2015)

Recent, microdroplet-based methods for scRNA-seq are scalable to many thousands of cells. Fluid flows are precisely controlled to generate nanoliter aqueous reaction droplets embedded in oil, which can then be channeled, fused and manipulated. In these approaches, single cells are individually encapsulated in droplets, together with a bead containing millions of copies of a barcoded primer (a different barcode sequence per droplet) and additional reagents. After cell lysis, the barcoded primers capture transcripts released within that droplet and are then used for reverse transcription and sequencing library preparation. Further library preparation and high-throughput sequencing are carried out on pooled samples, and the cell-of-origin of transcripts is inferred from the barcode sequence (Burgess 2015).

In this thesis the first commercial microfluidics single-cell system was mainly used – the Fluidigm C1 Single-Cell Auto Prep System. For Fluidigm C1 methods cells are captured using integrated fluidic circuits (IFCs), which enable analysis of up to 96 or 800 cells per IFC. Cell capturing is achieved by input of >800 cells into one inlet well of the IFC. Cells are being separated into individual

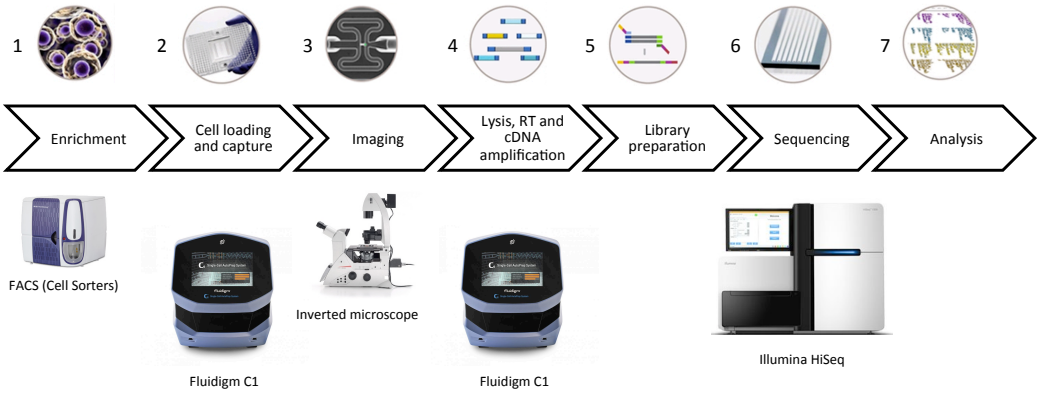

Figure 1: Workflow depicting the steps involved in performing single-cell mRNA-seq using the Fluidigm C1 system and Illumina sequencing. **1**: Cells of interest are enriched using fluorescence-activated cell sorting (FACS). **2:** Single-cell suspension of known concentration is transferred to one "cell inlet" of a Fluidigm microfluidic integrated fluidic circuit (IFC) plate. Cells are captured in IFC micro-chambers using the Fluidigm C1 instrument. **3**: Micro-chambers are documented using microscopy. **4**: Lysis, reverse transcription (RT) and cDNA amplification is performed using the Fluidigm instrument. **5**: Harvested material is subjected to Illumina NexteraXT library preparation. **6**: Pooled single-cell libraries are sequenced using Illumina sequencing. **7**: Derived sequencing data is processed and analyzed. Shown images were obtained from the websites of BD Biosciences, Fluidigm, Leica and Illumina.

micro-chambers that, by design, promote homing of individual cells. Cell capture is followed by microscopic screening, on-chip cell wash, lysis, reverse transcription and preamplification in nanoliter volumes. Library preparation for sequencing is carried out using individual samples for 96 cell IFCs and 20 pools (each with indexed 40 cells) for 800 cell IFCs. The cell-of-origin of transcripts is inferred from barcode sequences (Figure 1).

One limitation of the Fluidigm C1 method is that it only works for cells relatively homogeneous in size, since the capture sites are tuned to three size ranges (5–10, 10–17, and 17–25 microns in diameter). A second limitation is that the capture rate can be low for sticky, small or non-spherical cells, which can result in less cells being captured and sequenced (Kolodziejczyk et al. 2015a). However, overall single-cell capture rates are higher compared to droplet-based microfluidics techniques. Gained data quality, measured by number of detected genes per cell and uniform gene body coverage outperforms other microfluidics techniques to date. Additionally, the workflow is well established with optimized chemistry, low

hands-on-time and high protocol flexibility to sequence i.e. DNA or to apply other custom protocols.

1.4.2 Protocols for single-cell sequencing preparation

Many protocols have been developed to generate mRNA sequencing libraries from single cells (Tang protocol (Tang et al. 2009), STRT-Seq (Islam et al. 2011, Islam et al. 2012), SMART-Seq (Ramsköld et al. 2012), CEL-seq (Hashimshony et al. 2012), Quartz-Seq (Sasagawa et al. 2013), DP-Seq (Bhargava et al. 2013), MARS-Seq (Jaitin et al. 2014), CytoSeq (Fan et al. 2015), SC3-Seq (Nakamura et al. 2015), G&T-Seq (Macaulay et al. 2015)). Each protocol may be divided into the following steps: Cell lysis, reverse transcription, cDNA amplification, and sequencing library preparation. To avoid partial loss of material liquid manipulation is minimized and one-tube reactions are commonly used. Fast turn-around-times, cooling and chemistry selection for minimum inhibition effects (for subsequent steps) increase sensitivity. Most published methods use poly(T) priming to perform reverse transcription. Subsequent second-strand synthesis can be achieved by poly(A) tailing (Tang et al. 2009, Sasagawa et al. 2013) or, as used in this work, by template-switching mechanism at the 5' end of RNA template (SMART-Seq, Ramsköld et al. 2012). SMART-Seq protocols allow full-length transcript coverage, leading to reduction of 3' coverage biases originating from incomplete reverse transcription (Kolodziejczyk et al. 2015a). After reverse transcription, minute amounts of cDNA have to be amplified, which is achieved by either in vitro transcription (IVT, Hashimshony et al. 2012) or PCR (i.e. SMART-Seq). As for the SMART-Seq method applied with the Fluidigm C1 workflow, PCR-amplified cDNA constitutes the output material. Amplified cDNA samples are multiplexed, further processed for library prep and sequencing primers are added to increase throughput for next generation sequencing. Most protocols were designed for Illumina sequencing. Protocols for SOLiD sequencing (SC3-Seq, Nakamura et al. 2015) and PacBio sequencing (G&T-Seq, Macaulay et al. 2015) were recently developed.

1.5 Challenges of single-cell data analysis

Cells of the same type can show distinct transcriptomic signatures leading to phenotypic variation (Grün and van Oudenaarden 2015, Snijder and Pelkmans 2011). The goal of single-cell sequencing experiments is to find relations of cell types according to their similarity based on individual transcriptomes (Poulin et al. 2016).

Once, different sub-populations are found, their relationship needs to be deciphered. For example, the final output of data analysis can consist of a list of cell clusters, and a specific set of genes that can differentiate between found sub-populations. Alternatively or additionally, gene-centric analyses may be used. Gene-to-gene correlation analysis aids to define gene-regulatory modules (regulons, transcriptional circuits) that show synchronized expression of specific gene groups (Wagner et al. 2016). Although the single-cell data sets harbor a high resolution and a wealth of information, they are complex in nature and pose specific analytical and technical challenges (Wagner et al. 2016, Poirion et al. 2016). Single-cell data has a low signal-to-noise ratio (owing to technical noise and biological noise) (Brennecke et al. 2013), a high rate of dropout events (missing values, sparsity) (Macaulay and Voet 2014) and a small sample size compared to a high number of genes (Grün and van Oudenaarden 2015). Variation in gene expression values determined by scRNA-seq is in principal composed of i) technical variation, ii) intrinsic variation (transcriptional bursting, stochastic variation, "uncorrelated" variation) and iii) putatively functional extrinsic biological variation ("correlated" variation, single-cell variability).

Technical variation is introduced due to low amounts of starting material in individual cells. Mammalian cells contain about 1–50 pg of RNA with mRNA amounts of 0.01-2.5 pg mRNA per cell (Kawasaki 2004, Carter et al. 2005, Boon et al. 2011). Major contributors to technical variation include RNA degradation, absorption of molecules to liquid contacting materials, non-uniform PCR amplification, and varying sequencing efficiency (Bacher and Kendziorski 2016). These factors influence the usually low percentage of mRNA molecules from a cell that can be captured, amplified and finally sequenced (Liu and Trapnell 2016).

In addition, intrinsic biological variation may affect the overall noise level of single-cell gene expression data. Transcription is not a linear process but happens in bursts over time. This transcriptional bursting is a conserved phenomenon observed with many techniques ranging from microscopy (Raj et al. 2006) to other highly sensitive single-cell techniques such as single-cell qPCR (Bengtsson et al. 2005). The promoter of a gene switches between an active and an inactive state, which is intrinsically caused by the interplay between RNA polymerases on DNA (Fujita et al. 2016).

Extrinsic biological variation, single-cell variability or single-cell heterogeneity are the major target properties to be elucidated using single-cell transcriptome analysis. In this work, these terms are used to describe the diversity within an ensemble of macrophage cells, which has been previously considered as principally homogenous. Note that single-cell variability is not meant to refer to diversity of cell types that are clearly distinct (Dueck et al. 2016). Coordinated expression signatures of genes, derived from variation in single-cell gene expression, constitute a cell's identity. However, there may be partial dependencies between the multiple facets of a cell's identity, such that variation in one biological dimension may be a confounder for another (Wagner et al. 2016). For example, confounding factors such as the cell cycle can obscure biologically relevant molecular signatures in scRNA-seq data sets, i.e. single-cell variation inherent to the immune response (Stegle et al. 2015).

1.5.1 Limitation of traditional analysis strategies

Primary analysis of single-cell RNA-seq data follows similar workflows as for traditional bulk RNA sequencing, including data preprocessing (adapter trimming, paired-end data processing, nucleotide quality filtering), alignment, quality filtering (low quality cell removal, outlier cell removal and filtering genes with high biological variation) and normalization (confounding factor removal, size factor normalization, and normalization to internal controls). However, the problem of high data complexity, high dimensionality and high intrinsic variation levels entails further analytical challenges. Many standard multivariate analysis methods (i.e. hierarchical clustering or principal component analysis (PCA)) are limited in

defining cellular states based on whole transcriptomes (Grün and van Oudenaarden 2015). These methods are for example not robust for dealing with missing data and rare outliers. For PCA, high variability in expression levels among cells of the same type can cause a potentially underlying structure to be undetected by this otherwise useful approach (Bacher and Kendziorski 2016). Hierarchical clustering may define groups of cells with similar expression patterns but fails to represent the multivariate structure of the data (Wirth et al. 2011).

1.5.2 Self-organizing map machine learning

It becomes clear that studying multi-faceted biological processes at the single-cell level crucially depends on novel computational techniques that efficiently mine single-cell data sets. As for the remarkable growth of data from information technology (i.e. social media), unsupervised machine learning represents an ideal approach for exploiting the structures hidden in complex single-cell data. Especially, methods based on artificial neural network algorithms such as self-organizing maps (SOMs, Kohonen 1982) combine effective noise-tolerant data processing and dimension reduction with strong visualization capabilities (Löffler-Wirth et al. 2015). SOM analysis summarizes input data (i.e. a single-cell gene expression matrix) by gene vector quantization ("training") and simultaneously carries out topological preserving gene vector projection ("mapping"). Optimization of neighborhood kernels controls the extent to which the gene vector projection influences the vector quantization (Zhang and Fang 2012). By mapping from a higher-dimensional input space to a lower-dimensional map space, SOMs display similarity relationships of genes in two dimensional maps in which spatial proximity reflects expression pattern similarity (coordinately expressed gene sets) (Kim et al. 2015). Each node on the map (SOM component) is expressed as a prototype gene expression vector for the high-dimensional space. Thus, genes with the same or similar expression patterns are mapped to the same or nearby SOM component in the consensus of all cells. The density of genes mapped to this two-dimensional map follows the data density in the high-dimensional space.

SOM reduces the dimension of the expression data from thousands of genes to a few SOM components each component representing a cluster of co-expressed single

genes. SOM analysis arranges and classifies genes with high information content in the consensus of all cells. Those high-information-content-genes feature high expression and high correlation in a sufficiently large number of cells. It is assumed that genes with uncoordinated (random) expression values have low information content. Thereby, SOM analysis accounts for technical noise in single-cell data. Genes with high technical variation are separated from those genes with high biological variation, without the need of conservative filtering strategies (Brennecke et al. 2013). Importantly, SOM analysis improves the performance of downstream multivariate methods like hierarchical clustering, by maintaining representativeness and reducing noisiness (Wirth et al. 2011). Thus, it allows for robust cell state definitions. SOM component clusters that comprise co-expressed genes aid in defining cell state-specific gene signatures and co-expression modules. Therefore, this dimension reduction method helps to link clusters with prior knowledge to support functional interpretation.

1.6 Aims of the thesis

Immune cells such as macrophages show exceptional resilience and heterogeneity, instrumental to their function in immunity and homeostasis (Mosser and Edwards 2008). The objective of this work is to shed light on cellular strategies of macrophages at the onset of response towards external stimuli that mimic invading bacteria. As a model system, differentiated THP-1 macrophages left unstimulated is compared to macrophages stimulated with bacteria-derived lipopolysaccharide (LPS). By investigating isogenic cells under homogenous conditions macrophage heterogeneity in the absence of classical polarization strategies is explored using single-cell mRNA sequencing. Our main focus is to ask how non-genetic (or phenotypic) heterogeneity among individual macrophages might interact to causally generate higher-level function.

Firstly, we aim to unbiasedly characterize transcriptome signatures of individual macrophages by assessing multivariate distance and similarity of reconstructed cellular states. Instead of considering stimulation-induced changes only, we consider the use of self-organizing map machine-learning to holistically characterize vectors

of cellular identity and to guide functional annotation. Secondly, we analyze how cells adapt stimulation by quantifying cellular response of activated macrophage states. Distinct approaches are being implemented to mathematically describe the efficiency of intracellular signaling transduction and resulting transcriptional response under "normal" and disordering conditions. Thirdly, we predict central regulatory hubs that underly antagonistic gene-regulatory modules by integrative analysis strategies. Mutually exclusive expression of competing gene-regulatory factors is further confirmed in THP-1 and primary human macrophages using independent single-cell techniques, including single-cell qPCR, RNA-fluorescence *in situ* hybridization (RNA-FISH) and immunofluorescence. Fourthly, we aim to more functionally address macrophage dynamics. For example, we ask how macrophage state balance is shaped under elevated environmental triggers. Moreover, we aim to characterize how targeted perturbations of antagonistic factors influence cellular dynamics and shift macrophages towards different transcriptional and phenotypical identities.

Collectively, this work aims to provide an initial comprehensive conceptual framework for understanding intrinsic macrophage heterogeneity as a cellular strategy towards variant environmental conditions. We anticipate this single-cell data set of human macrophage activation to contribute to an enhanced appreciation of general mechanisms of transcriptional control, as well as the development of new mathematical models for signal integration and new therapeutic strategies for human disease.

Chapter 2

Materials and methods

2.1 Lab methods and computational analysis

2.1.1 Cell culture

Human THP-1 monocytic-like leukemia cells (ATCC, Cat. no. TIB-202, Auwerx 1991), THP1-XBlue cells (InvivoGen, Cat. no. thpx-sp) and THP1-XBlue-defMyD cells (InvivoGen, Cat. no. thpx-dmyd) were cultured with RPMI 1640 medium (Biochrom, Cat. no. FG1215) supplemented with 10% fetal bovine serum (FBS, Biochrom, Cat. no. S0615). Medium was filtered using 0.22 µm vacuum filtering system (Millipore, Stericup (Cat. no. SCVPU02RE) and Steritop (Cat. no. SCGPS01RE)). Cells were seeded from supplied stocks and initially cultured in T25 culture flasks (TPP, Cat. no. P90026). Following cultivation of cells was done in T75 flasks (Biochrom, Cat. no. P90076). Cells were incubated at 37 °C in a 5 % CO_2 atmosphere. Subculturing was done three times per week by the addition of fresh medium to gain final cell concentrations of 2×10^5 cells/ml. Cells were washed by centrifugation at 300 g for 5 minutes at RT and subsequent replacement of supernatant by fresh complete medium. Cell numbers were determined using C-Chip disposable counting chambers (Biochrom, Cat. no. PDHC-N01).

Human primary macrophages were isolated from at least four individual buffy coats donated by healthy volunteers (kindly provided by DRK- Berlin). Peripheral blood monocytes (PBMC) were isolated from buffy coats with Ficoll Paque by

density centrifugation for 40 minutes at 400g and subsequent washing steps with PBS supplemented with 0.5% BSA and 2mM EDTA. Afterwards, monocytes were isolated with MACS Monocyte Isolation Kit II with MACS LS columns (Miltenyi Biotec). Purity (>95%) was assessed using FACS analysis. Primary monocytes were cultured and differentiated to macrophages in RPMI 1640 medium (Biochrom, Cat. no. FG1215) supplemented with 10% human serum (Human Serum Type AB, PAN-BIOTECH, P30-2501) for 7 days at 37 °C in a 5 % CO_2 atmosphere.

2.1.2 Macrophage differentiation and treatment

THP-1 monocytes were differentiated to macrophages-like cells with 10 nM phorbol-12-myristate-13-acetate (PMA, Sigma, Cat. no. P8139) for 72 hours prior to LPS stimulation (Maeß et al. 2014). After 48 hours of differentiation cell medium was changed with fresh complete medium including 10 nM PMA. As a standard setting 6-well plates (Corning, Cat. no. 3736) were used with 1×10^6 cells total in a volume of 4 ml. Primary macrophages were seeded at the same cell concentration in 6-well plates. For 12-well plates and microscopic slide preparation (Corning, Cat. no. 3737) macrophages were seeded with 1 ml at a cell concentration of 2.5×10^5 cells/ml. Cells were treated with 100 ng/ml lipopolysaccharide (LPS, Sigma-Aldrich, Cat. no. L5293) unless mentioned otherwise for 2 hours. One µM dexamethason (kindly provided by Dr. Sebastiaan H. Meijsing) was used for macrophage treatments as indicated.

2.1.3 Cell cycle analysis

Cell cycle analysis was carried out by applying propidium iodide (PI)/RNase Staining Solution (Cell Signalling, Cat. no. 4087). Differentiated THP-1 macrophages were washed twice with 4ml pre-warmed (37°C) 1 x phosphate buffered saline (PBS, Sigma-Aldrich, Cat. no. D8537-24X500ML). One ml pre-warmed (37°C) TrypLE™ Express (Gibco, Cat. no. 12604021) was added and samples were incubated for 8-12 minutes at 37°C in a 5% CO2 atmosphere. Non-differentiated THP-1 monocytes were washed twice with 4ml pre-warmed (37°C) 1 x PBS. Centrifugation was carried out for 5 minutes at 180g on room temperature (25°C). Differentiated and

non-differentiated THP-1 cells were resuspended in 10ml of complete RPMI 1640 medium (Biochrom, Cat. no. FG1215) supplemented with 10% fetal bovine serum (FBS, Biochrom, Cat. no. S0615). Afterwards, samples were spun for 5 minutes at 180g at room temperature (25°C), washed with 1 x PBS and spun again as described. Finally, cell pellets were resuspended with 1ml 1×PBS. Fixation of cells was carried out by drop-wise addition of 2333ul ice cooled ∼100% ethanol while carefully shaking the sample. Then, samples were incubated for 15 minutes on ice or overnight at -20°C. Afterwards, cells were spun down at 200g for 5 minutes at room temperature (25°C). Pellets were resuspended in 500ul propidium iodide (PI)/RNase Staining Solution and incubated for 15 minutes at room temperature. Finally, samples were analyzed with analytical flow cytometry analysis using the BD FACSAria II.

2.1.4 Cell harvest

Supernatants from 6-well plate were discarded. Wells were washed twice with ∼4 ml 1 × phosphate buffered saline (PBS, Sigma-Aldrich, Cat. no. D8537) that was pre-warmed to 37 °C in a water bath prior to use. One ml pre-warmed TrypLE Express (Gibco, Cat. no. 12604021) was added to each well. Incubation was for 8-12 minutes at 37 °C in a 5 % CO2 atmosphere.

2.1.4.1 Cell harvest for population analysis

For population measurements, bottom of wells were flushed multiple times to recover incompletely detached cells. Samples were transferred into ice-cooled 1.5 ml or 15 ml tubes. Subsequently, each well was flushed again with 0.5 ml PBS (2 % FBS) and transferred into corresponding 1.5 ml or 15 ml tubes. Tubes were spun for 5 minutes at 2000 g and 4 °C. Supernatants were discarded and pellets were washed with ice-cold PBS. Samples were spun again for 5 minutes at 2000 g and 4 °C. Supernatants were again discarded, pellets were washed once more with 1 ml ice-cold PBS and transferred into 1.5 ml tubes. After an additional spun supernatants were discarded. To remove residual PBS a final centrifugation was carried out for 3 minutes at 2000 g and 4 °C. Remaining liquid was removed and

pellets were put on dry ice and finally stored at −80 °C.

2.1.4.2 Cell harvest for single-cell analysis

For single-cell measurements (including single-cell qPCR and single-cell mRNA-seq) 4 ml of ice-cooled medium with FBS was added to detached cells. Samples were transferred into ice-cooled 15 ml tubes. Tubes were centrifuged for 5 minutes at 150 g and 4 °C. Supernatants were discarded and pellets were initially gently resuspended with 1ml ice-cooled PBS including 2 % BSA (Sigma-Aldrich, Cat. no A7030). Addition of BSA to PBS was done because it prevents cell clumping. Thirteen ml of ice-cooled PBS including 2 % BSA was added to resuspended cells gently. Samples were spun for 4-5 minutes at 150 g and 4 °C. Supernatants were discarded and final resuspension was in 450 µl PBS including 2 % BSA. Five µl of 7-amino-actinomycin D (7-AAD, BD Biosciences, Cat. no 559925) per 1×10^6 cells were added to exclude dead cells during fluorescence activated cell sorting (FACS). After 5 minutes incubation in the dark on ice, resuspended cells were filtered through a 40 µm cell strainer (BD Biosciences, Cat. no. 352340). Finally, cells were transferred to FACS tubes (VWR, Cat. no 734-0443) and subjected to FACS sorting and analysis using BD FACS Aria II.

2.1.5 FACS for sc-qPCR and sc-mRNA-seq

For C1 single-cell mRNA sequencing workflows and C1 single-cell pre-amplification workflows cells were subjected to FACS sorting into 1.5 ml tubes prior to loading into Fluidigm IFCs. Target tubes for FACS sorting were pre-coated with PBS including 10 % BSA to prevent cell damage if cells were hitting the tube wall. Tubes were stored at 4 °C. Hundred ul 1 x PBS with 2 % BSA was added to tubes prior to spotting. For individual cell spotting to 96-well plates, cells were spotted into 5 µl water (Ambion, Cat. no. AM9937) and processed as described in 2.1.4.2. FACS cell selection (gating) was configured to ensure single-cell spotting specificity by subsequent gating of a) side scatter area (SSC-A) versus forward scatter area (FSC-A), b) forward scatter width (FSC-W) versus forward scatter area (FSC-A) and c) side scatter width (SSC-W) versus side scatter area (SSC-A). For a) the main

cell population was selected narrowly as guided by cell density visualizations. For b) and c) FACS event outliers with high width estimates were excluded (potential cell doublets). 7-AAD was detected using both a Cy5-5 filter (PerCP-Cy5-5, 695/40) and a mCherry filter (mCherry/mKate2, 615/20). Visualization of events was done by plotting SSC-W versus signals derived from filters mentioned above. Events were discriminated if they showed a higher fluorescence compared to the main population (intact cells).

2.1.6 Post-FACS cell preparation for Fluidigm C1 workflows

Applying cell preparation and FACS analysis as described (see 2.1.4.2 and 2.1.5) 1.5 - 3.5 $\times$ 10^5 cells were captured per tube. Cell sorting took 10-15 minutes per treatment group with a flow rate of 1 or up to 2. Target tubes were cooled to 8 °C by the use of a FACS Aria II cooling tube holder. After spotting cells were kept on ice whenever possible. After gentle resuspension, cells were counted using C-Chip disposable counting chambers (Biochrom, Cat. no. PDHC-N01). Cells were spun at 200 g for 5 minutes at 4 °C and supernatant was discarded. Pellets were resuspended in PBS with 2% BSA to reach a final concentration of 400 cells/µl. Cells were counted again to ensure that the final cell concentration was 300 - 400 cells/µl. Sixteen µl of cell mix was subsequently used for the Fluidigm C1 single-cell workflows.

2.1.7 Single-cell mRNA-sequencing

The Fluidigm C1 single-cell Auto Prep System was used to generate single-cell cDNA libraries for mRNA sequencing using C1 Single-Cell Auto Prep Arrays for mRNA Seq (IFCs, Fluidigm, Cat. no. 100-5761 and 100-5760) in combination with the C1 Single-Cell Auto Prep Reagent Kit for mRNA Seq (Fluidigm, Cat. no. 100-6201), the SMARTer Ultra Low Input RNA for Illumina Sequencing (Clontech, Cat. no. 634828) and the Advantage 2 PCR Kit (Clontech Cat. no. 639206). The workflow was done according to the Fluidigm protocol "Using C1 to Generate Single-Cell cDNA Libraries for mRNA Sequencing". The protocol in brief was as

follows. Lysis mix was prepared using 1ul C1 DNA loading reagent (Fluidigm), 0.5 µl RNase inhibitor (Clontech), 7 µl 3' SMART CDS primer IIA (Clontech) and 11.5 µl Clontech dilution buffer. For preparation of the lysis mix for cells treated with LPS 1 µl RNA spike mix dilution was added to the lysis mix instead of C1 DNA loading reagent. The RNA spike mix dilution was prepared as follows: ArrayControl RNA spikes (Thermo-Fisher„ Cat. no. AM1780) were thawed, and spikes #1, #4, and #7 were used. 1.5 µl spike #7 was added to 13.5 µl of RNA storage solution (Thermo-Fisher, The RNA Storage Solution, Cat. no. AM7000), 1.5 µl spike #4 was added to 12 µl of RNA storage solution and 1.5 µl spike #1 was added to 148.5 µl of RNA storage solution. Spike #7 mix was resuspended and spun briefly and 1.5 µl of the solution was added to the spike mix #4. Spike mix #4 was also mixed and spun briefly and 1.5 µl of the solution was added to the spike mix #1. Spike #1 mix was resuspended and spun briefly and 1 µl was finally added to 99 µl loading reagent (Fluidigm). One µl of the generated RNA spikes mix dilution was added to the lysis solution as described above.

For preparation of the reverse transcription (RT) reaction mix 1.2 µl loading reagent (Fluidigm), 11.2 µl 5×first-strand buffer (Clontech), 1.4 µl dithiothreitol (Clontech), 5.6 µl dNTP mix (dATP, dCTP, dGTP, and dTTP, each at 10 nM, Clontech), 5.6 µl SMARTer IIA oligonucleotide (Clontech), 1.4 µl RNase inhibitor (Clontech) and 5.6 µl SMARTScribe reverse transcriptase (Clontech) was combined, mixed and briefly spun.

For preparation of the PCR mix 63.5 µl PCR-grade water (Clontech), 10 µl 10×Advantage 2 PCR buffer (Clontech), 4 µl 50X dNTP mix (Clontech), 4 µl IS PCR primer (Clontech), 50×Advantage 2 polymerase mix (Clontech) and 4.5 µl loading reagent (Fluidigm) were combined, mixed and briefly spun.

To prime the Fluidigm IFCs, 200 µl C1 harvest reagent (Fluidigm) was added into accumulators A1 and A2 of the IFC. Twenty µl C1 harvest reagent was added into inlets P1 and P2 (40 wells total). Twenty µl C1 preloading reagent was added into inlet 2. Fifteen µl of C1 blocking reagent was added into the cell inlet (inlet C1) and cell outlet (inlet C2). Twenty µl of cell wash buffer was added into inlets 5 and 6. Afterwards, the IFC was placed into the Fluidigm C1 system and the Script "mRNAseq: Prime" was run. Runtime as ∼12 minutes.

For cell loading 60 µl of prepared cell mix (see 2.1.6) was added to 40 µl suspension reagent (Fluidigm). The cell mix was gently resuspended by setting a P200 pipette to 60 µl and slowly pipetting up and down 5-10 times. Blocking solution was then removed from the primed IFC from cell inlet (inlet C1) and outlet (inlet C2). Again, cell mix was gently mixed as described above. Six µl of cell mix was finally added to the cell inlet (inlet C1) and 20 µl cell wash buffer (Fluidigm) was added into inlet 1. The IFC was placed into the Fluidigm C1 system and the script "mRNAseq: Cell Load" was run. Execution of the complete script took ∼30 minutes.

After cell loading was completed, micro-chambers of the IFC were screened manually within 20-30 minutes using Zeiss Observer Z1 with a phase contrast 20×Objective. All cell pictures were summarized in Figure 28 on page 107. It was documented simultaneously if micro chambers were empty, had more then one cell, contained damaged cells or contained one intact individual cell.

As soon as microscopic documentation was completed, the IFC was prepared to run lysis, reverse transcription, and PCR. Therefor, 180 µl of C1 harvest reagent was added into four harvest inlet reservoirs of the IFC. Nine ul of lysis mix and 9 µl reverse transcription mix were added into inlet 3 and inlet 4, respectively. Twenty-four µl of PCR mix was added into inlet 7 and 8. Afterwards, the IFC was placed into the Fluidigm C1 system and the Script "mRNAseq: RT & Amp" was run over night (∼8.5 hours). The script contained the following thermal cycling protocols. Lysis was carried out for 3 minutes at 72 °C, 10 minutes at 4 °C and 1 minute at 20 °C. For reverse transcription 40 °C were applied for 90 minutes and 70 °C were applied for 10 minutes. The PCR started with heating for 1 minute at 95 °C followed by 5 cycles of 95 °C for 20 seconds, 58 °C for 4 minutes and 68 °C for 6 minutes. Afterwards, 9 cycles were run with 95 °C for 20 seconds, 64 °C for 30 seconds and 68 °C for 6 minutes. Subsequently, 7 cycles were run with 95 °C and 64 °C for 30 seconds each and 68 °C for 7 minutes. Finally, 72 °C were applied for 10 minutes.

After lysis, reverse transcription and PCR the IFC was removed from the C1 system. Three and a half µl from each of the 96 single-cell libraries (C1 harvest amplicons) were transferred from harvest outlets of the IFC into 10 µl of

C1 DNA dilution reagent (Fluidigm) placed into a 96-well plate (diluted harvest plate, Biozym, Cat. no. 621601) following pipetting instructions from Fluidigm. Afterwards, the plate was sealed, mixed for 10 seconds and spun to collect harvest products.

For library preparation for Illumina sequencing the Nextera XT DNA Sample Preparation Kit (Illumina, Cat. no. FC-131-1096) and Illumina Index Kit (Illumina, Cat. no. FC-131-1002, Illumina) were used. Two µl of harvest products were transferred into a new 96-well plate containing 2 µl C1 harvest reagent per well (diluted sample plate). After sealing and mixing for 20 seconds the plate was spun for 1 minute at 1500 g. Each well of a new 96-well plate (library prep plate) was filled with 3.75 µl tagmentation reaction mix that contained per well 2.5 µl tagmentation DNA buffer (Illumina) and 1.25 µl amplification tagmentation mix (Illumina). Finally, 1.25 µl of diluted samples from the diluted sample plate were added to 3.75 µl of tagmentation reaction mix. Plates were mixed for 20 seconds and spun at 4000 g for 5 minutes to collect contents and to remove bubbles. The plate was then transferred into a thermal cycler. Samples were incubated with a heated lid for 10 minutes at 55 °C followed by 10 °C for a maximum of 10 minutes. Once the sample reached 10 °C, 1.25 µl NT buffer (Illumina) was added to the tagmented samples of the library preparation plate for neutralization. Afterwards, the plate was sealed, mixed for 20 seconds and spun at 4000 g for 5 minutes. To amplify and index the DNA, 3.75 µl of Nextera PCR master mix (NPM, Illumina) was added to each well of the library prep plate. Subsequently, index 1 (N7xx) and index 2 (S5xx) primers (Illumina) were aligned to the rows and the columns of the 96-well plate, respectively. Firstly, 1.25 µl of index 1 primers (N7xx) were added into the corresponding well of each row of the library preparation plate. Secondly, 1.25 µl of index 2 primers (S5xx) were added into the corresponding wells of each column of the library preparation plate. Afterwards, the plate was sealed, mixed for 20 seconds, spun at 4000 g for 2 minutes and placed into a thermal cycler with lid heated during the incubation. The following thermal cycling protocol was used: Initial heating for 3 minutes at 72 °C, followed by 30 seconds at 95 °C. Twelve cycles of 95 °C for 10 seconds, 55 °C for 30 seconds and 72 °C for 60 seconds, followed by incubation for 5 minutes at 72 °C, and final cooling to 10 °C. Amplified

and indexed products were then subjected to pooling and purification. Therefor, 1 µl of each library (96 µl total) was mixed by pipetting with 87 µl of AMPure XP beads (Beckman Coulter, Cat. no. A63880). The bead mix was incubated for 5 minutes at room temperature and placed on a magnetic stand for 2 minutes. Afterwards, supernatant was carefully removed and 180 µl of freshly prepared 70 % ethanol was added. Incubation of ethanol on the magnetic stand was 30 seconds before ethanol was removed. After repeated ethanol wash, beads were allowed to air-dry at room temperature for 10 minutes. DNA was eluted with 96 µl of C1 DNA dilution reagent (Fluidigm). The tube was then mixed for 3 seconds, incubated at room temperature for 2 minutes and placed on a magnetic stand for another 2 minutes. The entire volume of supernatant was transferred to a new tube and AMPure cleanup was repeated, as described above except that elution was carried out with 144 µl of C1 DNA dilution reagent. The material was then tested with Agilent Bioanalyzer (Figure 5 D).

Libraries were quantified using Kappa Library Quant (Kapa Biosystems, Cat. no. KK4854). Illumina 100 nt paired-end sequencing was done on a Illumina HiSeq2000 by using TruSeq PE Cluster Kit v3 - cBot - HS (Illumina, Cat. no. PE-401-3001), TruSeq SBS Kit v3 - HS (Illumina, Cat. no FC-401-3001) and TruSeq Dual Index Sequencing Primer Box (Illumina, Cat. no. PE-121-1003).

2.1.8 Population mRNA-sequencing

RNA concentration measurement and quality control was carried out using Qubit 3.0 Fluorometer (Thermo Fisher Scientific) and Agilent 2100 Bioanalyzer (Agilent Technologies) with RNA 6000 Nano Kit (Agilent Technologies). Sequencing libraries were prepared using Illumina TruSeq RNA Library Prep Kit v2 (Illumina) and paired-end sequencing 2x100bp was performed on HiSeq 2000 (Illumina).

2.1.9 qPCR expression analysis of population samples

Reverse transcription was performed using qScript cDNA SuperMix (VWR, Cat. no. 733-1177) in standard thermal cycler (5 minutes 25°C, 30 minutes 42°C, 5minutes 85°C). HPLC-purified primers were obtained from Sigma Aldrich. Primer

working solutions (2 µM) were freshly prepared. PerfeCTa SYBR Green SuperMix (VWR, Cat. no. 733-1246) was used for all qPCR reactions. qPCR reactions were prepared in 10µl volume in 384-well plates (Fisher Scientific GmbH, Cat. no. PCR-384-LC480-W) and used LightCycler 480 II system (LC480, Roche) to perform a qPCR. Following primers were used:

Gene name	Ensemble gene ID	Forward primer	Reverse primer
CCL20	ENSG00000115009	CTGGCTGCTTTGATGTCAGTG	AGTCAAAGTTGCTTGCTGCTTC
CCL3	ENSG00000277632	CAAGGGGGCCCTCAGAGTGTCCT	TGTGACCTGACTTGGGGCTGGAG
CSF1	ENSG00000184371	TGCTGGAGAAGGTCAAGAATGT	TCACCACATCTTGGCTGGAG
GAPDH	ENSG00000111640	CTCCTCCTGTTCGACAGTCA	CGACCAAATCCGTTGACTCC
HIF1A	ENSG00000100644	GGACAGCCTCACCAAACAGA	TCAGGAACTGTAGTTCTTTGACTC
IL1B	ENSG00000125538	GGACAGGATATGGAGCAACAAG	AACACGCAGGACAGGTACAG
IL8	ENSG00000169429	CTGATTTCTGCAGCTCTGTG	GGGTGGAAAGGTTTGGAGTATG
IRAK3	ENSG00000090376	AGAGCTCTGCGCTGTTCTG	ACTCAACACTGCTCCCAGG
JAK2	ENSG00000096968	GGGGTTTTCTGGTGCCTTTG	CACTCCCAAAATTACCCTTGCC
MYD88	ENSG00000172936	AGCATTGAGGAGGATTGCCA	GGCCACCTGTAAAGGCTTCT
NFKB1	ENSG00000109320	TGAGTCCTGCTCCTTCCA	GCTTCGGTGTAGCCCATT
NR3C1	ENSG00000113580	CCGGGCCCAAATTGATATTCAC	ACATCTCCCCTCTCCTGAGC
PPARG	ENSG00000132170	TGGAAGACCACTCCCACTCC	GCAGGCTCCACTTTGATTGC
RUNX2	ENSG00000124813	CGCCGAGCTCCGAAATGCCT	AACTCTTGCCTCGTCCGCTCC
SOD2	ENSG00000112096	GGCACTCGTGGCTGTGGTGG	CCTGCTGGTGCCGCACACT
TNF	ENSG00000232810	CTCAGCTTGAGGGTTTGCTAC	GGACAGGATATGGAGCAACAAG

2.1.9.1 RNA isolation for population measurements

For RNA isolation samples were processed as described (see 2.1.4.1) and subsequently processed using RNeasy Mini Kit (Qiagen, Cat. no. 74106). RNA from each sample was derived following the manufacturers protocol "Purification of total RNA from animal cells using spin technology". DNase digest was done for 30 minutes on-column using RNase-free DNase set (Qiagen, Cat. no. 79254). RNA was eluted from columns with 30 µl RNase-free water. Elution was done twice to maximize RNA recovery. RNA was finally stored at −80 °C. Quality of RNA

was tested using gel electrophorese. Therefore, 1 % agarose gels were prepared with agarose (Biozym, Cat. no 840000). For running gels 1×lithium borate buffer (Faster Better Media LLC, Cat. no. LB20-1) was used according to (Brody et al. 2004). Sample preparation for electrophoresis was done with 1 µl RNA, 2 µl 5×LB loading medium (Faster Better Media LLC, Cat. no. LB5N-8) and 9 µl RNase-free water. Separation of RNA was done by applying 300 V for 5 minutes. 1 kb plus DNA ladder (Invitrogen, Cat. no 10787018) was used as reference marker. RNA concentrations were determined with NanoDrop 2000 (Thermo Scientific). For normalization of samples, isolated RNA samples were adjusted by the addition of ice-cooled RNase free water to reach similar concentration. RNA samples subjected to mRNA sequencing workflows were additionally measured using Agilent Bioanalyzer following manufacturer instructions.

2.1.9.2 Reverse transcription for population measurements

For reverse transcription of RNA into cDNA for qPCR workflows a reaction mix was generated that contained 2 µl qScript cDNA SuperMix (VWR, Cat. no. 733-1177) and 8 µl of RNA sample. Reaction was performed in PCR strips (Biozym, Cat. no 710990) in thermal cycler with heated lid (PC-100, MJ Research). Samples were incubated for 5 minutes at 25 °C, 30 minutes at 42 °C and 5 minutes at 85 °C, followed by final cooling to 4 °C. cDNA was stored at −20 °C or −80 °C (long term storage).

2.1.9.3 Quantitative real-time PCR for population measurements

Primer working solutions with forward and reverse primers were freshly prepared from 10 mM primer stocks to a final working concentration of 2 µM. PCR master mix was prepared consisting of nuclease-free water (Ambion, Cat. no. AM9937) and PerfeCTa SYBR Green SuperMix (VWR, Cat. no. 733-1246). The mix was stored on ice in the dark whenever possible. cDNA samples were thawed on ice and appropriate cDNA volumes were added to the according volume of prepared master mix. Samples were mixed and spun to collect contents. Two µl primer working solution was added into wells of a 384-well plate (Fisher Scientific GmbH, Cat. no. PCR-384-LC480-W) using a 12.5 µl Matrix pipette (Thermo Scientific,

Cat. no. 2009) or a Xstream dispenser (Eppendorf, Multipette Xstream "Kary Mullis" Limited Edition, Cat. no. 4986000203). Final concentration of primers was 0.2 µM per reaction. Eight µl master mix that contained cDNA as described was added using a 125 µl Matrix pipette (Thermo Scientific, Cat. no. 2011) or a Xstream dispenser. Finally, plates were sealed (Roche, with LightCycler480 Sealing Foil, Cat. no. 04729757001) and spun at 3000 g on room temperature. Then, plates were analyzed using the LightCycler 480 II system (Roche, LC480). The cycling protocol was as follows. For pre-incubation, heating was applied for 3 minutes at 95 °C. Afterwards, 40 to 50 cycles were carried out with denaturation for 10 seconds at 95 °C and annealing and extension for 45 seconds at 60 °C. Subsequently, melting curve analysis was done by heating up the plate from 65 °C to 95 °C over 10 minutes. Finally, temperature was hold at 40 °C until the plate was removed from the instrument.

To check if genomic DNA contributed to qPCR measurements, ValidPrime Human - SYBR assay was used (TATAA Biocenter, Cat. no. A105S25) according to (Laurell et al. 2012). The following calculation was used to evaluate if genomic DNA substantially contributed to observed signals: Cq is the detected Cq values for primer assays for genes of interest (gene), the ValidPrime primer assay for either the run cDNA samples (sample), a genomic DNA standard (gDNA).

$$\mathrm{Cq}_{RT-}^{gene} = \mathrm{Cq}_{gDNA}^{gene} + (\mathrm{Cq}_{sample}^{vp} - \mathrm{Cq}_{gDNA}^{vp})$$

2.1.9.4 Primary data analysis of qPCR results

Raw data was derived from the LightCycler 480 II system using the LC480 analysis software (Roche, v1.5.0.39). Abs Quant/2nd Derivative Max method was applied to calculate Cq values and curve profiles and the TM calling methods was used to calculate Tm values and melting curve profiles. Outputs were saved as tab-delimited text files that were used as input for custom-made R scripts to visualize derived values and curve profiles for quality assessments.

2.1.9.5 qPCR Expression data analysis for population measurements

For differential gene expression analysis log 2 fold-change expression method was used (Livak and Schmittgen 2001). Cq values from three PCR replicates (same cDNA tested in three different wells of the assay plate) were averaged and ΔCq was calculated as follows where ref indicates the reference gene (i.e. GAPDH) and gene indicates the gene of interest for a given treatment.

$$\triangle \mathrm{Cq} = \mathrm{Cq}^{ref}_{treatment} - \mathrm{Cq}^{gene}_{treatment}$$

This calculation was done individually for cell culture replicates (material from cells cultured in a different culturing unit, i.e. a different well plate). Subsequently, △Cq-values of three cell culture replicates were averaged. The △△Cq was calculated as follows using values from a reference samples (reference) and a sample subjected to a treatment (treatment).

$$\triangle\triangle \mathrm{Cq} = \mathrm{Cq}^{gene}_{reference} - \mathrm{Cq}^{gene}_{treatment}$$

In a final step fold changes were calculated for each cell culture replicate per treatment and gene as follows:

$$\mathrm{FC}^{gene}_{treatemnt} = 2^{-\triangle\triangle Cq}$$

For estimation of statistical significance, t-test was conducted with ΔCq-values. The statistical test was configured as a two-tailed non-paired test according to Goni et al. 2009.

2.1.10 qPCR expression analysis of single cells

Single cells and 40-cells controls were sorted into 5 µl of RNase-free water in 96-well plates using BD FACSAria II. After cell spotting, samples were snap-frozen. Single-cell and bulk samples were reverse transcribed using qScript cDNA SuperMix (Quanta Biosciences, Cat. no. 95048). Quantitative PCR was performed using PerfeCta SYBR Green SuperMix (Quanta Biosciences, Cat. no. 95054) on Roche LightCycler 480 II System. We used custom designed primers from Sigma-Aldrich (Supplementary Table 2) and RT2 Profiler Toll-Like Receptor Signaling Pathway PCR Array (Qiagen).

2.1.10.1 FACS sorting for single cell analysis

The FACSAria II cytometer (BD Biociences) with a BD Automated Cell Deposition Unit (ACDU) setup was used as described in 2.1.5. Individual cells were spotted into wells of 96-well plates (Biozym, Cat. no. 621601). Sporting to the center well bottom was calibrated by spotting 50-100 drops (Beads, BD Biosciences, Cat. no. 349502) and precise sledge adjustment. Practically, spots were hit on the center right region at well tops. Capture plates were filled with 5 µl nuclease-free water (Ambion, Cat. no. AM9937) per well and plates were kept at 4 °C or on ice. Single cells were spotted into wells A-H/1-11 and 40 cells were spotted into well A12 and B12. Fife µl 2 µM interplate calibrator (IPC, TATAA Biocenter, Cat. no. IPC250S) was added into wells C-E/12. Spotting took ∼1 minute per plate. Immediately after spotting, plates were sealed with adhesive aluminum foil (VWR, Cat. no. 60941-126) and frozen on a conductive aluminum 96-well rack placed on dry ice. Plates were stored at −80 °C.

2.1.10.2 Reverse transcription

All steps after thawing of frozen 96-well plates containing single cell material were done as quickly as possible, and samples were kept on a conductive aluminum rack on ice whenever possible. Plate contents were thawed for maximum 5 minutes at room temperature and spun for 1 minute at 2000 g at 4 °C. One µl qScript cDNA SuperMix was diluted at the ratio of 1:1 with RT-PCR grade water (Life technologies, Cat. no. AM9935). One µl diluted qScript was added into each well (total volume 6 µl) using multipette Xstream. The plates were sealed with adhesive aluminum foil, mixed and spun down briefly at 4 °C to collect contents. Reverse transcription was performed in a Peqlab thermal cycler (VWR, peqSTAR 96X Universal Gradient, Cat. no. 732-2887). Thermal cycling was performed as described in 2.1.9.2 for bulk RNA samples. After reverse transcription, 96-well plates were spun down at 2000 g at 4 °C and adhesive aluminum foils were removed. For testing 8 genes 35 µl nuclease-free water (Ambion, Cat. no. AM9937) was added into wells to dilute samples (total volume of 41 µl). Plate was sealed with adhesive sealing foil (Bio-Rad, Cat. no. RSN100033), spun at 2000 g at 4 °C and

put on ice. Foil was removed subsequently and samples were aliquoted into two 384-well plates (Fisher Scientific GmbH, Cat. no. PCR-384-LC480-W) using an automated 96-channel liquid handling robot (BiomekNX$_P$) using sterile P20 filter tips (AP96, Beckman Coulter, Cat. no. 71256). Aspiration volume was 20 µl and dispension volume was 5 µl. Finally, 384-well plates were sealed with sealing foil, spun at 3000 g at 4 °C and put on ice.

2.1.10.3 Single-cell quantitative real-time PCR

For each plate, master mix was prepared with gene specific forward and reverse primers (100 µM) and PerfeCTa SYBR Green SuperMix, and stored at 4 °C in the dark. Five µl master mix with primers were pipetted into appropriate cDNA containing wells and into water control containing wells of 384-well plate using multipette Xstream. Following primers were used:

Gene name	Ensemble gene ID	Forward primer	Reverse primer
CCL20	ENSG00000115009	CTGGCTGCTTTGATGTCAGTG	AGTCAAAGTTGCTTGCTGCTTC
GAPDH	ENSG00000111640	CTCCTCCTGTTCGACAGTCA	CGACCAAATCCGTTGACTCC
HIF1A	ENSG00000100644	GGACAGCCTCACCAAACAGA	TCAGGAACTGTAGTTCTTTGACTC
IL1B	ENSG00000125538	GGACAGGATATGGAGCAACAAG	AACACGCAGGACAGGTACAG
IL8	ENSG00000169429	CTGATTTCTGCAGCTCTGTG	GGGTGGAAAGGTTTGGAGTATG
IRAK3	ENSG00000090376	AGAGCTCTGCGCTGTTCTG	ACTCAACACTGCTCCCAGG
JAK2	ENSG00000096968	GGGGTTTTCTGGTGCCTTTG	CACTCCCAAAATTACCCTTGCC
NR3C1	ENSG00000113580	CCGGGCCCAAATTGATATTCAC	ACATCTCCCCTCTCCTGAGC
TNF	ENSG00000232810	CTCAGCTTGAGGGTTTGCTAC	GGACAGGATATGGAGCAACAAG

Four genes per 384-well plate were tested on 88 single-cell samples. Additionally, 5 µl PerfeCTa SYBR Green SuperMix were added into IPC containing wells. Finally, plates were sealed with adhesive aluminum foils, spun down at 3000 g and stored at −80 °C. Before samples were analyzed, 96-well plates were defrosted on ice and spun down at 2000 g. Then, adhesive aluminum foil was removed and plate was sealed with LightCycler480 sealing foil and spun down at 3000 g. Using LightCycler 480 II system cooled plates were analyzed using the cycler protocol below:

Step	Time	Temperature
Pre-incubation	180 s	95 °C
Denaturation	10 s	95 °C
Annealing, Extension	45 s	60 °C
Melting curves analysis	180 s	65 - 95 °C
Cooling	hold	40 °C

2.1.10.4 Absolute quantification

To estimate absolute mRNA transcript number, commercially available Inter-plate Calibrator (IPC) standard (c = 10^6 copies/ul, TATAA Biocenter, Cat. no. IPC250S) was diluted with yeast-tRNA (Ambion, Cat. no. AM7119). Dilution series (undiluted, 1:1, 1:10, 1:100, 1:1.000, 1;10.000, 1:100.000 and 1:1.000.000) were prepared in triplicates in PCR strips (Biozym, Cat. no. 710990). A master mix with IPC primer solution (2 µM) and PerfeCTa SYBR Green SuperMix was prepared. Three µl IPC dilution series was pipetted into a 384-well plate (Fisher Scientific GmbH, Cat. no. PCR-384-LC480-W) using a 12.5 µl Matrix pipette (Thermo Scientific, Cat. no. 2009). Afterwards, 5.4 µl master mix with IPC primer was pipetted into 384-well plate using a 125 µl Matrix pipette (Thermo Scientific, Cat. no. 2011). Plate was sealed with LightCycler480 sealing foil and spun down at 3000 g. Finally, cooled plates were analyzed using LightCycler 480 II system. Absolute quantification relative to the IPC standard curve (see below) was done according to Bustin 2000.

2.1.10.5 High-throughput qPCR analysis for primary macrophages

To generate pre-amplified cDNA from human PBMC-derived primary macrophages for subsequent Biomark HT-qPCR procedures were followed as described for Fluidigm C1 single-cell sequencing. C1 Single-Cell Auto Prep Array for PreAmp (17-25um, Cat. no. 100-5758) were used with C1 Single-Cell Auto Prep Reagent Kit (Cat. no. 100-5319) according to the protocol 'Using C1 to capture cells from cell culture and perform preamplification using delta gene assays' (PN 100-4904

K1 and PN 100-5875 C1, Fluidigm).

BioMark HT-qPCR was performed at TATAA Biocenter AB (Göteborg, Sweden). The pre-amplified samples were analyzed undiluted together with gDNA, IPC template and NTC controls with customer assays (Qiagen RT2 Profiler Array assays) together with ValidPrimeTM assay (TATAA Biocenter) to test if assays give heavy amplification of gDNA and Interplate calibrator assay (TATAA Biocenter) to compensate for variations between runs. The qPCR was performed using TATAA EvaGreen GrandMaster Mix Low ROXTM (Cat. no. TA06-250LR, TATAA Biocenter) and GE 96.96 Dynamic ArrayTM Sample & Assay Loading Reagent Kit (Cat. no. 85000802-R, Fluidigm), respectively. Sample Mix for BioMark (Fluidigm) for one sample was 5.5µl TATAA Probe GrandMaster® Mix LowROX, 0.55µl 20X Evagreen mix (Biotium), 0.5µl GE Sample Loading Reagent (Fluidigm), 0.12µl DNase/ RNase free water and 3.33µl undiluted pre-amplified sample. Assay Mix for BioMark (Fluidigm) for one sample was 4µl Assay and 4µl GE Assay Loading Reagent (Fluidigm). The qPCR was performed on BioMark (Fluidigm) using the 96.96 Dynamic ArrayTM IFC (Integrated Fluidic Circuit). The thermal protocol was a mixture of the recommended settings from the manufacturer for Qiagen RT2 Profiler Array assays. Settings are shown here:

Step	Temperature	Time	Cycles
Thermal Mix	50°C, 70°C, 25°C	120 s, 1800 s, 600 s	1
Pre-denaturation	95°C	1 min	1
Denaturation, Annealing/Elongation	95°C, 60°C	10 s, 35 s	40
Melting curve	60°C – 97°C	Continuous	1

Data were analyzed using the Fluidigm Real-Time PCR Analysis Software applying the linear derivative baseline correction. No amplification in the NTC was detected. Data indicated no detectable amplification of gDNA. Comparing amplification and melting curves of the gDNA control sample for ValidPrime and customer assays, a big difference was observed, indicating only true amplification for the ValidPrime assay. Some samples for few assays showed more than one

product or unspecific product in the melting curve analysis. Those assays were excluded from further analysis.

2.1.11 Protein expression analysis

Lysis buffer was prepared with 1 µM Trizma hydrochloride (pH 8.0) (Tris-HCL, Sigma, Cat. no. T2788-1L), 10 mM ethylenediaminetetraacetic acid (EDTA, Roth, Cat. no. 80402), 1 % sodium dodecyl sulphate (SDS, Sigma, Cat. no. 71736-100ML) and freshly prepared 1×PIC and 1×PS. Lysis buffer was added and cells were sonicated for two times 5 cycles using a Biorupter sonification instrument (Diagenode). Subsequently, samples were centrifuged for 5 minutes at 14 000 g and 4 °C. Finally, supernatant was transferred into new 1.5 ml tube and stored at −80 °C.

Protein contents from cell lysate were determined with Pierce 660 nm Protein Assay (Thermo Scientific, Cat. no. 22660) in combination with the accessory Ionic Detergent Compatibility Reagent (IDCR, Thermo scientific, Cat. no. 22663). The bovine serum albumin (BSA, Sigma, Cat. no. A3912-100G) standard curve was used to determine the protein concentrations. Following BSA standards were used in technical replicates: 1.53, 0.76, 0.38, 0.19, 0.05, 0 mg/ml. Ten µl of each BSA standard and sample lysates were transferred into a 96-well plate (TPP, Cat. no. 92096). Samples lysate were analyzed in biological and technical replicates. Pierce mix was prepared with Pierce 660 nm Protein assay solution and 50 mg/ml IDCR. Then, 150 µl Pierce mix was pipetted into the appropriate sample, and BSA standard, containing wells of a 96-well plate. Plates were shaken for 1 minute at 600 g at room temperature. Five minutes after adding IDCR solution, absorbance was measured at 660 nm using POLARstar Omega (BMG LABTECH). Raw data was generated using POLARstar Omega analysis software.

NuPAGE LDS sample Buffer (1×) (Life technologies, Cat. no. NP0007), 1 M Dithiothreitol (DTT, Life Technologies, Cat. no. D-1532) and nuclease-free water were added to sample lysates. Samples were denatured for 10 minutes at 70 °C. Using LDS-PAGE, proteins were separated according to their molecular weight in a polyacrylamide gel. 10 µl of each prepared sample (20 µg protein) was loaded onto NuPage 15-well Novex 4 - 12 % Bis-Tris gel (1 mm, Invitrogen,

Cat. no. NP0329BOX). Additionally, 5 µl of a 1:1 marker, consisting of Precision Plus Protein Dual Color Standard (Bio Rad, Cat. no. 161-0374) and western MagicMark XP Western Protein Standard (Invitrogen, Cat. no. LC5602) was added. Using XCell SureLock™ Mini-Cell Electrophoresis System (Invitrogen) gel run was performed at 80 V for about 10 minutes and subsequently at 150 V for 2.5 hours. As running buffer, NuPAGE MOPS SDS Running Buffer (Invitrogen, Cat. no. NP001) was used.

Separated proteins from SDS-PAGE were plotted on nitrocellulose membrane (Hybond ECL Nitrocellulose Blotting Membrane 0.45 µM, GE Healthcare/Amersham, Cat. no. RPN78D) at 400 mA for 2 hours at 4 °C. Blotting was done in an EasyPhor PAGE WetBlotter Mini System (Biozym).

After blotting, membrane was briefly washed in distilled water and stained with Ponceau S solution (Applichem, Cat. no. A2935.0100) to confirm protein transfer. Subsequently, membrane was destained in distilled water. Finally, membrane was cut to allow detection of different target proteins simultaneously.

Membranes were blocked with blocking solutions for each antibody for 1 hour at room temperature on a shaker. Afterwards, membranes were incubated with appropriate primary antibody at 4 °C over night. To remove unbound antibody, membranes were washed three times with washing solution (1×TBS + 0.1 % Tween20 (Sigma, Cat. no. P1379-500ML)) for 10 minutes at room temperature. Then, membranes were incubated with a corresponding second antibody conjugated with horseradish peroxidase (HRP) for 1 hour at room temperature on a shaker. After three washing steps, luminescence was detected using chemiluminescence-reagent (ECL, Perkin Elmer, Cat. no. 104001EA) and visualized using FUSION-SL Advance 4.2 MP gel documentation system (Peqlab).

2.1.12 Immunofluorescence staining

THP-1 cells or primary monocytes were seeded on poly-L-lysin (Sigma-Aldrich) coated glass slides in 24-well cell culturing plates (Corning). After differentiation and treatment, cells were fixed and permeabilized using Transcription Factor Buffer Set (BD Pharmingen), and immunofluorescent double labelling for different antibodies pairs was prepared as follows: Cells were washed twice with ice cold PBS.

100µl of Fix/Perm buffer was added into each well and plates were incubated on 4°C for 45 minutes. After incubation cells were washed twice with Perm/Wash buffer. Two-hundred µl of primary antibodies mix was added into each well and plates were incubated at 4°C overnight. Primary antibodies used were GR (H-300, sc-8992, dilution 1:200, rabbit polyclonal), IL1B (sc-52012, 1:100, mouse monoclonal), IL-8 (H-60, sc-7922, 1:200, rabbit polyclonal) FKBP51 (D-4, sc-271547, 1:200, mouse monoclonal) and IRAK-M (XX-6, sc-100389 1:100, mouse monoclonal). Primary antibodies mix was prepared by combining 200µl of Perm/Wash buffer and a pair of primary antibodies (mouse and rabbit) to obtain working concentration of 1.5µg/ml for each antibody. After incubation with primary antibodies, glass slides with attached cells were washed twice with 200µl of Perm/Wash buffer and 100µl of secondary antibodies mix was added to each well, followed by one hour incubation in the dark at 4°C. Secondary antibodies mix was prepared by combining 100µl of Perm/Wash buffer per well with a pair of goat anti-mouse and goat anti-rabbit fluorescently labelled secondary antibodies to obtain a concentration of 4mg/ml for each antibody. Secondary antibodies from Thermo Fisher Scientific used were Novex Goat anti-Mouse IgG (H+L, Alexa Fluor 594, A11032), Novex Goat anti-Rabbit IgG (H+L, Alexa Fluor 488, A11034), Novex Goat anti-Rabbit IgG (H+L, Alexa Fluor 594, A11012). Glass slides with cells were washed twice with 200µl ice cold Perm/Wash buffer and mounted on microscopic slides using ProLong Gold Antifade Reagent with DAPI (Thermo Fisher Scientific). Samples were dried at room temperature overnight and stored at 4°C in the dark over night until imaging was performed.

2.1.13 RNA fluorescence *in situ* hybridization

RNA fluorescence *in situ* hybridization (RNA FISH) was performed following the Stellaris RNA FISH protocol preparation, which is based on the methods of Raj et al. 2008. Therefor, 10^6 cells (microscopy: 3×10^2 cells on poly-L-lysin coated coverglass) after treatment were fixed with fixation buffer (3.7% formaldehyde (Sigma, Cat. no. F8772-25ML), 10×PBS (Sigma, Cat. no. P5493-1L), and nuclease-free water (Ambion, Cat. no. AM9937) for 10 minutes at room temperature. Fixed cells were washed and and permeabilized in 75% ethanol

at 4°C overnight. After washing (wash buffer: 20 x saline sodium citrate (SSC, Sigma, Cat. no. S6639-1L), 10% formamide (Sigma, Cat. no. F9037-100ML), and nuclease-free water) for 5 minutes at room temperature, cells were incubated (37°C, 4,5 hours) with 125nM of different RNA FISH fluorescent probes (order from Stellaris via Biosearch Technologies, design of probes was done using online probe design software from BT) in hybridization buffer (100 mg/ml dextran sulfate (Sigma, Cat. no. D8906-10G), 20 x SSC, 10% formamide, nuclease-free water). Afterwards, cells were resuspended in wash buffer for 30 minutes at room temperature. Finally, cells were resuspended in 1×PBS and analyzed with BD Biosciences FACSAria II flow cytometer. For microscopic analysis, cells were finally washed with 2×SSC buffer for 5 min at room temperature. Microscope slides were prepared with Prolog Gold anti-fade reagent with DAPI (ThermoFisher, Cat. no. P36931). Probes for NR3C1, KAK2, FKBP5, IRAK3, IL1B and IL8 were labeled with Quasar 670. Probes for IL1B were labeled with TAMRA. Probes for GAPDH (Biosearch Technologies, SMF-2026-1) and XIST (BioCat GmbH, SMF-2038-1-BS) were labeled with Quasar 570. Following custom probes probes were used:

NR3C1	JAK2	FKBP5	IRAK3	IL8	IL1B
cgcagccgagataaacaact	ttctgaaaccggctacacag	tagagaacctggaaggaggg	aggtcgaacagcagcgtgtg	actagagaacttatgcaccc	ttgtgcctcgaagaggtttg
ctttggagtccatcagtgaa	ccatttctgtcatcgtaagg	acaatctttaatactcccct	cagaacagcgcagagctctc	cggtggctttttatatcatc	gattggctgaagagaatccc
tcttctctaccaggagttaa	tttcttctgcaacatactcc	gcctttgccaagactaaaga	gaaggactcaacactgctcc	tctctgaaagtttgtgcctt	tgcttcagacacttgagcaa
ctcctcttagggttttatag	tacacaggtgtgataccaca	catatctctcctttcttcat	accttcctgataactcttct	ctagaagcttgtgtgctctg	atcatttcactggcgagctc
agggtgaagacgcagaaacc	gtagagtacattatgcctgg	catattctggtttgcacagt	attatccacggtgacattgg	gcttggaagtcatgtttaca	cctcattgccactgtaataa
ggagtctgattgagaagcga	cactgcaatacccaacgagga	gaattttagggagactgcca	ccttttttcattatgttcagg	ctgcagaaatcaggaaggct	gccatcagcttcaaagaaca
caaccaaaagtcttcgctgc	gagatattccatgccgatag	gtttggttctccggataatg	gctgatggaagatttaagca	gcaaaactgcaccttcacac	aggagcacttcatctgttta
attgcttactgagccttttg	attcttcctgtgtttcatga	ctccttcgtttggatttgaa	tttctagttccttctatgat	tctaagttctttagcactcc	cggagattcgtagctggatg
tatacagtcccattgagagt	tttgatcgttttcttttggct	attggaatgtcgtggttcttc	tccactctgtatacctcaaa	ctctcaatcactctcagttc	tggccacaacaactgacgcg
tttgcaatgctttcttccaa	ttctctgtgtagaaggcaga	aaccatatcttggtccaaga	gacagcatatgttaggtttt	ataatttctgtgttggcgca	aaggtctgtgggcagggaac
gaacactggtcgacctattg	gttgcaaaaatctcctcacc	ctcagcattaggttcaatgc	gtttgggtgatgaaacagta	tctcttccatcagaaagctt	gatgaagggaaagaaggtgc
cagtggatgctgaactcttg	gtaaatcctgttctgtcagt	attctttggccttttcgaag	aatatgcagccaactctagt	agcccttctcaaaaacttct	tcccatgtgtcgaagaagat
tttggaaactccttctctgt	ggatagttacaactcggctt	gctccaatttttcttttggta	gacagaacttctcagtctct	attcttggataccacagaga	catcgtgcacataagcctcg
ccttcaaatgttgctgttct	cttcccttaatgagctaagt	ttcccttctctttgacaatg	gtgttccatttctcatgtat	aagtttcactggcatcttca	cagttcagtgatcgtacagg
tacaatttcacattgccacc	tgtgcatctgcagttaatct	atcttcccatactgaatcac	ctacacactgcaatctgtca	agtgttgaagtagatttgct	caagctttttgctgtgagt
atgtcaaaggtgctttggtc	tcgaaattgggccatgacag	tattccatctctaaccagga	attcgaatgtgccaagggag	caacagacccacacaataca	ggtacagattcttttccttg
ggggacccagaagaaaactc	tgattacctgctttcttcag	cagaagctttcgattccttt	gaatggctttggatattcct	agttcggatattctcttggc	tgtagagtgggcttatcatc
gactctcattcgtctcttta	atgacattttctcgctcgac	ggtgtattctctaagcttca	catggttgaacgttgtgcag	cattctagcaaacccattca	ttttgggatctacactctcc
tggaggagagcttacatctg	ctgctgaagttcttctttgt	ttgtcacagcattcaacagc	atatactgccacagatgacc	ccatcatttttatgtgatgc	ggaactgggcagactcaaat
tgacatcctgaagcttcatc	acagtttccatctggtaaca	atacaagcctttctcattgg	tccaaaaggatgtttgcact	attcatcttctatttttcca	cttgagaggtgctgatgtac
ctttacagcttccacaagtt	tgggggacagcatttagtaa	ttggctgactcaaactcgtt	gttagtttgggttgaaactg	ctggcaatgacaagactggg	aggaagacgggcatgttttc
ttccactgctcttttgaaga	caccattcgttctgaagact	ttttctggcacatggagatc	ggaagtgtgccatggcaaaa	tcaacacagcactaccaaca	gaagtcagttatatcctggc
tccagcacataggtaattgt	ctctgtaatgttggtgaggt	gaacatgttggcgtatatcc	aactctgatgttctaggtgg	gttctaactcattattccgt	gctctctttaggaagacaca
gggcagtttttttcttcgaat	tgccaactgtttagcaactt	ttccttttttcattagtgacc	gcatgtaccacagatgttta	attgactgtggagttttggc	ctagggattgagtccacatt
acattttcgatagcggcatg	gcacatacattcccatgaat	catttgcttccagaatcaca	taatggaaagtttcccctgt	acaagtttcaaccagcaaga	caaaaacctttctgttccct
ttaccaggatttttcagaggt	tgccaggatcactaagtttg	ttgttaggatgatctccagg	ccaaagctgtagacatctgt		acaggaaagtccaggctata
ggtgagttgtggtaacgttg	tcctgaagaatgtcctttgg	taagtcagcaagcaagtggc	cactactctacatcctgtta		atggacaggagatcctctta
ttcaggttcaatatacctcca	tttcaatgcattcaggtggt	gaaagccactctccacaagga	gctggatatgttttggatca		cctgaaaggagagagctgac
agctatcatatcctgcatat	actgcagatttcccacaaag	tcattgctgaagggtgtttt	aattctctaaggagatcccg		ctggctcaacaaaagggctg
ctccaagttgagtctggaac	ctttgagaatccagagcact	atccagaaactctcatctgc	agagaaattccgagggcagg		tcaggcgggctttaagtgag
catgttgagcgtagtcatga	gctctgaaagaaggcctgaa	gcacaattctgattgctctt	ctgccaaacagaagagcttg		tgctcatcagaatgtgggag
catttcactgctgcaatcac	taggtgctcttcagtactat	ctgggaggaagtactgttgta	aagctggcttgagtactttc		ttgccccctttgaataaatt
aaacatccaggagtactgca	aatgttgtcatgctgtaggg	aaatagatccactccaggtc	ggacacctgaaggactttag		aggctcttttacagacactg
ttgtctatatgatctccacc	ccttgcatatctgagatgtg	ccctagtgtagaagagcaac	cattctccaggaatagagga		attgaattgattccatagct
ggagcaaaacacagcaggtt	cctgtggatatacctttttg	cgagcaactgcgtgtcaaac	tcttccactggaatacttgg		taaagagagcacaccagtcc
cagcatgtgtttacattggt	ggagcataccagaatatggg	aagctgacagggcaggaaa	attgttattctggctttcat		
atacctgaagcctgtgtaac	tacagaaccactccaaagct	tttcacaactcacgccagaa	aggccttcatcagaaggtag		
tctaggccttcatatttcat	gtggacttttactcttctca	catgggaagctgtcttcaac	gttttctgagtcattctgtc		
atcttggtgtcacttactgt	cttgtttgtcattgccaatc	ctggagatttaggctactgg	tcagactggctgcattcaaa		
tcatatacctctctgtttct	cattattgttccagcattct	cacatttaagacttgcccta	ctttttgtccaagctcagaa		
tcttatcaacagagatcccct	gagctagatccctaaaggag	gtttacccgtaaggactgaa	gtcctgggatggaactatat		
aagcacaccttttctaggat	ttatccctttatttgatccac	catgagtgtttcttaggctg	atatttaccttatagggcct		
atgctatgttaaccaatccc	atcacacaagatgccaaggt	tcagcttttgctcttcatat	ctggagcttctgaagaagga		
aatctctgacaatccagctc	gacaatattcctggcattct	tcccaacagtttagcaagta	ttcatattcatcccaggaaa		
tgcaacatccatagcttaca	aatgttattggcagtcagca	gttatttgctcagaaccact	aaggtcatacctatgctcag		
agatgaatgtgcgctttgga	gttcatgagcataaatccca	cgtgaagtgtcttcttgagt	cttatggagccaatgtcttc		
atctttatcgggttctcttg	taacctgctgcacttcttaa	gtctgtggacttctacacaa	attgatcattctcttggcat		
aagtgtaccgctacaggtaa	ggtgtctaaagtggagtagc	tccatatgcagcctaaaagg	ttatctgcatcacccaaact	GAPDH as provided (SMF-2026-1)	

2.1.14 Microscopy

Images were taken with a Zeiss Z1 Observer wide-field fluorescence microscope with a 60x oil immersion objective or a Plan-Apochromat 40x/1.4 Oil DIC (UV) VIS-IR M27 objective using Zen Software (Version 2.31). Five Z spacings with 0.3µm were done. For each sample, 8x8 or 10x10 tiles were recorded. Binning was set to 3x3. Scaling per pixel was 0.330µm x 0.330µm. Bit depth was 14 bit. Channel settings were as follows:

	Channel 1	Channel 2	Channel 3
Reflector	50 Cy 5	38 HE Green Fluorescent Protein	49 DAPI
Beam Splitter	660	495	395
Filter Ex. Wavelength	625-655	450-490	335-383
Filter Em. Wavelength	665-715	500-550	420-470
Contrast Method	Fluorescence	Fluorescence	Fluorescence
Light Source	HXP120 V	HXP120 V	HXP120 V
Channel Name	Alexa Fluor 594	Alexa Fluor 488	DAPI
Excitation Wavelength	280	493	353
Emission Wavelength	618	517	465
Imaging Device	Axiocam 506	Axiocam 506	Axiocam 506

For background subtraction and normalization of tiles Gaussian processing with high kernel density settings (∼400) was performed to generate a background model for shading correction. Tiles and Z-stacks were aligned. Maximum intensity projection of deconvoluted images was used for fluorescence intensity quantification using EBimage (Pau et al. 2010). Briefly, for FISH analysis images from different channels were normalized by subtracting the channel mean intensity from every pixel of the image, nuclei were segmented and used for propagation to accomplish cell segmentation, as described by Pau et al. 2010. After cell intensity-based background subtraction, mean intensities per cell per channel were calculated and transformed $((SD_{cell}\text{-}SD_{ac})\times M_{cell})^2$, SD_{cell}: standard deviation of cell intensity,

SD_{ac}: mean standard deviation of all cells per acquired picture, M_{cell}: mean intensity per cell). Cell size and eccentricity were calculated as described (Pau et al. 2010).

2.1.15 Live-cell imaging analysis

Live-cell imaging was done on a heated stage using Zeiss AxioObserver Z1 wide-field fluorescence microscope with a 10x objective at 37°C in a 5 % CO2 atmosphere. Cells were seeded in standard 6-well plates as described for cell culture cells.

2.2 Analysis of sequencing data

Most analyses were carried out using R-project statistical environment (http://www.r-project.org) and Bioconductor (http://www.bioconductor.org) or using Python. Primary data analysis was done within Unix shell environment.

2.2.1 Primary analysis of population RNA sequencing data

BCL Illumina files were demultiplexed and converted to FASTQ file format using bcl2fastq Conversion Software v1.8.4 (Illumina). Quality of raw reads was assessed with FASTQC (Andrews 2010) and RseQC (Wang et al. 2012a). Reads were mapped to the human reference genome (GRCh37/hg19) using STAR aligner version 2.4.0d (Dobin et al. 2013). Adapter trimming was omitted because STAR aligner removes adapter sequences at the end of reads (soft clipping, Wilson and Stein 2015). Gene expression estimation was determined using htseq-count (from HTSeq version 0.6.1, Anders et al. 2015). Differential expression analysis of population RNA-seq data was done with DESeq2 (Love et al. 2014) with standard settings. Unless otherwise mentioned, p-value cut-off was < 0.001 and fold change ($\log_2$) was >2 or a percentile range as described in figure captions.

2.2.2 Primary analysis of single-cell RNA sequencing data

Initial steps of data analysis were as described for primary analysis of population RNA-seq (see above). Quality of libraries was comparable to published SMART-seq data. Data from selected libraries was excluded due to low quality (see Supplementary Table 2). Aggregated single-cell expression data was in agreement with the matching bulk controls (see Figure 6 E). Gene expression estimation was determined using htseq-count (from HTSeq version 0.6.1, Anders et al. 2015) for raw reads. Gencode annotation (release hg19/GRCh37.p13) was used as reference. Cells were filtered based on microscopic observations, mean expression and sequencing quality (see Supplementary Table 2 on page 114).

2.2.3 Assessment of technical noise

To determine a way to distinguish biological variation from technical variation, sequencing of mRNA from population samples near single-cell quantity together with RNA-spike assays (ERCC RNA Spike-In Mix, Cat. no. 4456740, Life Technologies) was applied using the Fluidigm C1 single-cell Auto Prep System. At mean expression levels of >20 counts per gene population RNA samples and spike RNA but not single-cell RNA showed normal distribution of gene expression values (Supplementary Figure 27). Analysis was done according to Piras and Selvarajoo 2015 using shapiro.test R function. To enrich for genes with high biological variability and low technical noise levels, genes were selected with mean count >20 (5367 ± 267 genes (average $\pm$ s.d.)).

2.2.4 Normalization of single-cell sequencing data

Expression values of single cell data vectors were $\log_{10}$-transformed, divided by the mean expression per cell and quantile normalized.

2.2.5 Dimension reduction and cell distance visualization

To separate cells based on their transcriptome-differences, dimension reduction using Kohonen's Self-Organizing Maps (SOM) following methods implemented

in oposSOM (Löffler-Wirth et al. 2015) were used. The grid size was 10×10 for analysis and 30×30 for transcriptome visualization. The dimension reduced matrices were used to build correlation matrices with rcorr (R, Hmisc package). Significant pairwise correlations were kept (p-value $< 1\times10^{-5}$) for hierarchical clustering analysis to determine basic cell states. For assessing the uncertainty in hierarchical clustering reproducibility was estimated with bootstrapping using pvclust (Suzuki and Shimodaira 2006).

SOM-reduced gene expression matrices were used for independent component analysis (ICA) using fastICA R package to visualize distances for cells. In ICA-space cells were annotated according to results from hierarchical clustering (Figure 9 B). For treatment-independent cell distance visualization cell-cell-correlation networks were computed using iGraph R package (Csardi and Nepusz 2006, Figure 9 A).

T-distributed stochastic neighbor embedding (t-SNE) analysis was done with Rtsne R package.

2.2.6 Exploratory single-cell analysis

To identify genes specific for cell-states, differential gene expression analysis was performed including computation of fold-changes, weighted average difference (WAD) scores and shrinkage t-scores according to Wirth et al. 2012. State-specific genes were then used for gene set analysis (over-representation analysis) to characterize cell states (see 2.2.7, Kamburov et al. 2013). Next, we moved from cell-specific markers to marker genes expressed in sub-clusters of cells. Using treatment-specific average SOM-portraits we identified ∼10 correlation clusters (CCs) for each treatment (Figure 17 A). Some CCs showed strong restriction of CC-specific gene expression (high t-scores and beta-score) and expression in a high percentage of cells. For each treatment-specific macrophage state the most representative CC was identified by gene-overlap analysis. Thus, strong mean gene expression of genes from these CCs in the respective macrophage states in ICA space was observed. Additionally, similarity of CCs for each treatment was determined to align similar CC for further analysis (see Supplementary Figure 32 and 33).

To identify state-specific major regulatory hubs, CC-specific genes were used as input for FANTOM4 EdgeExpressDB analysis (Severin et al. 2009). GeneOverlap R package (v. 1.10.0) was used for gene overlap analysis. Overlap was tested by hypergeometric test.

2.2.7 Functional annotation of gene lists

Molecular concept-based analysis of gene lists (pathway analysis) was carried out using ConsensusPathDB (http://consensuspathdb.org/, Herwig et al. 2016, Kamburov et al. 2013) Over-representation analysis and Wilcoxon enrichment analysis was done to define pathway-based sets. Minimum number of measured genes per term was 4 and p-value cutoff was 0.01. However, for small gene lists p-value cutoff was set to 1 to aid annotation of genes.

2.2.8 Responsiveness analysis

Characterization of single-cell responsiveness upon external stimuli was achieved by projection of bulk RNA-seq differential expression analysis to cell-specific genes. Cell-specific genes were determined with sample-specific SOM portrait analysis by selecting SOM components that were over-expressed (over-expression spots) for a given cell as described (Wirth et al. 2012). Differential expression of bulk data was done with Deseq2 (Love et al. 2014). Upper-quartiles (80th percentile for up-regulated and down regulated) of differential expressed genes (p-value$<$0.001) were joined to cell-specific genes. Mean expression for all cell-specific genes was calculated per cell.

2.2.9 Stability analysis and intra-cluster correlation

Stability scores were calculated using silhouette function from the R package 'cluster'. Intra-cluster correlations as shown were derived from pair-wise Pearson correlation coefficients of cell correlation matrices for each cell cluster.

2.2.10 Entropy analysis

Entropy analysis was done according to Teschendorff et al. 2014 and Teschendorff 2016. Log-transformed data from genes with mean expression of >75 counts were quantile normalized and joined with (PPI) network from the Human Protein Reference Database (HPRD, v13Jun12) for high-confidence (small size) network construction. For entropy analysis of low-confidence (maximum size) PPI networks all genes were selected showing counts in at least one cell. The average of the normalized local entropies for each gene in the network was calculated to maintain cell/sample entropy rates for further analysis of variance (ANOVA, non-parametric, Kurskal-Wallis test, Dunns post test with $\alpha = 0.05$ (95% confidence interval)).

Chapter 3

Results

3.1 Model system and mRNA population measurements in activated macrophages

Stimulation with LPS is widely considered to produce M1-like macrophage phenotypes (Martinez and Gordon 2014, Wang et al. 2014). M1-like macrophages express for example IL1B, IL8 and other genes associated with the primary innate immune response triggered by TLR-4 signaling. THP-1 cells have become one of most widely used cell lines to investigate the function and regulation of monocytes and macrophages (Auwerx 1991). To analyze to which extent archetypical innate immune response markers (i.e. IL1B, IL8 and HIF1A) are expressed among individual macrophages the following model was used: THP-1 monocytes were first differentiated for three days in the presence of 10 nM PMA. PMA-induced differentiation of monocytes (suspension cells) to a macrophages-like status (adherent cells) was accompanied by morphological changes (Figure 2A). Flow cytometry analysis of DNA content showed that ∼97% of cells were in G0 phase (cell cycle arrested) after three days of differentiation (Figure 2B). For primary macrophages isolated from human blood, CD14 positive PBMCs were cultured in human serum for 7 days to accompany differentiation. Primary macrophages showed similar morphological properties compared to THP-1 macrophages (Figure 2C).

To assess innate immune response differentiated macrophages were either

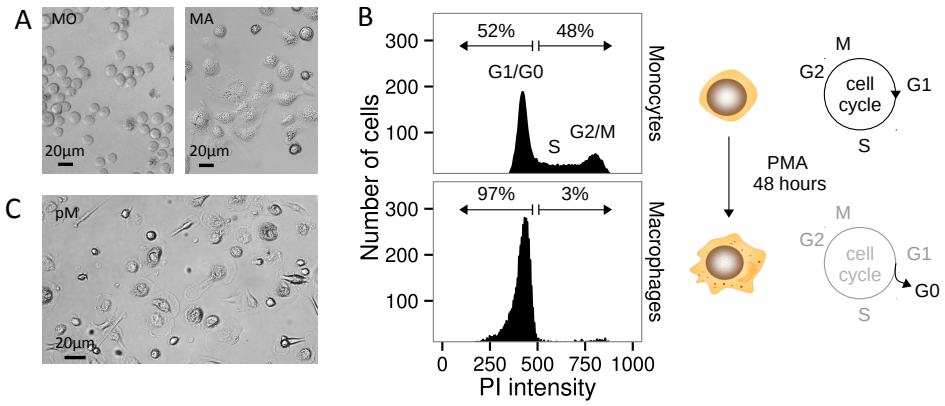

Figure 2: Microscopic observations of THP-1 and primary macrophages and cell cycle analysis. **A**: Microscopic observation of THP-1 monocytes (MO) and THP-1 macrophage cells differentiated with 10nM PMA for 72 hours (MA). **B**: Flow cytometric analysis of cell cycle with propidium iodide in non-differentiated THP-1 monocytic cells and differentiated THP-1 macrophage cells. This experiment was repeated three times, and similar results were obtained. The representative flow cytometry pattern is shown. The cycle of G0 (resting phase) / G1 (gap 1 phase), S (DNA synthesis phase), G2 (gap 2 phase), M (mitosis) and G1 is shown schematically. **C**: Microscopic observation of human primary macrophages differentiated with human serum for seven days from healthy human donor blood-derived monocytes.

left unstimulated (resting macrophages, untreated, UN) or were stimulated with 100ng/ml LPS (activated macrophages, LPS-treated, LPS) for two hours (Figure 3A). Stimulation with high, near-saturation levels of LPS for two hours renders an early inflammatory response. The selection of this early time-point was done to detect primary response transcriptional networks rather than secondary response effects (Parnas et al. 2015, Ramirez-Carrozzi et al. 2009).

At the population level RT-qPCR results from LPS-treated THP-1 macrophages showed strong up-regulation of immune-response markers including IL1B, IL8, NFKB and TNF and down-regulation of RUNX2, which is inhibited by TNF and IL1B (Ding et al. 2009, Figure 3B). Strongest expression was observed after 2 hours of LPS stimulation for selected marker genes IL1B, IL8 and RUNX2 (Figure 3C). Also transcriptome-wide population RNA-seq data showed strong macrophage response towards LPS: 775 ($\log_2$ fold-change > 2) to 4061 ($\log_2$ fold-change > 0) genes were up-regulated and 3228 ($\log_2$ fold-change < 0) to 295 ($\log_2$ fold-change < -2) genes were down-regulated (q-value <0.001, Figure 3D), including many known inflammatory marker genes. Top pathways for up-regulated genes (292 pathways) and down-regulated genes (16 pathways) were general pathway terms associated to signal transduction and immune response. More specific pathways were found including TNF signaling, MYD88/TLR4 signaling and nuclear receptor meta-pathway for up-regulated genes and G protein–coupled receptor (GPCR) signaling for down-regulated genes (Figure 3E, Supplementary Table 3 for pathways including up-regulated genes and Supplementary Table 4 for pathways including down-regulated genes).

3.2 Single-cell response of selected markers

To tackle the question to what extent theses global results (based on population measurements) reflect the expression landscape in individual cells different single-cell expression analyzes were carried out. Results from single-cell RT-qPCR (sc-qPCR), fluorescence *in situ* hybridization (FISH) coupled to microscopic screening and FISH coupled to flow cytometry analysis (FISH-flow) showed that IL1B, and other pro-inflammatory transcripts, although highly expressed on average, were

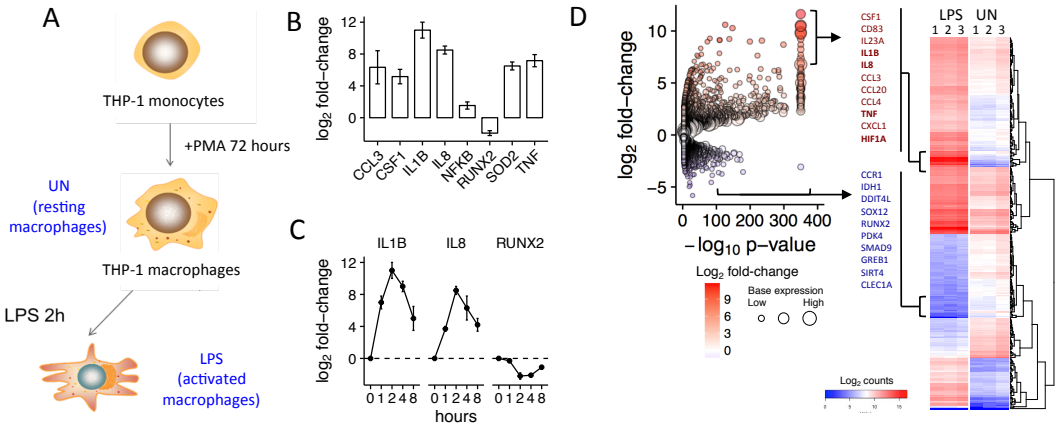

E

Pathways up-regulated

Nr. of genes	q-value	Pathway
122	6.1×10^{-19}	Signal Transduction
109	4.2×10^{-17}	Immune System
42	6×10^{-11}	Adaptive Immune System
62	7.3×10^{-10}	Innate Immune System
37	9.5×10^{-10}	Nuclear Receptors Meta-Pathway
35	2.5×10^{-9}	JAK STAT pathway and regulation
34	4.8×10^{-9}	TNF signaling pathway
24	1.7×10^{-6}	NF-kappa B signaling pathway
11	0.003	MyD88-independent TLR3/TLR4 cascade
9	0.010	MyD88 dependent cascade
9	0.010	HIF-1 signaling pathway

Pathways down-regulated

Nr. of genes	q-value	Pathway
31	6.8×10^{-8}	Signal Transduction
25	2.2×10^{-6}	Immune System
20	4.6×10^{-5}	Signaling by GPCR
18	0.0001	Innate Immune System
17	0.0002	Metabolism
15	0.0007	GPCR downstream signaling

Figure 3: Gene expression changes upon innate macrophages activation. A: Monocyte derived THP-1 macrophages left untreated (resting macrophages, UN) or treated with 100ng/ml LPS for 2 hours were used to investigate macrophage heterogeneity. **B**: RT-qPCR analysis of selected LPS-responsive genes. All fold changes were significant, p-value < 0.05. **C**: RT-qPCR analysis carried out with cells treated for 1, 2, 4 or 8 hours with LPS showed peak expression of two hours after LPS stimulation. **D**: Volcano plot representation (fold-change vs. p-value) and heatmap (top up- and down-regulated genes with biological replicates) of differentially expressed genes from population RNA-seq data determined from activated macrophages compared to resting macrophages (LPS vs. UN). Dot size is relative to to the abundance of a given transcript (base expression). **E**: Pathway enrichment analysis for up- and down-regulated genes (see 2.2.7).

heterogeneously expressed within individual cells.

Single-cell qPCR results showed expression of IL1B and IL8 in 20.5±4%(mean+s.e.m) and 25.4±1.3% of activated macrophages treated with LPS, respectively (Figure 4A). In resting macrophages expression of IL1B and IL8 was virtually absent. However, rare cells were observed by sc-qPCR analysis, which showed expression of IL1B or IL8 for resting macrophages (Supplementary Figure 29A). In comparison GAPDH was found expressed in 89±8% of macrophages (Figure 4A). FISH-flow analysis showed the presence of 46±8% IL1B positive cells and 92±5% GAPDH positive cells. To rule out that heterogeneity in the original THP-1 cell culture material had an impact on partial IL1B expression in activated macrophages, assays were repeated for clonal macrophages, derived from individually cultured and expanded single THP-1 cells, with highly similar outcomes (Supplementary Figure 29C). In agreement with sc-qPCR results and FISH-flow analysis FISH microscopy screenings also showed that IL1B and IL8 expression was restricted to a fraction of activated THP-1 macrophages (Figure 4C). Some cells clearly did not express any of the highly differentially inflammatory genes identified from population measurements of activated macrophage transcriptomes. As in sc-qPCR, rare IL1B positive cells were found in resting macrophages using FISH analysis (Supplementary Figure 29B).

Considering these findings, it remains uncertain if observations for IL1B/IL8 positive cells were only due to stochastic fluctuations of mRNA transcripts over time. To assess if inflammatory gene expression is likely to co-occur in some cells mRNA expressions of several genes was assayed in the same cells. Sc-qPCR data suggested that functional related genes (i.e. IL1B and IL8 and HIF1A, a LPS-inducible transcription factor) were expressed in a coordinated fashion. Gene pairs with functional relation showed high Pearson correlation values (IL1B vs. HIF1A r=0.82 and IL1B vs IL8 r=0.78) compared to genes with no direct biological association that showed low Pearson correlation coefficients (GAPDH vs IL1B r=-0.07, Figure 4D). Similarly, FISH microscopy analysis showed overlapping expression patterns of IL1B and IL8 (Figure 4E). This relation was quantified for ∼800 cells per gene pair by acquisition of multiple pictures and subsequent per-cell fluorescence quantification. High Pearson correlation values were determined for IL1B and

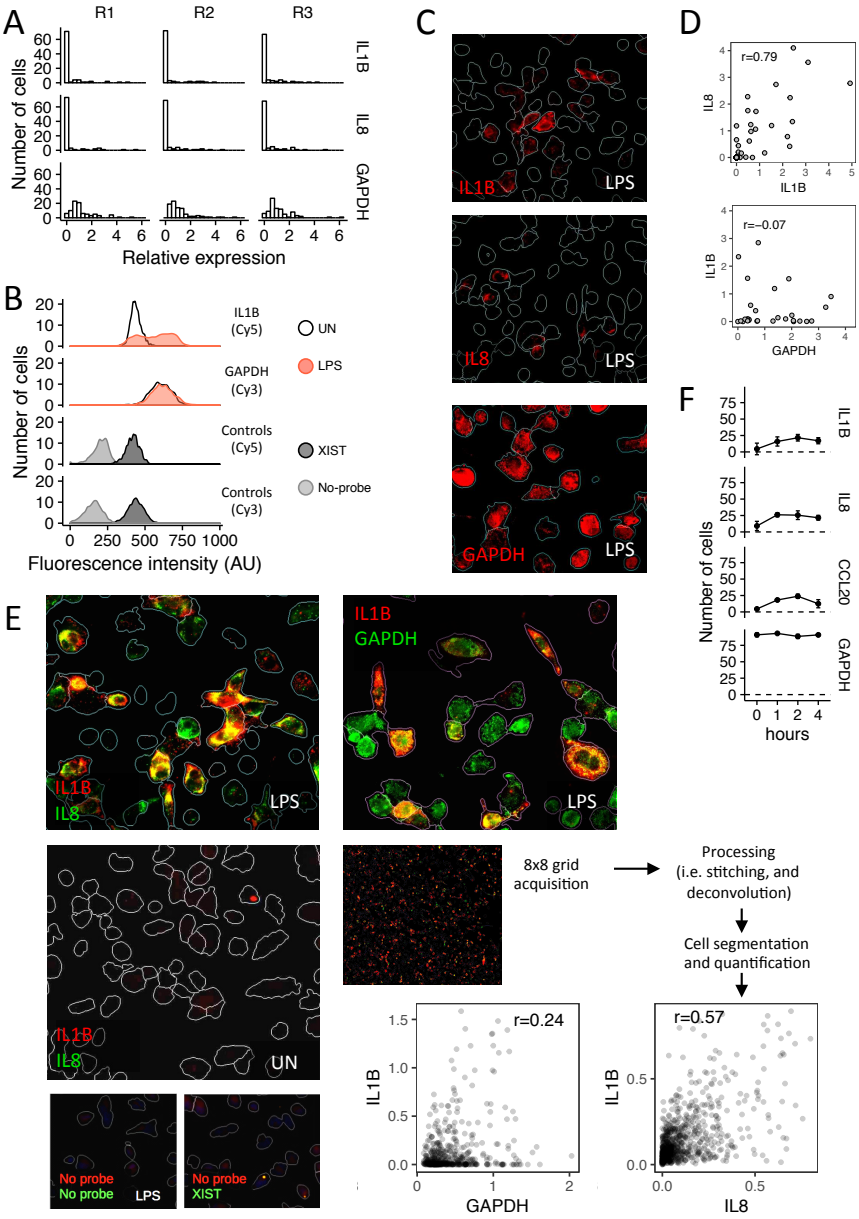

Figure 4: LPS-responsive genes show partial and coordinated gene expression. **A**: Distribution of gene expression in individual activated macrophages determined by sc-qPCR analysis. **B**: Distribution of IL1B and GAPDH expression from activated and resting macrophages analyzed by RNA fluorescence *in situ* hybridization coupled to flow cytometry analysis (FISH-flow). XIST is not expressed in THP-1 cells and acts, together with unstained cells (no-probe), as background subtraction control. **C**: RNA-FISH analysis of selected transcripts and schematic representation of the analysis workflow. **D**: Correlation analysis of sc-qPCR readouts for selected transcripts. **E:** RNA-FISH analysis and correlation analysis for selected gene pairs based on relative fluorescence quantification. **F**: sc-qPCR analysis for selected transcripts treated with LPS for 1, 2 or 4 hours or left untreated. Two times ∼88 cells per time point were analyzed. r indicates Pearson's correlation coefficient.

IL8 (r=0.57) and lower Pearson correlation values were determined for IL1B and GAPDH (r=0.24, Figure 4E). The effect of partial inflammatory gene expression was also found 4 hours after LPS stimulation (Figure 4F) The number of cells that were positive for selected inflammatory genes remained constant (IL8) or declined (IL1B) from 2 hours to 4 hours after LPS stimulation. However, approximately at most half of the cells did not express any of the classical inflammatory genes but expressed GAPDH homogeneously in almost all cells.

To conclude, in the case of IL1B and IL8 a specific function, the LPS-induced primary response, is restricted to a subpopulation of cells rather than affecting the whole macrophage population. Results corroborate a model including digital all-or-none gene expression. Similarly, this was observed for dendritic cells at single-cell resolution (Shalek et al. 2013, Shalek et al. 2014). For inflammatory marker genes transcriptional heterogeneity upon a specific stimulation appeared to be highly synchronized at the single-cell level. This suggests that high correlation of gene expression observed in single-cell gene expression measurement is a potential proxy to evaluate putative joined functions of gene groups by the guilty-by-association principle (Oliver 2000, Wolfe et al. 2005). Using whole transcriptome data this property may aid the definition of cellular states. Moreover, this approach would help characterize those cells that surprisingly showed absence of classical inflammatory expression signatures. In summary, these results suggest that gene expression response of macrophages towards LPS results in subpopulations or cellular states with distinct transcriptomes.

3.3 Transcriptome-wide assessment of macrophage heterogeneity

To examine cellular heterogeneity of individual THP-1 macrophages transcriptome-wide the Fluidigm C1 workflow was used to generate single-cell cDNA libraries for mRNA sequencing (Figure 5A). After FACS-based discrimination of cell debris, cell aggregates and dead cells (Figure 5B), 93 resting macrophages and 96 LPS-treated cells were captured in Fluidigm integrated fluidics circuits (IFCs) micro-chambers (examples see Figure 5C). Cells were screened in individual micro-chambers of IFCs.

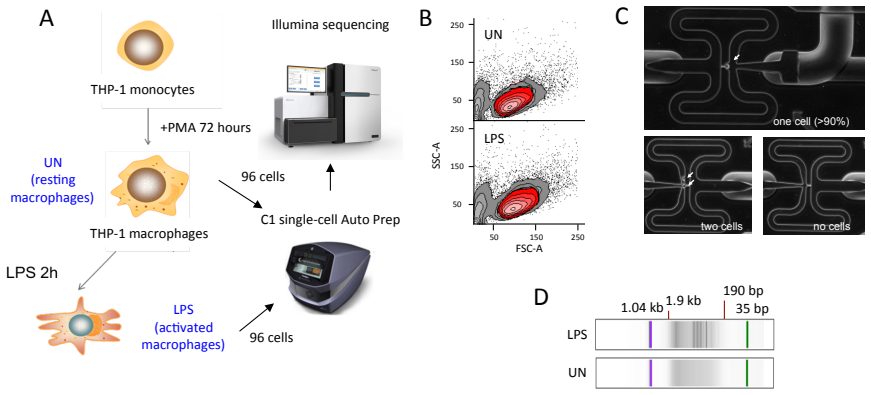

Figure 5: Single-cell sequencing workflow. **A**: Fluidigm C1 workflow to generate single-cell cDNA libraries for Illumina sequencing. **B**: FACS plots show final gating used to isolate viable single cells based on forward scatter (FSC) and side scatter (SSC). **C**: Selected images of microfluidic integrated fluidic circuit (IFC) micro-chambers (carrier wells) empty, loaded with one cell or loaded with two cells. See Supplementary Figure 28 for images of all micro-chambers. **D**: Representation of electrophoresis traces of multiplexed sequencing ready cDNA libraries.

Three micro-chambers were empty on the IFC used for resting macrophages and cell doublets or deformed cells were found in 8 and 7 micro chambers for resting and activated macrophages, respectively (Supplementary Figure 28). Individual single-cell cDNA libraries (not shown) and pooled and indexed libraries showed expected patterns in gel electrophoresis (Supplementary Figure 28D).

Paired-end low-coverage sequencing of pooled libraries showed high base call accuracy (Figure 6A). Mapped reads covered full length transcripts and reads showed only mild bias towards the 3'-end of gene bodies (Figure 6B). Gene-mappable sequencing reads per cell ranged from 1.564 (empty wells) to 15.534.370 (on average 4.093.295 reads/cell) reads for resting macrophages and from 13.248 to 1.715.592 (on average 588.692 reads/cell) for activated (LPS-treated) macrophages. Data of IFC micro-chambers with cell doublets, no cell or damaged/deformed cells or cells with low sequencing quality were excluded to generate a clean dataset from 73 and 83 intact single cells for untreated and LPS-treated macrophages, respectively (Supplementary Table 2). Complexity of single-cell transcriptomes is low compared to population RNA-seq derived transcriptomes. High sequencing depth is not required to capture single-cell library complexity (Pollen et al. 2014). Sequencing-depths of $\sim$ 0.5-3 million mappable reads per cell were sufficient, as

indicated by saturation curve analysis estimating the number of detected genes in subsampled sequencing data (Figure 6C).

The entire single-cell dataset datasets comprised 15.684 genes with a cut-off of one read. Individual cells showed on average 3047 genes expressed with more than 20 sequencing reads per gene and 6724 genes with more than one read count (Figure 6D). In total, for both resting and activated macrophages 5420 unique genes were detected with an average minimum gene expression cut-off of 20 reads per gene. At a mean expression level of 20 reads per gene, data derived from minute amounts of IFC-processed bulk RNA but not single-cell data showed normal (Gaussian) distribution. This suggests that genes with mean gene expression counts above 20 reads in single-cell data show transcriptional variability above technical noise levels (Piras and Selvarajoo 2015, see Materials and methods 2.2.3 and Supplementary Figure 27). Number of detected genes was comparable to other studies with similar setups (i.e. Björklund et al. 2016). Despite the higher sequencing coverage compared to activated macrophages, resting macrophages showed 1.25 times higher numbers of detected genes per cell under different cut-off settings (Figure 6D). Comparison of results from population RNA-seq data (from aliquots from the same cells subjected to IFCs) with mean expression from single-cell data, indicated coherent single-cell sequencing results (Figure 6E). Pearson correlation coefficients of 0.95 and 0.93 were determined for untreated and LPS-treated cells, respectively.

3.4 Macrophages are present in three transcriptional states

The generated single-cell dataset builds a complex and high-dimensional dataset manifested as a gene expression matrix with hundreds of experimental samples (cells) and thousands of genes. Thus, inferring cellular heterogeneity requires sophisticated data sorting, simplification and visualization strategies to exhibit gene modules and distances of single-cell transcriptomes. To gain an initial insight into the single-cell expression landscape, data from top expressed ∼2500 genes was clustered using hierarchical clustering. Heatmap representation of the data showed good separation between activated (LPS–treated) and resting macrophages but

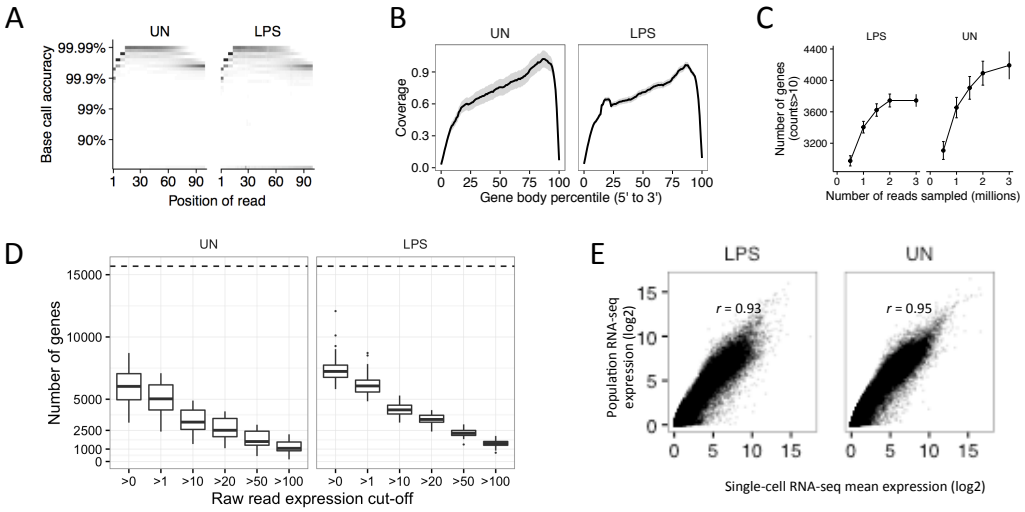

Figure 6: Quality evaluation for single-cell sequencing data. **A**: Per base phred quality scores indicated good sequencing accuracy for single-cell libraries generated from activated (LPS) and resting (UN) macrophages. **B**: Distribution of mapped sequencing fragments shown along gene bodies (gene body coverage). **C**: Sequencing depth saturation curve analysis. Each dot was generated by random downsampling of raw reads from each single-cell datafile, subsequent mapping, quantification and final counting of genes with mean expression of >10 counts. Error bars indicate standard error. **D**: Number of detected genes per expression bin. **E**: Correlation between average single-cell expression values and population RNA-seq gene expression measurements.

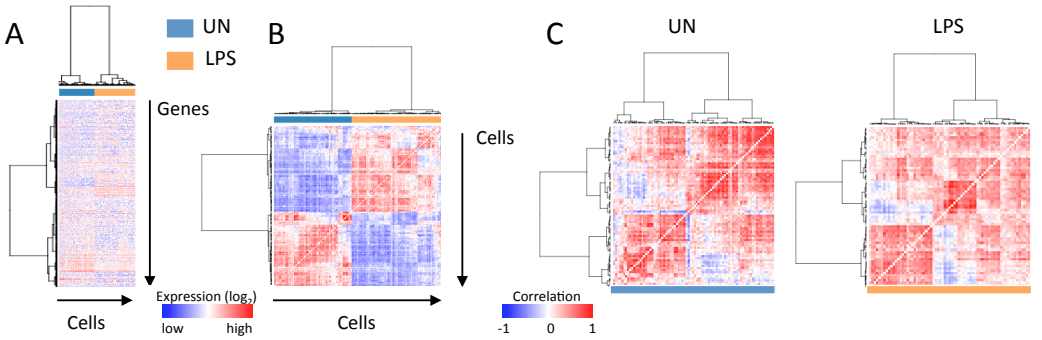

Figure 7: Cell distance estimation with non-dimension reduced single-cell data. A: Hierarchical clustering of ∼2500 top expressed genes. **B and C:** Hierarchical clustering of pair-wise Pearson correlation matrix of top highly expressed genes for cells from both treatments together (**B**, resting, UN and activated, LPS) and for the treatment models individually as indicated (**C**).

intra-treatment differences could not be easily observed (Figure 7A). Similarly, this was the case for cell-to-cell correlation matrix analysis performed on combined data for resting and activated macrophages (Figure 7B).

Cell-to-cell correlation analysis represents an obvious classification strategy for potentially detecting different cellular states. Once cell-to-cell correlation analysis was performed individually for both macrophage models, distinct clusters were observed indicating the presence of transcriptionally different macrophage states (Figure 7C). However, determined clusters were not reproducible as indicated by low bootstrap probability (BP) values (median BP=0.11 for resting macrophages and median BP=0.15 for LPS-treated macrophages, Figure 8D). A BP value of 1 would indicate that a dataset could be clustered with maximum reproducibility.

The observation of incomplete separation with low reproducibility is not surprising, because the power of many multivariate statistical methods (i.e. hierarchical clustering) is limited owing to the character of single-cell data. Single-cell data has a low signal-to-noise ratio, missing values and small sample size compared to a high number of genes. Thus, hierarchical clustering of normalized expression matrices gained an initial visualization of the data but remained impractical for further exploratory analysis and reproducible macrophage state definition.

Inspired by studies with similar challenges (high sample numbers with unknown relation) machine learning-based self-organizing maps analysis (SOM analysis,

Löffler-Wirth et al. 2015) was used to initially reduce the dimensions of the dataset from several thousand genes to 100 SOM components to facilitate further downstream analysis (Figure 8A). 5280 genes for untreated macrophages and 5115 genes for LPS-treated macrophages (mean gene expression > 20 counts) were mapped to 100 SOM components. Genes gathered in one SOM component exhibit coordinated, most similar and high level expression patterns. Thus, genes with high information content can be conveniently identified.

SOM analysis-derived, single-cell SOM portraits are simplified two dimensional visualizations of detectable single-cell transcriptomes (Figure 8B). SOM portraits visualize the similarity relationships of genes in which spatial proximity reflects expression pattern similarity. The locations of genes on the SOM portraits from different cells remain constant. SOM portraits intuitively revealed that only a fraction of expressed genes were coordinated and highly expressed in each individual cell. On average 130 genes for resting macrophages and 279 genes for activated macrophages showed high expression with high correlation within groups of cells in the dataset (Figure 8C). Compared to clusters gained with normalized raw counts (Figure 7) clusters were robust to bootstrapping and reproducible after SOM components were subjected to hierarchical clustering of cell correlation matrixes (median BP of 0.9 for untreated macrophages and 0.82 for LPS-treated macrophages, Figure 8D). Cell-to-cell correlation matrixes computed with SOM components showed clear separation of at least three sub-clusters for activated and resting macrophages. This suggests the presence of three distinct macrophage states (clusters I-III, Figure 8E and F).

To maintain a framework to further explore the molecular identities of individual single cells, different cell distance visualizations were performed. Cell-to-cell correlation network visualization was applied for activated and resting macrophages individually to intuitively arrange cells from the different clusters according to their whole-transcriptome correlation distance. Each cell was assigned a color according to its location in hierarchical clustering readouts (Figure 9A). While all three clusters from activated macrophages (LPS) were well separated from each other, cluster I and II from resting macrophages (UN) showed a less distinct pattern (Figure 9A). These results may indicate that many cells might have been in

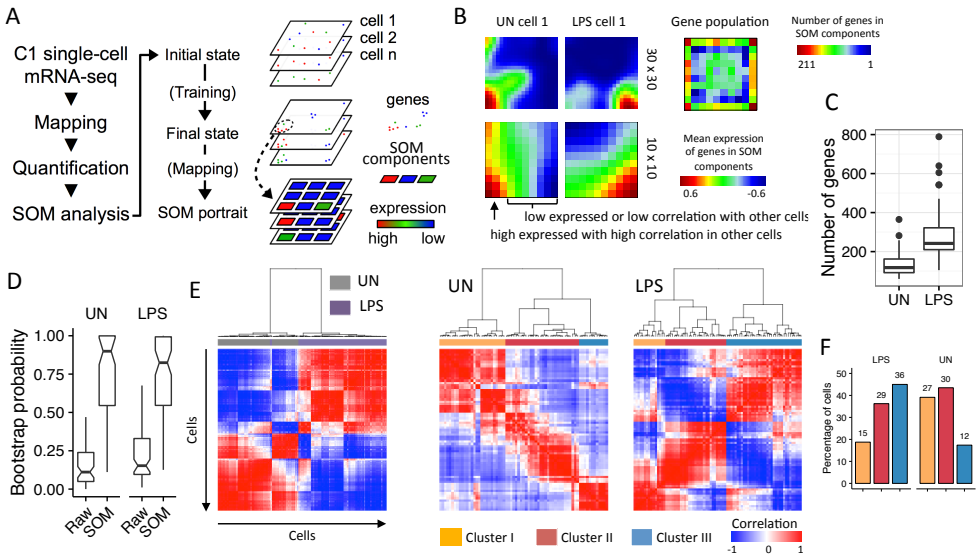

Figure 8: Macrophages segregate towards three transcriptional states. **A**: Schematic presentation of the data analysis workflow using SOM machine learning dimension reduction. **B**: SOM portraits ("expression landscapes") for selected cells with different grid sizes. Every dot represents a SOM component, representing a gene group of co-expressed genes and indicating the mean expression of genes within the component by gradient coloring (over-expression spots (red) and under-expression spots (blue)). Gene population maps indicate how many genes were associated to each component. **C**: Box plot showing the number co-expressed genes per cell (cell-specific genes). Genes were defined by selection of samples-specific over-expression spots from SOM portraits. **D**: Distribution of Bootstrap Probability (BP) values computed by normal bootstrap resampling, indicating how strong clusters (hierarchical clustering) are supported by the data (RAW: non-dimension-reduced single-cell data; SOM: dimension reduced data (SOM components). **E**: Hierarchical clustering of pair-wise Pearson correlation matrices of SOM components for cells for both treatments analyzed together (resting, UN and activated, LPS) and individually, as indicated. Main clusters were color assigned, based on similarity of clusters between both treatment models. **F**: Percentage of cells that were assigned to the classified clusters.

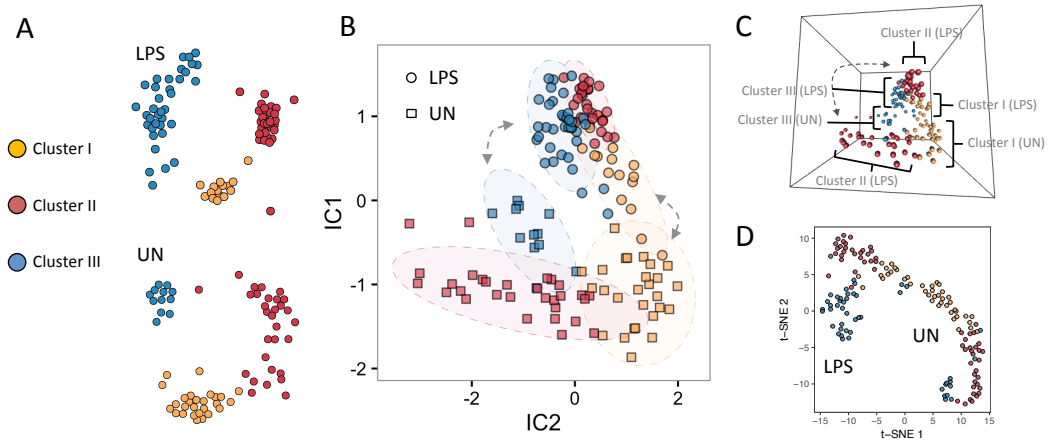

Figure 9: Cell-to-cell distance visualizations uncovers relations of defined macrophage states. **A**: Correlation networks for activated (LPS) and resting (UN) macrophages visualizing the distances between cells based on Pearson correlation. **B**: Two-dimensional independent component analysis (ICA) representation visualizing the distances between cells from both treatment model. Arrows highlight that states from both treatments are positioned in close proximity. **C**: Three-dimensional ICA representation indicates that clusters II from both treatment models are related (arrow). **D**: Representation of t-distributed stochastic neighbor embedding (t-SNE) analysis.

transition between two macrophage states and thus showed a mixed transcriptome profile.

In general, combined visualization of clusters from resting and activated macrophage models by means of correlation distance analysis is impractical due to the differences of transcriptomes from activated and resting macrophages (Figure 8E). Therefore, visualization of cell distances for both macrophage models was accomplished by independent component analysis (ICA) of SOM components computed with the combined dataset from activated and resting macrophages (Figure 9B). ICA representation showed that cells of different clusters separated partially on IC2 (I and II resting macrophages and II and III activated macrophages) and IC1 (resting I/II and III). Separation of resting and activated macrophages was observed along IC1. Although distantly separated in two-dimensional ICA space, three-dimensional ICA representation underlined the association of clusters II from resting and activated macrophages (Figure 9C). These cluster relations were also supported by t-SNE analysis of SOM components, in which cells from resting and activated macrophages states were mirrored along t-SNE axis 1 (Figure 9D).

3.5 Gene expression of macrophage states suggest different biological functions

After having defined groups of cells based on distinct correlation patterns using clustering and association of cells from different clusters in terms of transcriptome distances, integrative analysis was carried out to characterize molecular identities of macrophage states based on genes and pathways. SOM component visualization indicated strikingly differential gene expression patterns per gene cluster for both macrophage models (Figure 10A). Irrespective of intra-cluster heterogeneity a broad definition of cluster-specific genes was achieved based on SOM portrait analysis to select most representative cluster-specific genes for resting and activated macrophages (Figure 10B). Projection of mean expression of most significant cluster-specific genes (p-value < 0.01) underlined macrophage state-restricted expression in ICA space (Figure 10C). While cells of cluster I and III showed similar expression pattern for treatment-specific genes, cluster II showed more differential expression patterns between activated and resting macrophages. Inspection of derived gene lists revealed that archetypical pro-inflammatory marker genes (i.e. IL1B, IL8 and CCL3) with strong differential expression in population measurements (Figure 3D) showed high and coordinated expression in cluster II in activated macrophages (Figure 10D and Supplementary Table 5). In cluster II of resting macrophages pro-inflammatory marker gene expression was absent. Inspection of cluster-specific genes from the other clusters I and III did not intuitively indicate its associations to specific macrophage-related functions. However, the three clusters from both macrophage models showed also common gene expression signatures, as supported by overlap analysis (Figure 10E).

To gain a better picture on the putative function of found macrophage states, selected genes from different clusters were subjected to over-representation pathway analysis. 564 pathway terms were determined with >5 genes per pathway term and a pathway significance of q-value < 0.05. 328 pathway terms overlapped for any cluster of both macrophage models (Figure 11A). 219 pathways overlapped significantly for the associated clusters from both macrophage models. Determined pathways for cluster I showed highest significance estimates for pathway

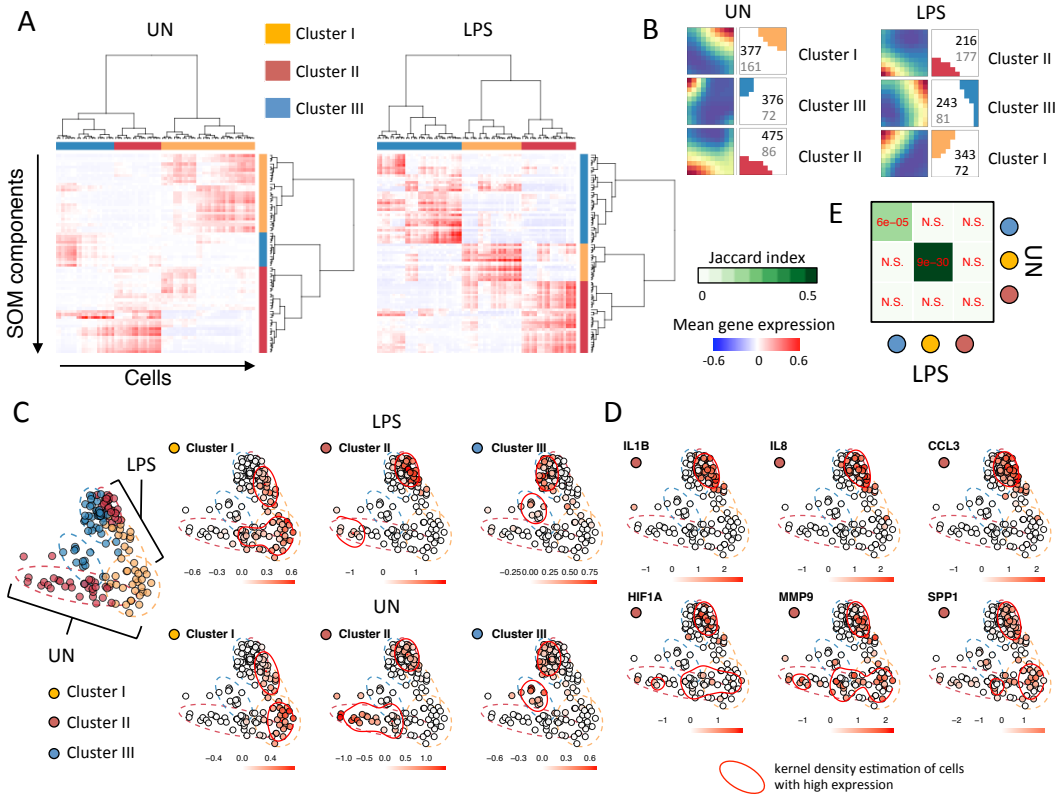

Figure 10: Cell states show distinct gene expression signatures. **A**: Heatmaps illustrating state-specific gene expression for resting (UN) and activated (LPS) macrophages (mean gene expression per SOM component). **B**: Strategy of state-specific gene selection and gene ranking guided by average state-specific SOM portraits for different clusters. Black numbers indicate the number of all state-specific genes derived from over-expression spots. Grey numbers indicate the number of most significant cluster-specific genes (p-value < 0.01). **C:** Schematic representation of cells in ICA space. Projection of mean gene expression (indicated by red gradient) of most significant cluster-specific genes onto ICA coordinates. Note, that expression values were scaled. Red circles mark calculated kernel density estimations that highlight cells with high expression values for a particular gene. **D**: Projection of normalized gene expression (not from SOM components) for selected state-specific genes onto ICA coordinates. **E**: Overlap analysis of state-specific genes indicates relation between states for resting and activated macrophages. Significant overlap was determined for clusters I and III but not for clusters II.

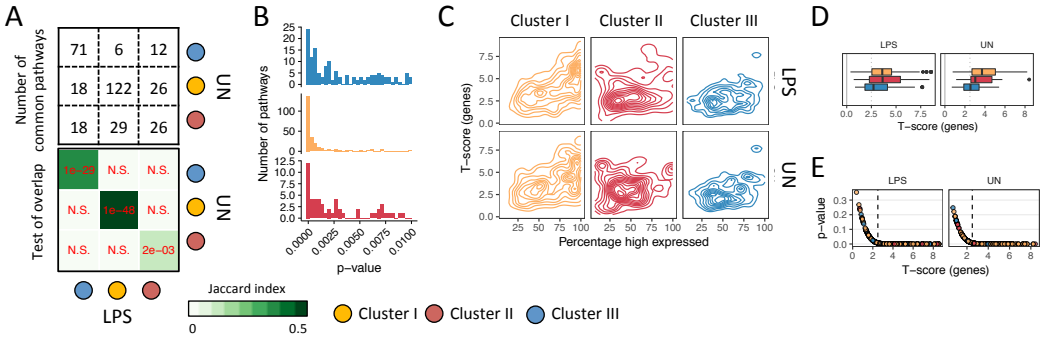

Figure 11: Characterization of state-specific pathway terms. **A**: Overlap analysis for determined pathway terms comparing pathway terms found for resting (UN) and activated (LPS) macrophage states/clusters. Top: Number of found pathways. Bottom: Representation of results from tests for significance of overlaps. Overlap analysis indicates relation between all states for resting and activated macrophages. **B**: Distribution of determined pathway significance estimations. **C**: Density plots showing the relation of t-score estimates per gene relative to the percentage of cells the gene is expressed in. Every data point underlying the density distribution represents a gene. Note that many genes for cluster I have high t-scores but show expression in a high percentage of cells. **D**: Distribution of t-scores of state-specific genes. **E**: Relation of p-value estimates and t-score estimates indicate that gene expression restriction towards a state is significant for t-scores $\sim$>2.5.

enrichments (Figure 11B).

Calculated gene-specific shrinkage t-scores linked differential gene expression (fold-change) between clusters with variance estimates. This facilitated robust gene ranking. Thus, t-scores were calculated for every gene to get a significance measure of how well a gene expression is restricted for its associated cluster. Generally, t-scores were higher for cluster I and cluster II compared to cluster III (Figure 11D). However, t-score estimates together with the percentage of cells showed that cluster II and III have a high degree of cluster-restricted gene expression compared to gene expression in cluster I (Figure 11C). This is because a gene may be expressed in almost every cell but its expression maximum lies within a specific cluster. At a t-score level of >2.5 the t-score estimate was evaluated significant ($p<0.05$, Figure 11E). Consequently, genes from cluster I have a lower restriction of gene expression compared to cluster II and III.

Twenty-nine pathways with the highest degree of overlap to major molecular pathways were selected (Herwig et al. 2016). The following classification was gained for the three main cell clusters in untreated and LPS-treated macrophages,

indicating functionally different states (Figure 12 and Supplementary Figure 30).

- *Homeostasis-preserving macrophages* (cluster I): Similarity associated clusters I for both macrophage models showed significant enrichment of pathway terms mostly unrelated to immune functions (Figure 12A). Pathway terms were associated to metabolic pathways including metabolism, glycolysis and gluconeogenesis and mitochondrial electron transport chain but to a low extent to immune-related processes (i.e. interferon-gamma signaling). For example, the expression of genes associated to metabolism-related pathways was similar and significantly restricted (average p-value<0.0013) in untreated (resting) and activated macrophages. However, metabolism associated genes were expressed above average in ∼78% cells in resting macrophages compared to ∼33% of cells in activated macrophages. Taken together, found pathways suggest that macrophage cells associated to cluster I exhibit low response upon LPS stimulation. In this work, these cells are termed "homeostasis-preserving macrophages" according to their putative function within the whole macrophage population. The presence of these cells may prevent excessive population transition in response to LPS stimulation and maintain homeostasis for the macrophage population.

- *Pro-inflammatory macrophages* (LPS, clusters II) *or macrophages with pro-inflammatory potential* (UN, cluster II): Cluster II for resting and activated macrophages showed over-represented pathways associated to classical inflammation (i.e. NF-κB, TNF- and TLR-signaling, average p-value<0.004, Figure 12B). Both cases showed restricted expression of genes from the canonical NF-κB pathway including TNFAIP3, IKBKB, NFKBIA, and ERC1. Those genes represent regulators of the NF-κB response rather than pro-inflammatory NF-κB response gene products. For example, TNFAIP3 is critical for limiting inflammation by terminating TNF-induced NF-κB responses (Zhou et al. 2016). Only in activated macrophages, additional NF-κB effector genes including IL1B and IL8 were expressed (Supplementary Table 6). Constitutively expressed genes of the NFKB machinery were expressed in fewer cells in resting compared to activated macrophages. Those cells did not show i.e.

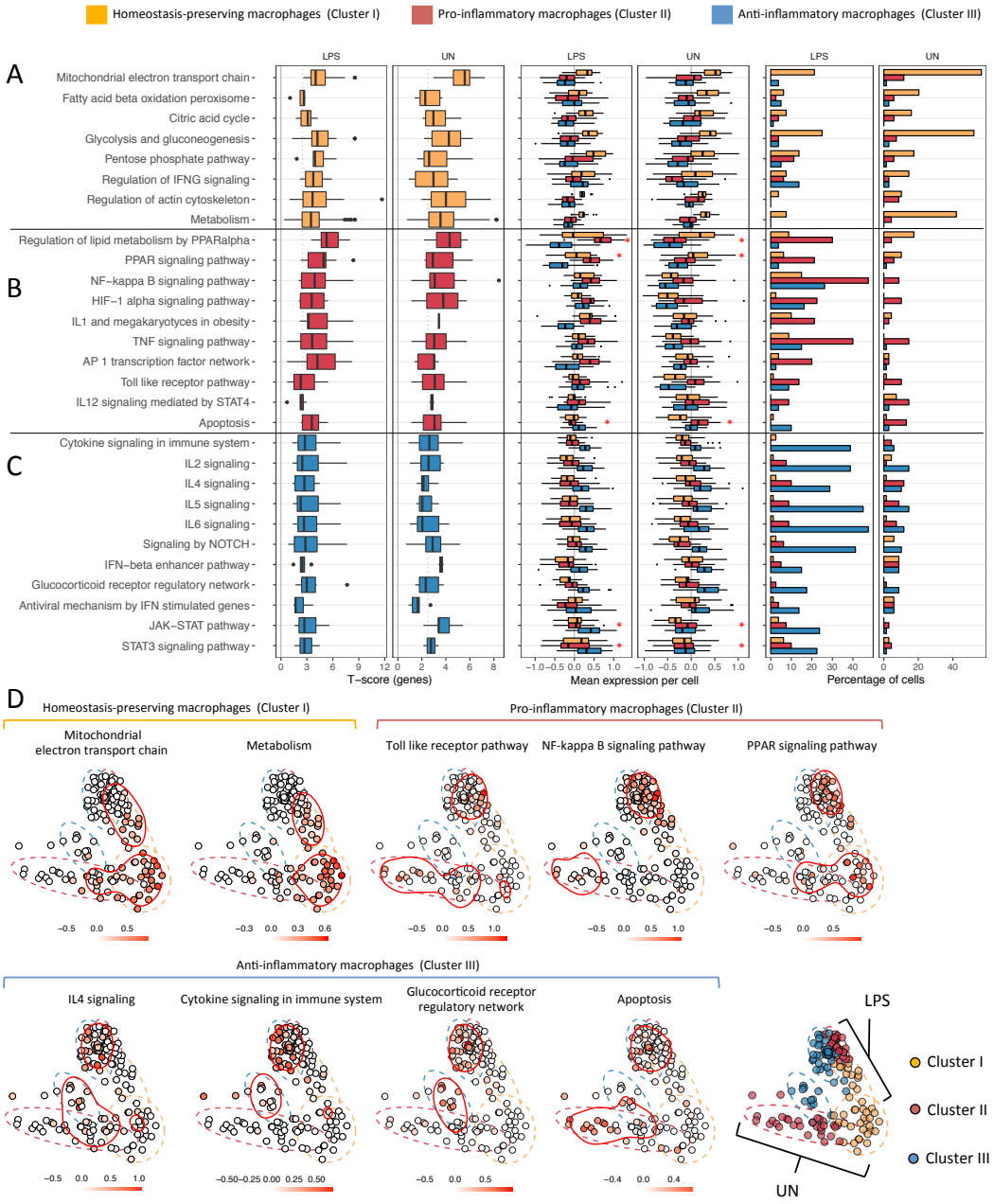

Figure 12: Pathway annotation analysis suggests distinct functional properties for macrophage states. A-C: Determined pathway terms that overlap for resting (UN) and activated (LPS) macrophages, along with distributions of t-scores for pathway-specific genes, mean pathway-specific gene expression per cell and the percentage of cells that show high expression for pathway-specify genes (mean expression > 0.3). Asterisk indicate differential state restriction. **D**: Visualization of pathway gene expression in ICA space. Horizontal color bars indicate mean expression levels of pathway-specific genes. White indicates low expression and red indicates high expression per cell.

IL1B expression and therefore did not show classical M1-like macrophage expression patterns. Resting macrophages with expression of NF-κB genes may represent cells with pro-inflammatory potential. For most pathways gene expression was similarly restricted to associated clusters of activated and resting macrophages. However, PPAR signaling pathways showed a switch like cluster-specific expression pattern. Genes of the PPAR signaling pathways were detected in homeostasis-preserving cells (cluster I) or pro-inflammatory cells for resting or activated macrophages, respectively (Figure 12B, asterisk). Strikingly, pathway analysis revealed that only ∼30% of cells from activated macrophages showed gene expression signatures of classical M1-like macrophages with high expression for pro-inflammatory pathways.

- *Anti-inflammatory macrophages* (clusters III): Clusters III from untreated and LPS-treated macrophages showed overrepresented pathways associated with immune regulatory pathways with genes connected to reduced inflammation (Figure 12C) including regulatory IL-signaling (average p-value<0.003, Supplementary Table 6), JAK-STAT signaling (p-value<0.004, including JAK2) and cytokine signaling (p-value<0.0007, including IRAK3) and glucocorticoid receptor regulatory network (p-value<0.0020, including FKBP5). Thus, these cells showed pathways associated to anti-inflammatory M2-like macrophage states. Intriguingly, cluster III grouped functionally tightly related genes such as NR3C1 (glucocorticoid receptor, GR) and IRAK3. Glucocorticoid receptor, promotes suppression of pro-inflammatory regulators such as NF-κB or activator protein 1 (AP-1) (Luecke and Yamamoto 2005, Busillo and Cidlowski 2013). Similarly, IRAK3 is a negative regulator of Toll-like receptor signaling and promotes alternative macrophage activation (Kobayashi et al. 2002, Ballinger et al. 2015). Both factors function in concert, as GR suppresses inflammation via the up-regulation of IRAK3 (also called IRAK-M, Miyata et al. 2015). Although JAK2 inhibition prevents innate immune responses (Peña et al. 2010), M2 polarization was shown to be enhanced through Jak2-mediated signaling in human macrophages (Yuan et al. 2014, Bhattacharjee et al. 2011). The number of cells expressing regulatory signaling pathways was higher in activated macrophages compared

to resting macrophages. IL2/4/5/6 pathway terms here again render the basal pathway machinery (i.e. PTK2B, Interleukin-6 receptor subunit beta precursor (IL6ST) and RASGRP3) of macrophage regulatory programs including sensing of anti-inflammatory interleukins. Classical pro-inflammatory gene expression with effector gene expression of chemokines, cytokines or interleukins was low or absent in the anti-inflammatory state of macrophages.

Despite the strong expression changes upon LPS-stimulation, pathway analysis revealed similar cluster-specific pathways for activated and resting macrophages. However, the lowest overlap of cluster specific genes (Figure 10E) and cluster-specific pathways (Figure 11A) was determined for the pro-inflammatory macrophages state (cluster II). This indicated that the majority of the differentially expressed gene was restricted to cells of the pro-inflammatory state.

However, to systematically gain further insight of the changes for this cluster upon LPS-stimulation, differential pathway analysis was performed for cluster II (Figure 13A, Table 1 and Supplementary Figure 31). As expected, typical pro-inflammatory pathways were again found for activated macrophages (i.e. NFκB pathway, p-value$<6.9\times10^{-6}$) as well as genes related to oxidative stress. For macrophages oxidative stress and inflammation are two major responses to fight invading bacteria. Oxidative stress is the result of elevated reactive oxygen species (ROS) production that is critical for the activation and functions of M1 macrophages (Covarrubias et al. 2013). Found genes for the oxidative stress pathway were those that reduce ROS-induced stress (i.e. SOD2 Kozakowska et al. 2015). Interestingly, nuclear receptors meta-pathway was found as LPS-exclusive pathway including the inflammation-limiting RXRα target gene GCLC (Wu et al. 2004).

Classical pro-inflammatory pathways including TNF-α signaling pathway (p-value<0.004) and HIF-1α signaling pathway (p-value$<4.4\times10^{-5}$) were also found for resting macrophages. The example of TNF-α signaling pathway highlights the separation of non-response genes for resting macrophages versus the responsive inflammatory genes in activated macrophages that show clearly distinct expression patterns (Figure 13B). Surprisingly, differential pathway analysis revealed the expression if IL-signaling pathways (average p-value$<7\times10^{-5}$) similar to the pathway terms found for anti-inflammatory macrophages (clusters III). This for example in-

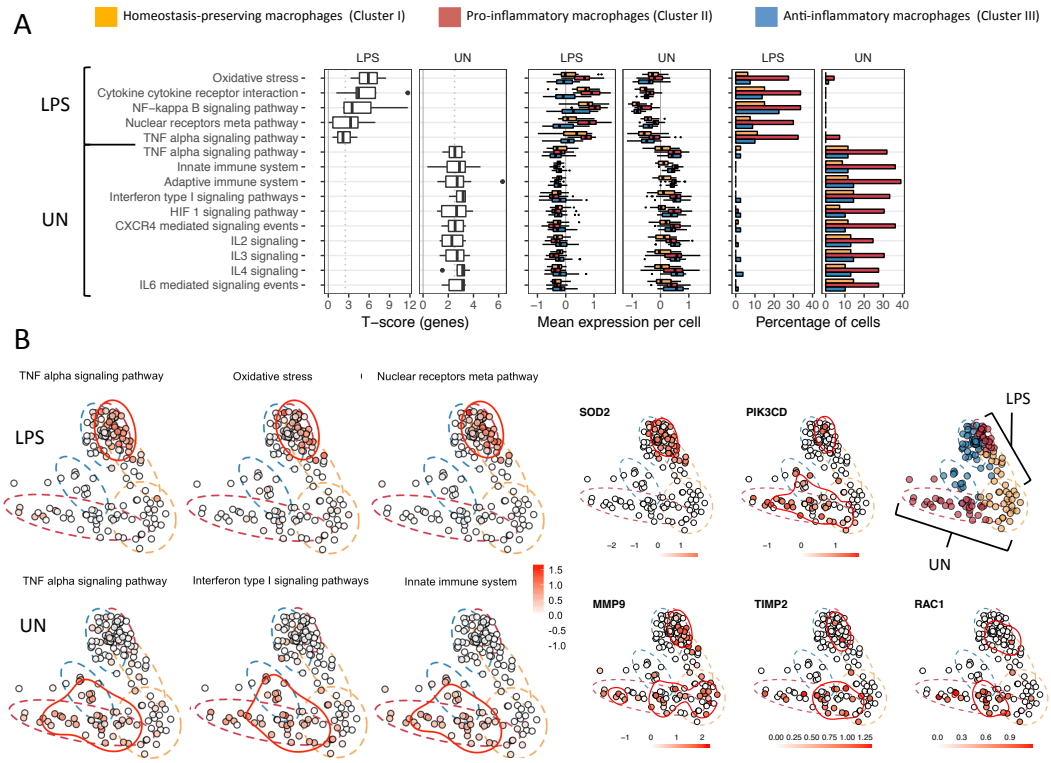

Figure 13: Differential pathway analysis of pro-inflammatory macrophage states. **A**: Pathway analysis was restricted to those pathway terms that showed differential state-specific gene expression between pro-inflammatory state activated macrophages (LPS) and resting macrophages (UN) with pro-inflammatory potential. TNF-α signaling pathway was selected as an example to highlight differential gene expression between the two states. Left: Distributions of t-scores for pathway-specific genes, mean pathway-specific gene expression per cell and the percentage of cells that show high expression for pathway-specify genes (mean expression > 0.3). **B**: Visualization of mean expression from pathway specific genes and expression for selected genes for cells in ICA space. Horizontal color bars indicate mean expression level of pathway-specific genes. White indicates low expression and red indicates high expression per cell.

	Pathway	p-value	q-value	Source	Number of genes	Pathway size	Genes
LPS	Oxidative Stress	9.84E-07	4.96E-04	Wikipathways	6	30	GCLC, MGST1, GSR, SOD2, NQO1, TXNRD1
	TNF signaling pathway - Homo sapiens (human)	4.74E-06	7.96E-04	KEGG	11	110	TNFRSF1B, TRAF1, CXCL2, MMP9, CCL20, TNFAIP3, IL1B, PIK3R5, CXCL1, MAP4K4, RFFL
	Nuclear Receptors Meta-Pathway	6.89E-05	4.96E-03	Wikipathways	13	316	GCLC, MGST1, GCLM, AHRR, GSR, CCL20, TNFAIP3, IL1B, SLC39A8, SLC7A11, SERPINB9, NQO1, TXNRD1
	NF-kappa B signaling pathway - Homo sapiens (human)	9.53E-05	5.30E-03	KEGG	7	95	TRAF1, CXCL2, TNFAIP3, IL1B, BCL2A1, CXCL8, LYN
	Cytokine-cytokine receptor interaction - Homo sapiens (human)	9.42E-04	1.28E-02	KEGG	10	265	TNFRSF1B, TNFRSF9, CXCL2, CCL20, IL1B, CCR7, IL18, IFNAR2, CXCL1, CXCL8
UN	IL6-mediated signaling events	9.62E-06	1.57E-04	PID	7	48	MAPK14, SOS1, RAC1, LMO4, PIK3R1, IL6R, GRB2
	Innate Immune System	1.36E-05	1.80E-04	Reactome	41	1309	ITGAL, RNASET2, TIMP2, PIK3CB, KCNAB2, NFATC3, APBB1IP, MEF2C, MAP3K1, SNAP29, CYB5R3, TNRC6B, PYGL, DNAJC5, PYCARD, DUSP3, MLEC, MAPK14, LY86, GCA, SOS1, WIPF1, QSOX1, PADI2, CTSD, LRMP, TRIM25, CAT, ARHGAP9, RAC1, CNPY3, IDH1, PFKL, PIK3R1, MNDA, SYK, GUSB, PIK3CD, GRB2, LAMP1, NHLRC3
	IL2	3.04E-05	2.84E-04	NetPath	8	76	PIK3CB, PIK3CG, MAPK14, SOS1, PIK3R1, SYK, PIK3CD, GRB2
	HIF-1 signaling pathway - Homo sapiens (human)	4.35E-05	3.56E-04	KEGG	9	103	PIK3CB, MKNK2, PIK3CG, LTBR, EGLN1, PFKL, PIK3R1, IL6R, PIK3CD
	IL4	7.53E-05	4.87E-04	NetPath	7	64	MAPK14, PIK3R1, SYK, INPP5D, PIK3CD, GRB2, FES
	IL3	1.65E-04	8.83E-04	NetPath	6	51	PIK3R1, SYK, INPP5D, PIK3CD, GRB2, FES
	Interferon type I signaling pathways	1.77E-03	4.43E-03	Wikipathways	5	54	MAP3K1, MAPK14, RAC1, PIK3R1, PIK3CD
	Adaptive Immune System	2.11E-03	4.98E-03	Reactome	24	807	ITGAL, MRC2, AP2S1, PIK3CB, BTBD1, PAG1, FYB, FBXO7, TNRC6B, FBXO9, RNF130, ITGA4, SOS1, CTSD, CLTA, HERC2, RAC1, HERC3, PIK3R1, UBE2Q1, SYK, INPP5D, PIK3CD, GRB2
	CXCR4-mediated signaling events	2.70E-03	6.15E-03	PID	6	88	PIK3CB, PAG1, PIK3CG, RAC1, PIK3R1, INPP5D
	TNF alpha Signaling Pathway	3.99E-03	8.24E-03	Wikipathways	6	93	MAP3K1, PYGL, SOS1, RAC1, GRB2, MAP3K3

Table 1: Differential pathway analysis. Results from differential pathway analysis as shown in Figure 13.

cludes the IL2-signaling pathway (p-value$<3\times10^{-5}$) and several PIK3 isoforms that are involved in limiting lipopolysaccharide-induced activation of signaling pathways, for example the expression of inflammatory mediators (Guha and Mackman 2002). Other pathway terms and associated genes putatively explain how a different cellular status is maintained in resting macrophage cells with pro-inflammatory potential. For example, the M2 macrophage marker gene TIMP2 (innate immune system pathway, p-value$<1.4\times10^{-5}$) is exclusively expressed in resting macrophages with pro-inflammatory potential and not in pro-inflammatory macrophages. TIMP2 is known to inhibit i.e. MMP9, a classical pro-inflammatory M1 macrophages factor that is required for inflammatory macrophage migration (Bourboulia and Stetler-Stevenson 2010, Laquerriere et al. 2004). Similarly, found interferon type I signaling pathway (p-value<0.002) induces the MYD88-independent pathway (Michalkiewicz et al. 2015) and activates RAC1 to down-regulate phagocytosis in human monocytic cells (Frausto-Del-Río et al. 2012). Taken together, these observations suggest that resting macrophage cells with pro-inflammatory potential are inhibited but maintain a basic machinery of pro-inflammatory pathway genes to rapidly react towards potentially invading bacteria.

3.6 Macrophage states exhibit different levels of responsiveness

State-specific expression of NF-κB effector genes (i.e. IL1B) in activated macrophages suggested that macrophage states exhibit heterogeneous responsiveness upon LPS stimulation. To assess cellular responsiveness to LPS in individual macrophages systematically, differential gene expression was assessed in respect to population RNA-seq readouts from activated and resting macrophages. To connect differential population expression data to single-cell data, cell-specific genes were identified by SOM analysis (Figure 8C). Specifically, for every cell those SOM components were selected that showed high level of gene expression and high correlation in the consensus of similar cells (SOM portrait over expression spots, Wirth et al. 2012). This allowed to classify cell-specific genes for every cell. Associated macrophage clusters in activated and resting macrophages showed different numbers of cell-specific genes (Figure 14A). Further, it was evaluated if these genes were differentially expressed in activated compared to resting macrophages at the average cell population level (bulk RNA-seq, Figure 14B). The number of cell-specific differentially expressed genes and the degree of differential expression (fold-change) thus allowed to analyze if and in which way (up- or down-regulation) a cell globally reacts upon stimulation.

Response of 45% of cells remained overall low for activated macrophages (Figure 14C and D). Macrophages from the pro-inflammatory state showed strikingly more cell-specific differentially expressed genes compared to other macrophage states (up to ∼100 differentially expressed genes per cell, Figure 14C). Notably, the distribution of cells with low and high numbers of cell-specific differentially expressed genes was bimodal for pro-inflammatory and anti-inflammatory state macrophages (Figure 14C). Remarkably, homeostasis-preserving cells showed overall low response levels (low response state, Figure 14D). The term low-response macrophages can be therefore used as alternative term for homeostasis-preserving cells. Whereas, almost all pro-inflammatory state macrophages showed LPS-response with average up-regulated cell-specific gene expression (Figure 14D, 93% of cells defined as high response state), only half of anti-inflammatory macrophages

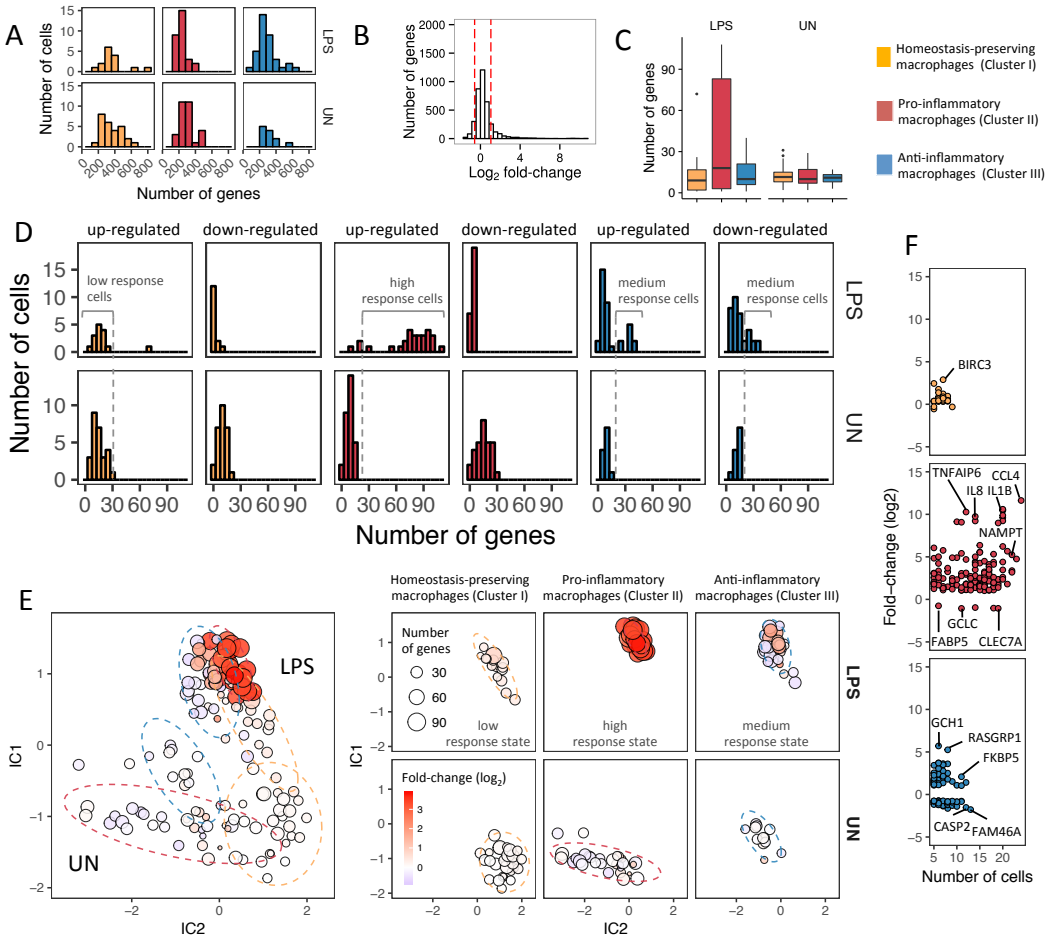

Figure 14: Analysis of macrophage responsiveness towards LPS stimulation. **A**: Distribution of cell specific genes per cell determined by SOM analysis and visualized for defined states for resting (UN) and activated (LPS) macrophages. **B**: Determined fold-change cut-offs for selecting differentially expressed genes from population RNA-seq data (LPS vs. UN). **C**: Number of cell-specific differentially expressed genes per macrophage state. **D**: Histograms show the distribution of cells agains the number of assigned cell-specific differentially expressed genes. **E**: ICA visualization of mean fold-changes ($\log_2$) per cell. **F**: Scatter plots show genes in respect to their fold-change ($\log_2$) vs. the number of cells the gene is expressed in (cell-specific genes) for each macrophage state.

showed response with average up or down-regulated gene expression (Figure 14D, 53% of cells defined as medium response state).

In homeostasis-preserving state low-response macrophages only 31 genes were expressed (>5 cells) with an average fold-change of 0.7 ($\log_2$, Figure 14F, Supplementary Table 7). Genes with the highest differential expression were for example BIRC3 and DUSP2. While BIRC3 is an important regulator of innate immune response and inhibits apoptosis (Wang et al. 2012b), DUSP2 is required to initiate LPS-triggered TLR cascades via MAPK signaling (Lang et al. 2006).

For activated macrophages, the strongest gene expression in respect to determined gene-specific fold-changes (275 genes with average fold-change of 2.8 ($\log_2$)) was observed for cells of the pro-inflammatory state (Figure 14F, Supplementary Table 7). In several cells genes were expressed with high fold-changes compared to resting macrophages; i.e. NAMPT, CCL4, IL8, IL1B and TNFAIP6. The M1-macrophage marker NAMPT, once secreted as protein, promotes cell survival for macrophages and other cells in inflammatory environments (Halvorsen et al. 2015, Li et al. 2008). Also CCL4 (MIP-β) is a typical M1-marker responsible for early inflammation induction and a chemoattractant for natural killer cells, monocytes and a variety of other immune cells (DiPietro et al. 1998, Bystry et al. 2001). TNFAIP6 can be induced by pro-inflammatory cytokines and is involved in positive regulation of cell migration but also balancing inflammatory response (Dyer et al. 2016). Few genes were down-regulated in pro-inflammatory state macrophages including GCLC and CLEC7A. Down-regulation of GCLC leads to elevated inflammation (Wu et al. 2004) and CLEC7A (Dectin-1) is suggested a M2-marker (Lefèvre et al. 2010).

The alternative, anti-inflammatory macrophage state showed weaker response (262 genes with average fold-change of 1.9 ($\log_2$ up-regulated) and -1.0 ($\log_2$ down-regulated)). Forty percent of anti-inflammatory cells showed overall up-regulated cell-specific gene expression with known anti-inflammatory functions (i.e. FKBP5, GCH1 and RASGRP1, Figure 14F, Supplementary Table 7). GCH1 promotes macrophage M2-like polarization and its inhibition shifts the phenotype of tumor associated macrophages from the proangiogenic M2 towards M1 macrophages (Pickert et al. 2013). RasGRP3 limits Toll-like receptor-triggered inflammatory response

in mouse macrophages (Tang et al. 2014). FKBP5 is involved in glucocorticoid receptor coordinated anti-inflammatory response (Chinenov et al. 2014). Genes down-regulated in anti-inflammatory state macrophages included for example FAM46A and CASP2 whose functions are unknown or not linked to macrophage biology.

In summary, projection of average population differential expression data to single-cell data suggested that defined macrophage states are similar to previously defined M1/M2-like polarization models. This is remarkable because this clearly suggests intrinsic macrophage heterogeneity towards M1/M2 signatures independent of targeted polarization (with i.e. IL4 towards M2 macrophages). In this regard it is not surprising that state-specific gene expression signatures do not fully recapitulate M2 macrophage profiles for found anti-inflammatory macrophages.

Many genes were classified according to macrophage states that are still incompletely functionally described or not specifically associated to macrophage biology (Supplementary Table 7). Remarkably, single-cell analysis showed that only a fraction of cells react strongly upon LPS-stimulation (M1-like, high response cells). Therefore, most of the cellular response is restricted to macrophages of cluster II (pro-inflammatory state macrophages). This underlines that top differentially expressed genes classified with population gene expression readouts (Figure 3D) are biasedly derived from ∼30% of the whole macrophage population. Contrary, gene expression of cells with low pro-inflammatory potential or cells with anti-inflammatory gene expression characteristics (M2-like, medium response cells, Figure 14D and E) were underrepresented in population expression data.

3.7 Macrophage state characteristics upon environmental changes

To further mathematically characterize the differential response of macrophages to changing environmental triggers in respect to defined macrophage states, gene expression stability, intra-cluster correlation and signaling robustness was analyzed by means of whole transcriptional noise characteristics and by means of signaling entropy, respectively.

In order to measure stability of macrophage states, each cell's estimated stability level was assessed in the context of its associated state within the whole macrophage population. Therefore silhouette coefficients (stabilities) were calculated. Silhouette coefficients hereby contrast the average distance of one cell to other cells in the same state with the average distance to samples in the other states (Rousseeuw 1987). Silhouette coefficient has a value between -1 and 1 where a higher value indicates that the sample is well-matched to its own group, and poorly-matched to the other groups (Xiong et al. 2014). Homeostasis-preserving state macrophages showed highest (median S = 0.39) and lowest (median S=-0.05) stability for resting and activated macrophages, respectively (Figure 15A and B). Homeostasis-preserving cells present the dominating state in resting macrophages and form a high-stability population. These cells may generate a reservoir from which cells change states towards a more responsive pro-inflammatory or anti-inflammatory condition. Upon macrophage activation anti-inflammatory and pro-inflammatory macrophages remained at similar stability medians suggesting a similar status of paired states in activated and resting macrophages (Figure 15A).

In order to calculate the degree of macrophage similarity within macrophage states, irrespective of the whole macrophage population, intra-state correlations were computed between all cell pairs of their respective clusters. Therefore, Pearson correlation coefficients were determined for each state based on SOM components. Similar to results from responsiveness analysis (see 68) pro-inflammatory (median r=0.92) and anti-inflammatory (median r=0.89) state activated macrophages showed higher intra-state correlation compared to homeostasis-preserving cells (median r=0.81, Figure 15C). This suggests, that upon LPS-stimulation, both responsive states develop towards increased coordination. Compared to data from activated macrophages, resting macrophages showed higher spread of Pearson correlation coefficients. Notably, in this case, cells from different states did not show significant changes for Pearson correlation coefficients. This observation highlights that pro-inflammatory and anti-inflammatory states, specifically for activated macrophages, feature a high degree of coordination. This would represent a strategy to generate efficient pathogen defense functionality by still maintaining balanced macrophage states for flexible responses and to maintain homeostasis of

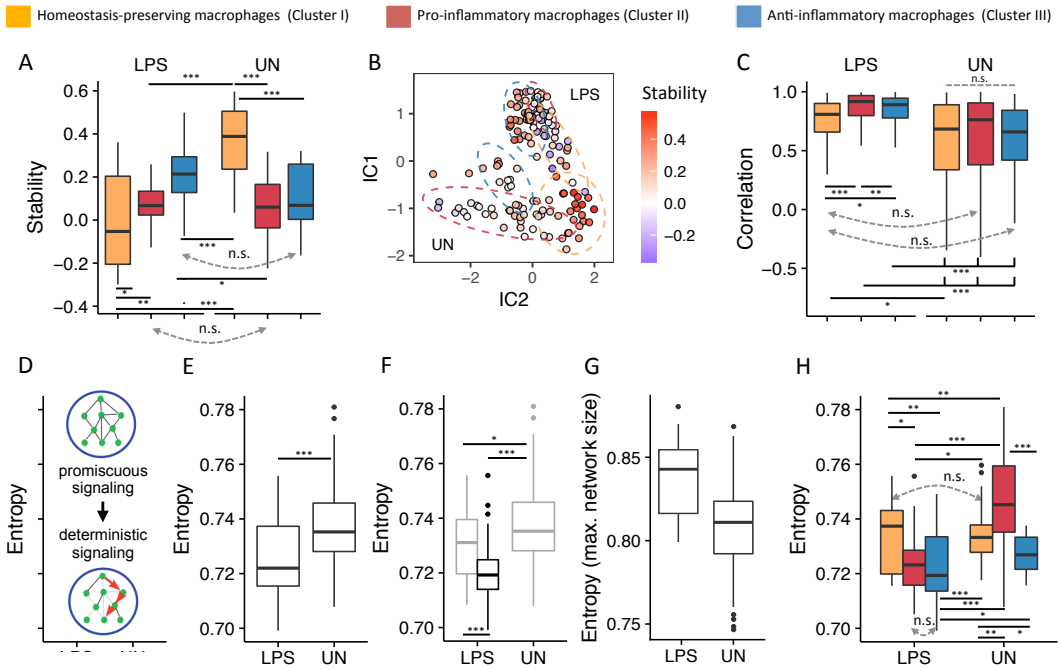

Figure 15: Stability, intra-cluster correlation and signaling entropy. **A**: Stability scores were used here to quantify if a cell lies well within its cluster (high stability) or tends to lie rather in between clusters. Box plots summarize the cells stability scores. **B**: Stability per cell projected to ICA representation. **C**: Single-cell heterogeneity was assessed by intra-cluster correlations of gene expression. High coefficients reflect lower heterogeneity of cells within a defined state and vise versa. **D-H**: Signaling entropy quantifies signaling pathway promiscuity computed from the integration of single-cell gene expression data with an interactome (PPI network, Teschendorff et al. 2014). High signaling entropy indicates high amount of uncertainty, whereas low signaling entropy suggests a more deterministic cellular response. **D**: Schematic representation for interpretation of the signaling entropy concept. **E**: Normalized local signaling entropy per cell for activated and resting macrophages using small high-confidence PPI networks. **F**: Signaling entropy per cell for low response cells (grey, LPS) and medium and high response cells (black, LPS) using small high-confidence PPI networks. See Figure 14 for definition of cellular responsiveness. **G:** Normalized local signaling entropy per cell for activated and resting macrophages using low-confidence PPI networks with maximum network size. **H**: Signaling entropy per cell, shown for defined macrophage states using small high-confidence PPI networks. UN: resting macrophages. LPS: activated macrophages. Statistical analysis was done with one-way ANOVA followed by Dunn's multiple comparison test (n.s. p-value > 0.05; * p-vale < 0.05; ** p-value < 0.01; *** p-value < 0.001).

the entire macrophage population (Figure 15C). Significantly lower intra-cluster correlations were determined for homeostasis-preserving cells in activated and resting macrophages.

Neither stability nor intra-state correlation analysis took into account the underlying gene regulatory pathways that are triggered upon stimulation. These analyses depend on the single-cell transcriptome data alone. Instead, signaling entropy quantitatively captures a system's efficiency to transduce signals by making use of protein-protein-interaction (PPI) network constructed pathways (Teschendorff et al. 2014). Normalized local signaling entropy quantifies the degree of coordination for cells and selected pathways in different treatment situations. To quantify the amount of uncertainty of signal transduction, combined analysis of PPI networks and single-cell gene expression data was applied to determine mean signaling entropy per cell according to Teschendorff 2016 using small high-confidence PPI networks. Loosely defined, signaling entropy of a system refers to the amount of overall "disorder" of underlying pathways. High signaling entropy indicates high amount of uncertainty of events, whereas low signaling entropy suggests low uncertainty and a more deterministic, coordinated response of cells (Figure 15D).

Intriguingly, activated macrophages exhibited a significantly lower entropy rate compared to resting macrophages (p-value$<9.7\times10^{-8}$, Figure 15E). Thus, LPS-stimulation resulted in quantifiable lower levels of uncertainty and more deterministic signaling, which might help to shape cellular function. Lower entropy rates were also determined for high/medium response activated macrophages compared to activated macrophages with low response (as defined in 3.6 and Figure 14D). Low response cells showed entropy rates closer to those of resting macrophages (Figure 15F).

High-confidence PPI networks were constructed using genes with high expression levels (on average >75 counts per gene). However, these interaction networks did not show scale-free topology and constituted small PPI networks with several hundreds of genes connected. Thereby, a basic requirement for the entropy approach described by Teschendorff was neglected. Low-confidence interaction networks constructed with all genes that showed any expression (count >0) in any cell generated bigger networks with scale-free (or near scale-free) topology. Activated

macrophages exhibited a significantly higher entropy rate compared to resting macrophages (p-value$<2.1\times10^{-3}$, Figure 15G) if low-confidence networks were used. Therefore, computing cell-specific entropy estimates with maximum network size (low-confidence networks) or small network size (high-confidence networks) showed opposite trends. The work presented here considered high-confidence networks. This strategy was chosen because the selection of high expressed genes minimizes the impact of low expressed genes for entropy estimations. However, low-confidence network-based entropy estimation may represent a more wholistic approach to qualify a system's efficiency to transduce signals.

For defined macrophage states, homeostasis-preserving state macrophages showed high entropy rates using small high-confidence PPI networks, similar to rates observed for resting (untreated) homeostasis-preserving macrophages (no significant difference, Figure 15H). Anti-inflammatory and pro-inflammatory state macrophages showed significantly lower signaling entropy rates compared to other macrophage states. While pro-inflammatory cells of activated macrophages showed low entropy rates, resting macrophages with pro-inflammatory potential showed remarkable higher entropy rates (p-value$<1.2\times10^{-7}$) indicating that those cells exhibit highly promiscuous signaling in the absence of LPS stimulation. In summary, determined signaling entropy rates revealed for both responsive states more deterministic signaling to putatively generate a balanced response of macrophages to bacterial triggers like LPS.

The signaling entropy framework was primarily developed for quantifying a samples mean entropy. However, differential gene-specific entropy rates showed similar trends for selected pathways inferred from constructed PPI-expression datasets (Figure 16A). For activated macrophages in particular pathways including TNFR1 signaling, TNF-α, NF-$\varkappa$B signaling and TLR4 cascade showed significantly higher degree of organization compared to resting macrophages, as indicated by lower signaling entropy rates (Figure 16B). Entropy rates helped to identify pathways with more deterministic signaling in resting macrophages including IL-12 signaling (p-value < 0.001). Other pathways showed only trends of lower entropy rates for resting macrophages, including CD28 dependent signaling, androgen receptor signaling, IL-2 signaling and Notch signaling. Although significantly changed

A

Short name	Pathway	p-value	q-value	Source	Number of genes	Pathway size
Innate	Innate Immune System	2.15E-18	4.74E-16	Reactome	123	1309
Adaptive	Adaptive Immune System	2.96E-07	3.44E-06	Reactome	65	807
EGFR	EGFR1	2.52E-13	1.25E-11	NetPath	57	458
TNFR1	Regulation of TNFR1 signaling	2.60E-03	9.01E-03	Reactome	5	23
TNF	TNFalpha	3.17E-05	2.06E-04	NetPath	25	241
NFKB	NF-kappa B signaling pathway - Homo sapiens (human)	2.05E-06	1.94E-05	KEGG	16	95
TLR4	Toll Like Receptor 4 (TLR4) Cascade	1.16E-03	4.85E-03	Reactome	14	128
IL12	IL12-mediated signaling events	9.37E-06	7.39E-05	PID	12	64
IL3	IL3	1.42E-03	5.74E-03	NetPath	8	51
CD28	CD28 dependent PI3K/Akt signaling	2.58E-03	9.01E-03	Reactome	6	33
AR	Androgen receptor signaling pathway	3.60E-08	5.36E-07	NetPath	31	151
IL2	IL2	1.52E-03	6.09E-03	NetPath	10	76
IL6	IL6	8.10E-05	4.72E-04	NetPath	12	77
IL4	IL4-mediated signaling events	1.81E-03	6.99E-03	PID	9	65
NOTCH	Canonical Notch Signaling Pathway	5.77E-06	4.82E-05	PID	11	51

B

C

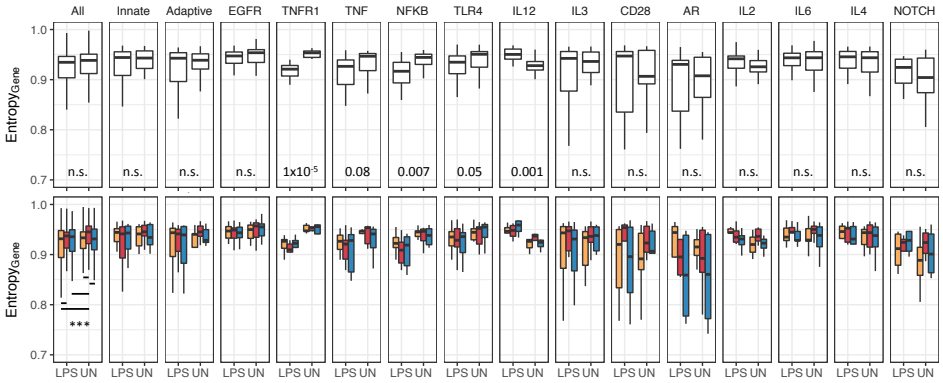

Figure 16: Signaling entropy for selected pathways. Genes (nodes within PPI-networks) were ranked according to differential entropy using Wilcoxon rank sum tests to derive for each gene a p-value, which reflects the statistical significance of the difference in the local normalized entropy of the given gene between the two treatments (Teschendorff 2014). **A**: Selected pathways enriched in gene lists integrated in PPI networks with single-cell gene expression including pathways with genes. **B**: Visualization of gene-specific entropy estimates per pathway per treatment model (LPS: activated macrophages, UN: resting macrophages). **C**: Same as in B but shown for defined macrophage state. Note that for B and C outliers are not shown and axis was scaled for better representation. Statistical analysis was done with nonparametric Kruskal-Wallis test followed by Dunn's post hoc multiple comparison method (n.s. p-value > 0.05; * p-vale < 0.05; ** p-value < 0.01; *** p-value < 0.001). Note that all genes, except of genes from pathways termed "Innate", "Adaptive", "IL6" and "IL4" showed differential pathway entropy using Wilcoxon rank sum tests.

entropy rates between macrophage states were determined if considering all 557 investigated genes of the PPI network, genes of general pathways including genes from terms 'innate immune system' and 'adaptive immune system' and EGFR1 showed similar entropy rates (Figure 16C). Inflammatory (TNFR1, TNF, NF-$\varkappa$B and TLR4) and regulatory (IL3, CD28, AR, IL2, IL6, and IL4) pathway terms showed lower entropy rates for defined pro-inflammatory or anti-inflammatory macrophage states, respectively. Interestingly, genes from Notch signaling pathway showed lower entropy rates for homeostasis-preserving state macrophages. Notch signaling is considered a central molecular switch towards M1 macrophages, producing a systemic low-grade inflammation state (Bi and Kuang 2015). This suggests that Notch signaling may be functionally important to regulate macrophage activation from a low response state (M0-like) towards and a pro-inflammatory state (M1-like).

Different approaches were used to characterize individual cells based on whole-transcriptome data. All approaches feature different properties of the data. Stability of cells compared to the entire macrophage population was similar for pro- and anti-inflammatory macrophages. Homeostasis preserving cells showed higher stability scores for resting macrophages. Within-cluster correlation suggested highest "cellular synchronization" for pro- and anti-inflammatory macrophages confronted with LPS. Similarly, signaling entropy indicated a more deterministic signaling for these states and promiscuous signaling in case of homeostasis-preserving cells and cells with pro-inflammatory potential in case of resting macrophages.

3.8 Transcriptional networks unveil major regulatory hubs for different macrophage states

After definition of cell-specific and state-specific genes and pathways and subsequent quantification of cellular information transduction in untreated and LPS-treated macrophages, these findings were integrated with underlying co-expression networks (regulatory modules). Regulatory module classification by means of gene to gene correlation analysis was achieved by analyzing SOM components. Ten gene correlation clusters were defined using SOM portrait analysis (Figure 17A) and

visualized as Euclidean distance heatmap representations (Figure 17B).

The high number of identified correlation clusters suggested a more detailed representation of the diversity of coordinated gene expression fluctuations. Defined macrophage states and correlation clusters were aligned to characterize the way correlation clusters operate through different macrophage states. Three correlation clusters with highest beta test statistics (Binder et al. 2014, Läuter et al. 2009) for included correlation clusters matched best with defined macrophage states (Figure 17C). Other correlation clusters showed intermediate expression patterns with expression in more than one defined macrophage state. For example, genes of correlation cluster E for activated macrophages are expressed in anti-inflammatory state macrophages and homeostasis preserving cells.

To identify hub genes that putatively drive macrophage state-specific functions, correlation clusters were aligned to macrophage states and rendered the association to either pro-inflammatory, anti-inflammatory and homeostasis-preserving cells (Supplementary Figure 32 (LPS) and Supplementary Figure 33 (UN)). Genes from correlation clusters were then subjected to FANTOM4 edge express analysis (Severin et al. 2009). This analysis allows to join genes based on regulatory interactions in THP-1 cells, that were investigated by functional and correlation-based high-throughput experiments. Central hub genes with high connectivity tend to encode regulatory essential genes (Goh et al. 2007). Notably, most central hub genes with high degree of connectivity were not strongly differentially expressed between resting and activated macrophages, which does not depreciate these factors as functionally less relevant (Figure 17D).

The generated map of degree-ranked hub genes provided an enriched selection of putatively important regulators (mostly transcription factors and chromatin remodeling enzymes) in the context of macrophage heterogeneity (Figure 17E). Many of the identifies hub genes represent rather novel findings in the context of M1/M2 macrophage biology.

For activated pro-inflammatory macrophages ETS1, ETS2, MITF and HIF1A were identified with treatment-specific regulation. Forkhead box O3 (FOXO3) and ARID5B were not regulated in activated macrophages in respect to resting macrophages (Figure 17E, correlation cluster J, LPS). Considering previous knowl-

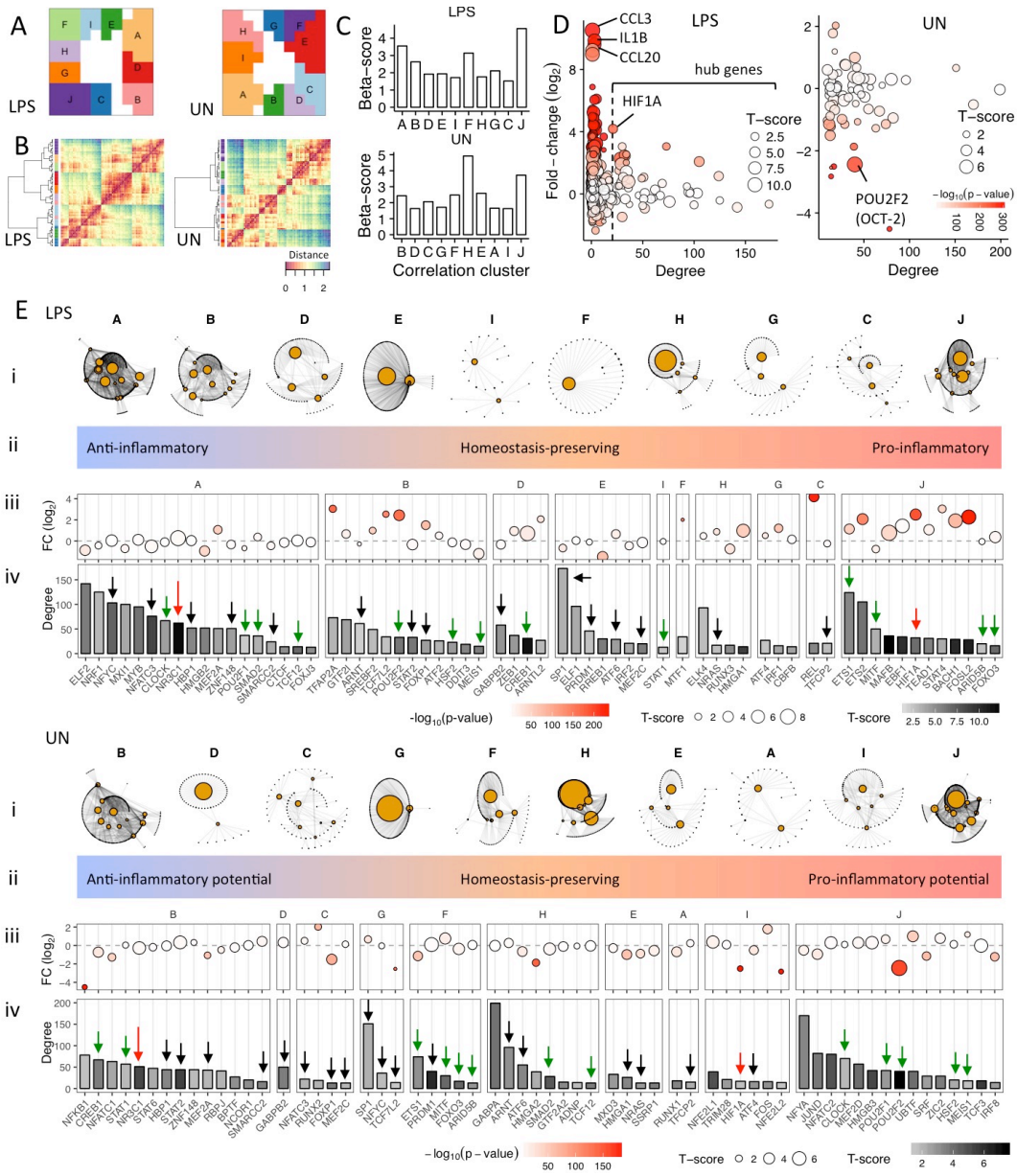

Figure 17: Prediction of hub genes underlying gene regulatory modules. **A**: Representation of correlation cluster (CC) selection from defined spots of co-regulated SOM components for resting (UN) and activated (LPS) macrophages. **B**: Heatmap indicating co-expression between SOM components measured by Euclidean distances. **C**: Multi-test-adjusted correlation test based on beta-test statistics to estimate significance of coordinated expression of genes in each of the selected CCs (as defined Binder et al. 2014). **D:** Representation of interacting (FANTOM) genes per treatment. Fold-change (reciprocal for UN) and p-value from population RNA analysis. Degree from interaction connectivity within CC networks. T-score estimates indicate significant CC-specific expression. **E, i:** Representation of interaction networks for CCs (A-J). **ii**: Gradient illustrating associations of CCs to defined macrophage states. **iii**: Properties (FC and t-score) of listed hub genes assigned in D. **iv**: Degree sorted hub genes. Color represents gene-specific t-score estimates. Black arrows indicate that particular hub genes were found in associated CCs (i.e. LPS-A vs. UN-B) between resting and activated macrophages. Green arrows indicate that hub genes were found in non-associated CCs. Red arrows mark NR3C1 and HIF1A.

edge, determined factors may indeed constitute functional state-specific regulators in macrophages. For example, ETS2 determines the inflammatory state of endothelial cells in advanced atherosclerotic lesions (Cheng et al. 2011). FOXO3 is known to maintain vitality and prevent apoptosis during inflammation (Jonsson et al. 2005). Notably, many pro-inflammatory hub genes for this regulatory network were associated to homeostasis-preserving cells of resting macrophages (Figure 17E, green arrows). Many hub genes for resting macrophages with pro-inflammatory potential represent crucial factors that are required for macrophage activation, including NFYA, JUND (AP-1), high-mobility group protein B3 (HMGB3) and POU2F1 (OCT1). NFYA is associated with lipid metabolism by PPARα. AP-1 is a determinant of macrophage activation. AP-1 knockdown in rat and human primary macrophages led to significantly reduced macrophage activity and cytokine secretion (Behmoaras et al. 2008). HMGB3 is a known mediator of inflammation and tissue regeneration and regulates the balance between cells with self-renewal and differentiation potential in hematopoietic stem cell (Andersson and Rauvala 2011, Nemeth et al. 2006).

Several hub genes overlapped for homeostasis-preserving cells in resting and activated macrophages. These factors, including trans-acting transcription factor 1 (SP1), ELF1 and GABPA, may be associated to suppress inflammation. For example, SP1 induces IL-10 expression and IL-10 in turn inhibits macrophage activation (Brightbill et al. 2000, O'Farrell et al. 1998).

Anti-inflammatory state cells in activated macrophages were associated i.e. to ELF2, nuclear respiratory factor 1 (NRF1), NFYC and HMG-box transcription factor 1 (HBP1) transcriptional regulation, pointing towards repression of specific inflammatory programs and M2-like promotion of anti-inflammatory signaling (Martinez et al. 2013, Galván-Peña and O'Neill 2014). For example, HBP1 down-regulates the inflammatory cytokine macrophage migration inhibitory factor (MIF, Tian et al. 2014). Intriguingly, NFKB1 was down-regulated in resting anti-inflammatory state macrophages. Further, highly ranked hub genes included also cAMP responsive element binding protein 1 (CREB1). In the setting of acute overnutrition of macrophages CREB inhibits the production of inflammatory mediators and contributes to the maintenance of insulin sensitivity (Luan

et al. 2015). Importantly, for resting and activated macrophages, nuclear receptor subfamily 3 group C member 1 (NR3C1) transcripts, which encode glucocorticoid receptor (GR), showed highest state-restricted expression (high t-scores) towards anti-inflammatory cells.

3.9 Independent experiments confirm mutually exclusive expression of pro-inflammatory and anti-inflammatory genes

Single-cell qPCR and FISH analyses were performed to independently validate the state-exclusive expression of hub genes from both sides of the macrophage spectrum (Figure 17E), including NR3C1 (anti-inflammatory) and HIF1A (pro-inflammatory) and other anti-inflammatory macrophage associated genes, including the GR target gene FKBP5, as well as JAK2 and IRAK3. In agreement with sequencing data cell state-specific expression of antagonistic transcriptional regulators was observed (Figure 18A and B). For example, in activated macrophages a clear trend of mutually exclusive expression was found for IL1B versus NR3C1 (r=0.05), JAK2 (r=-0.06) and IRAK3 (r=0.11) (Figure 18B). Contrary, highly correlated expression of HIF1A (r=0.82) or IL8 (r=0.79) with IL1B, and NR3C1 with IRAK3 (r=0.79) was observed, suggesting coordinated action of these inflammatory and anti-inflammatory regulators, respectively. Strikingly, high-throughput single-cell qPCR experiments using $CD14^+$ peripheral blood mononuclear cells (PBMCs) derived primary human macrophages with a diverse genetic and physiological background of healthy donors supported these results (Figure 18C).

Considering IL1B as a proxy for pro-inflammatory macrophages, another independent experiment confirmed state-exclusive expression in ∼1000 cells using FISH analysis (Figure 18D and E and Supplementary Figure 34). IL1B and IL8 showed highly correlated expression (r=0.57), whereas low correlation was found for IL1B versus NR3C1 (r=0.1), IRAK3 (r=-0.13), JAK2 (r=-0.11) and FKBP5 (r=0.04), indicating once more mutually exclusive cellular expression of these antagonistic genes (Figure 34D).

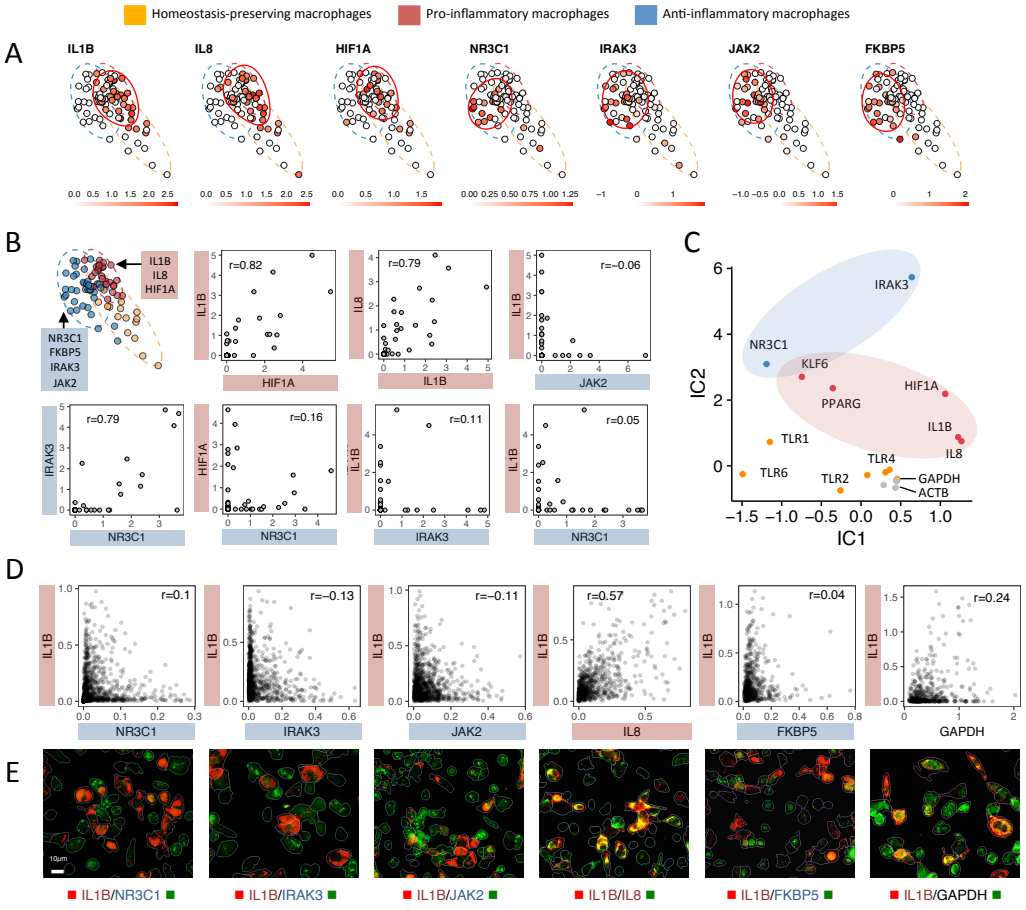

Figure 18: Validation of mutual exclusive expression of pro- and anti-inflammatory marker genes. **A**: Activated macrophages in 2-dimensional independent component analysis (ICA) space for state-specific genes that were selected for validation experiments. Each dot represents a cell. Expression levels are indicated by color gradients. White indicates low expression and red indicates high expression per cell. **B**: ICA representation for activated macrophages and sc-qPCR analysis results ($\geq$88 cells). C_q-values were transformed ($2^{C_q/-3.32}$) and scaled. **C**: ICA representation of HT-sc-qPCR results from human PBMC-derived primary macrophages. Single-cell processing was done as described in 2.1.10.5. Color indicates macrophage state associations. **D**: FISH analysis for indicated gene pairs. Relative expression per cell was computed from 8×8 tiled images as described in 2.1.14. **E**: Representative images from acquired and segmented FISH images. Samples were prepared as described in 2.1.13. r indicates Pearson's correlation coefficient. Cells were stimulated with 100ng/ml LPS for 2 hours.

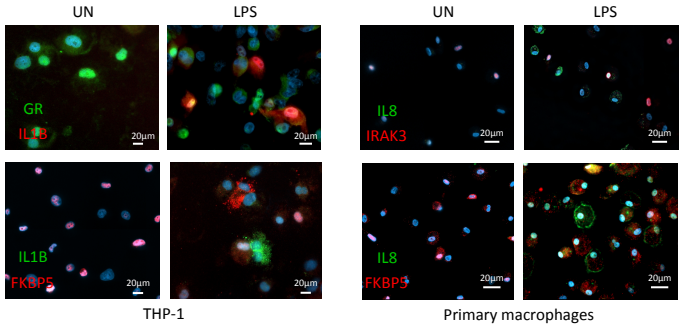

Figure 19: Mutually exclusive protein expression of pro- and anti-inflammatory genes. THP-1 macrophages and human PBMC-derived primary macrophages left unstimulated (UN) or treated with 100ng/ml LPS for 4 hours were double stained. Expression of pro-inflammatory marker genes IL1B and IL8 and anti-inflammatory marker genes GR and FKBP5 were visualized by immunofluorescence. Cell nuclei were stained with DAPI. (see Materials and methods 2.1.12 and 2.1.14).

Although mRNA data can reveal basic transcriptional mechanisms, proteins do execute major biological functions. Therefore, qualitative microscopic analysis of proteins in isogenic THP-1 and primary human macrophages were preformed using immunofluorescence double staining for selected gene pairs. Consistent with single cell mRNA expression data, protein analyses showed mutually exclusive expression of proteins from central antagonistic gene pairs such as anti-inflammatory/inflammatory GR (NR3C1) or FKBP5 vs. IL1B and IRAK3 or FKBP5 vs. IL8 (Figure 19). Nuclear localization of GR was observed in some cells for resting macrophages. Images suggested that LPS-treated cells with nuclear GR occupancy were less likely to express IL1B. Similarly, this was observed for anti-inflammatory factors IRAK3 and GR target gene FKBP5 with LPS-induced cytoplasmic translocation.

3.10 Elevated stimuli doses segregate cells towards pro- and anti-inflammatory signatures

To investigate in which way higher doses of external signals such as LPS would influence the expression of state-specific genes, macrophages were stimulated with

different doses of LPS over two hours and subjected to single-cell qPCR analysis. The number of macrophages expressing primary pro-inflammatory response genes HIF1A or IL1B increased significantly with the concentration of LPS (Figure 20A, top). Notably, for a different macrophage state, a simultaneous increase of the number of cells expressing anti-inflammatory NR3C1 was observed. The level of expression of all these first-line regulatory genes remained generally constant within individual macrophages (Figure 20A, bottom). Only for the effector gene IL1B elevated levels of transcripts per cell were detected.

Interestingly, NR3C1-induced secondary response genes (modifiers) such as IRAK3 appeared to be expressed at higher levels within few macrophages but remained largely unaffected by increasing concentrations of LPS. The entirety of these results suggests that increasing levels of external stimuli may result in an overall balanced transcriptional response of pro- and anti-inflammatory macrophage states. Accordingly, the number of cells with pro- and anti-inflammatory marker gene expression increased with elevated LPS doses, suggesting that responsive macrophage states increase. Although, marker genes from homeostasis-preserving macrophages were not specifically assessed, this suggests that pro- and anti-inflammatory state macrophages could be recruited from low these response cells. Thus, the population of these macrophages may act as a reservoir and decrease in number upon higher elevated LPS stimulation.

These single-cell data challenges the common perception of a direct molecular antagonism of major anti-inflammatory transcriptional regulators such as NR3C1. Instead, results corroborate a model including digital all-or-none gene expression switches of primary transcriptional events (Figure 20B). Cellular expression of antagonistic regulators such as NR3C1 can lead to an almost complete depletion of inflammatory mediators within the same cell. In contrast, cells devoid of such antagonistic factors might more freely express pro-inflammatory genes.

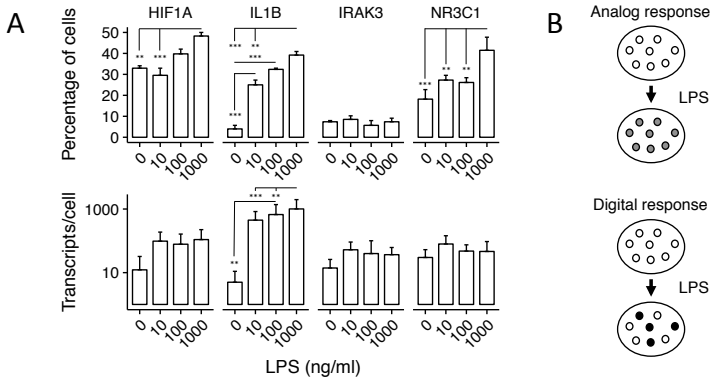

Figure 20: Elevated LPS-doses induce increasing numbers of cells with pro- and anti-inflammatory gene expression. **A**: Single-cell qPCR analysis of macrophages treated with 10ng/ml, 100ng/ml or 1µg/ml LPS or left untreated. Two times 88 cells per dose were analyzed. Shown is mean (bars) and standard deviation (error bars). Absolute quantification was done relative to IPC standards (see Materials and methods 2.1.10.4 on page 33). Statistical analysis was done with one-way ANOVA followed by Dunn's multiple comparison test (n.s. p-value > 0.05; * p-vale < 0.05; ** p-value < 0.01; *** p-value < 0.001). **B**: Model of analog or switch-like digital response.

3.11 Knockdown and activation of state-specific factors shift macrophage expression signatures towards an M2-like status

It was functionally evaluated how perturbations of major state-specific regulatory factors would influence transcriptional profiles of macrophage states. LPS-treated THP-1 macrophages deficient in MyD88 expression (Figure 21A) and activated macrophages subjected to dexamethason-induced GR activation were analyzed using RNA-sequencing. Differential gene expression data was joined with cell-specific gene expression as previously applied to determine responsiveness of macrophage states (see 3.6 and Figure 14). While MyD88 represents a major factor required for pro-inflammatory state macrophages, GR is considered here as a regulator of anti-inflammatory state macrophages.

As expected, pro-inflammatory signaling was markedly reduced in activated macrophages deficient in MyD88 activity determined by population RNA-seq (Figure 21B). 288 genes were significantly up-regulated ($\log_2$ fold-change > 2) and 722 genes were down-regulated ($\log_2$ fold-change < -2, q-value <0.001). Up-

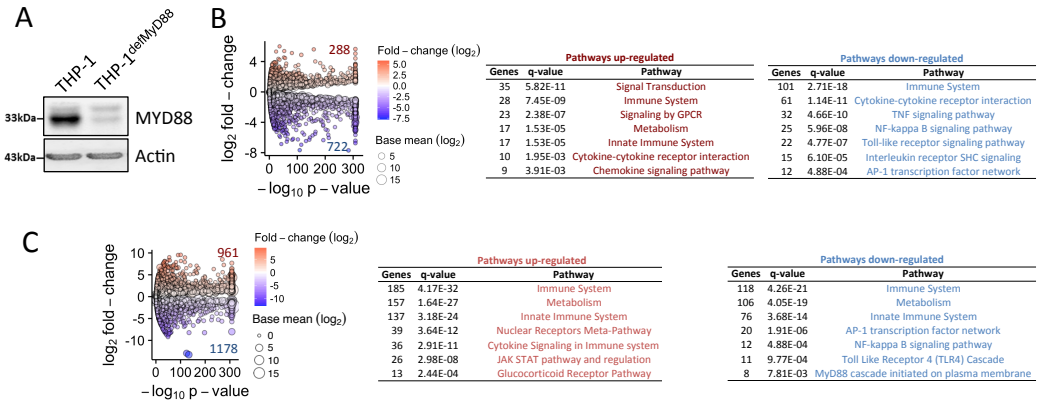

Pathways up-regulated

Genes	q-value	Pathway
35	5.82E-11	Signal Transduction
28	7.45E-09	Immune System
23	2.38E-07	Signaling by GPCR
17	1.53E-05	Metabolism
17	1.53E-05	Innate Immune System
10	1.95E-03	Cytokine-cytokine receptor interaction
9	3.91E-03	Chemokine signaling pathway

Pathways down-regulated

Genes	q-value	Pathway
101	2.71E-18	Immune System
61	1.14E-11	Cytokine-cytokine receptor interaction
32	4.66E-10	TNF signaling pathway
25	5.96E-08	NF-kappa B signaling pathway
22	4.77E-07	Toll-like receptor signaling pathway
15	6.10E-05	Interleukin receptor SHC signaling
12	4.88E-04	AP-1 transcription factor network

Pathways up-regulated

Genes	q-value	Pathway
185	4.17E-32	Immune System
157	1.64E-27	Metabolism
137	3.18E-24	Innate Immune System
39	3.64E-12	Nuclear Receptors Meta-Pathway
36	2.91E-11	Cytokine Signaling in Immune system
26	2.98E-08	JAK STAT pathway and regulation
13	2.44E-04	Glucocorticoid Receptor Pathway

Pathways down-regulated

Genes	q-value	Pathway
118	4.26E-21	Immune System
106	4.05E-19	Metabolism
76	3.68E-14	Innate Immune System
20	1.91E-06	AP-1 transcription factor network
12	4.88E-04	NF-kappa B signaling pathway
11	9.77E-04	Toll Like Receptor 4 (TLR4) Cascade
8	7.81E-03	MyD88 cascade initiated on plasma membrane

Figure 21: Differential expression analysis of MyD88 knockdown and GR activation in activated macrophages. **A**: Western blot analysis of THP1-XBlue-defMyD and THP-1 cells confirmed markedly decreased Myd88 protein levels. Analysis was carried out in triplicates. The knock-down efficiency was >90% determined by qPCR analysis (not shown). **B**: Volcano plot representation of differentially expressed genes (population RNA-seq data) determined with activated macrophages compared to activated macrophages with MyD88 deficiency (LPS vs. $LPS^{defMyd88}$). Tables show significantly enriched pathways for up-regulated genes (left) and down-regulated genes (right). **C**: Data visualization as in B determined with activated macrophages compared to activated macrophages additionally treated with 1 µM dexamethason (LPS vs. LPS+Dex).

regulated genes were associated to i.e. chemokine signaling and down-regulated genes significantly overlapped with classical inflammatory pathways, such as TLR signaling and NF-κB signaling (Figure 21B).

Effects of Dexamethasone (Dex), a synthetic activating GR ligand, rendered similar pathway enrichments in activated macrophages (Figure 21C). Anti-inflammatory effects of Dex-induced GR activation in macrophages are known (Meijsing et al. 2007). GR acts as a coordinating hub in anti-inflammatory responses via coordinated transcription factor-dominated regulatory networks (Chinenov et al. 2014). Beside down-regulation of genes involved in pro-inflammatory pathways, genes associated to nuclear receptor pathways and cytokine signaling were up-regulated (Figure 21C).

Integration of these population measurements with single-cell data allowed to dissect those genes with a potential involvement in macrophage heterogeneity. For activated macrophages deficient for MyD88 significant changes in transcriptome signatures were mainly found for pro-inflammatory state macrophages with striking

specificity (Figure 22A). Precisely, the majority of differentially expressed genes specific for pro-inflammatory cells was down-regulated in MyD88-deficient activated macrophages. Homeostasis-preserving cells and cells with anti-inflammatory profiles were less affected. However, anti-inflammatory state macrophages showed increased expression of IRAK3 and other anti-inflammatory mediators, suggesting that macrophages are shifted towards M2-like profiles.

In contrast, GR activation triggered a more specific regulation of smaller gene sets in pro-inflammatory cells (Figure 22B). These included down-regulation of NF-ϰB pathway genes (IL1B, IL8, IL18 and DUSP6) and up-regulation of inflammation-limiting factors (i.e. ADAM28, ACSL1, MAFB) and macrophage polarization pathways (i.e. PPAR signaling pathway, and, FOXO signaling and NRF2 pathway). This is intriguing from a functional perspective. For example, the metalloproteinase ADAM28 is a sheddase of TNF-α implicated in negative regulation of inflammation in obesity and type 2 diabetes (Jowett et al., 2012). Similarly, ACSL1 protects macrophages from the inflammatory effects in diabetes models (Kanter et al. 2012). Activation of MAFB was shown to directly influence macrophage M1/M2 polarization balance and to induce alternative macrophage fates (Bakri et al. 2005).

Intriguingly, highly significant changes were observed for genes specific for anti-inflammatory cells upon Dex treatment. SOCS2, JAK2, FKBP5 and IRAK3 expression was up-regulated (Figure 22B). An important role for SOCS2 in driving M2 polarization and limiting M1 polarization has been shown (Wilson 2014). Contrary, genes of the NCAM1 interactions pathway were down-regulated in anti-inflammatory cells, indicating attenuation of cell adhesions in these cells.

In summary, both functionally investigated factors had a significant impact on state-specific gene expression, indicating a shift from M1-like to M2-like macrophages. While MyD88, as an required adapter protein for TLR-4 signaling, was highly specific for pro-inflammatory cells only, GR, as a major regulator of transcription factor networks, influenced both pro- and anti-inflammatory state macrophages.

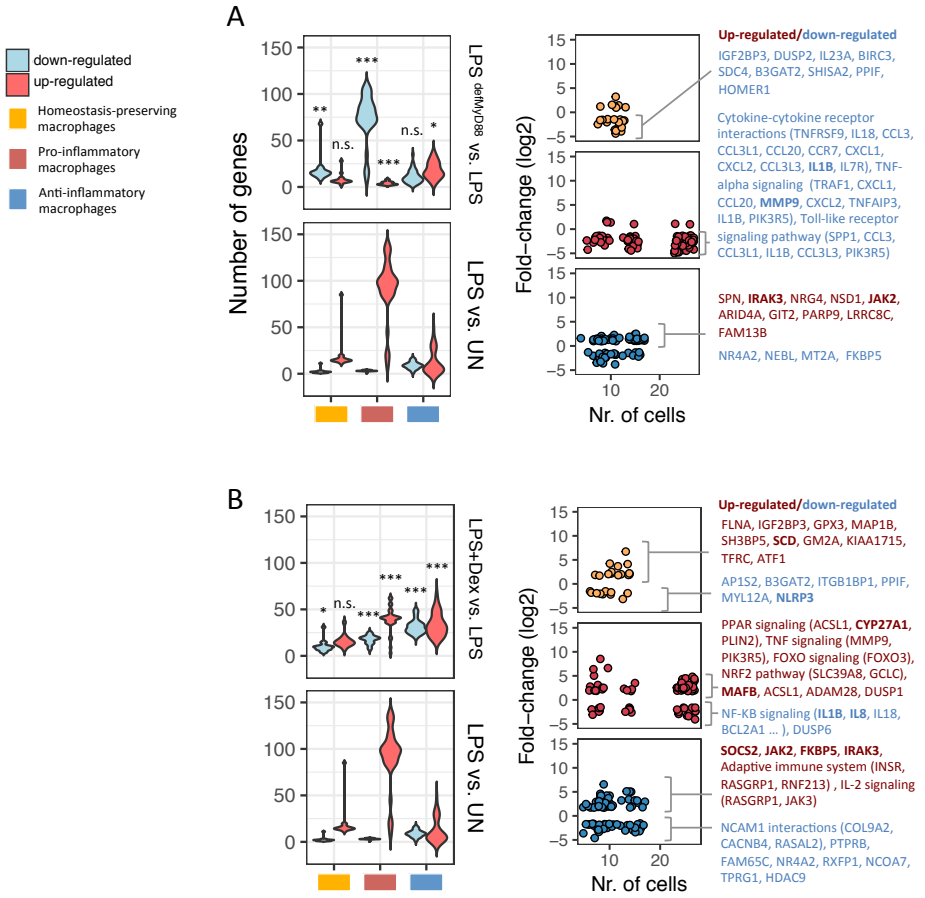

Figure 22: State-specific gene expression upon MyD88 knockdown or GR activation. **A** and **B**: Data analysis for THP1-XBlue-defMyD cells (stable MyD88 knockdown) treated with 100ng/ml LPS for two hours (**A**) and THP-1 cells treated with LPS and 1µM dexamethason. Analysis was done as described for responsiveness estimation (see 3.6, Figure 14 and Materials and methods 2.2.8). Briefly, differential expression data (LPS vs. $LPS^{defMyD88}$and LPS vs. LPS+Dex) from population RNA-seq was joined to cell-specific genes. Data was compared to the same analysis carried out with RNA-seq data from the comparison of resting macrophages and activated macrophages (LPS vs. UN). *Violin plots* show the number of cell-specific differentially expressed genes *per cell* for each macrophage state. Thus, every underlying data point represents a cell. Statistical analysis was done with one-way ANOVA followed by Dunn's multiple comparison test (n.s. p-value > 0.05; * p-vale < 0.05; ** p-value < 0.01; *** p-value < 0.001). *Scatter plots* show *genes* in respect to their fold-change ($\log_2$) vs. the number of cells the gene is expressed in (cell-specific genes) for each macrophage state. Selected genes are shown in blue (down-regulated) and red (up-regulated).

3.12 Different macrophage morphologies correlate with state-specific gene expression

Differentiated macrophages exhibit distinct heterogenous morphologies, including cells with round and flattened properties and increased size and granularity (Figure 23A). In contrast, macrophages deficient for Myd88 showed a round shape (Figure 23B). Similarly, macrophages treated with Dex shifted over time towards a small round morphology, comparable to monocytes, and showed reduced numbers of flattened shaped macrophages (Figure 23C). However, compared to monocytes these cells stayed attached and viable and did not float in the cell culture medium. Similarly, macrophages develop towards this small/round morphology after polarization with i.e. IL4 (Buchacher et al. 2015, Vogel et al. 2014).

FISH data was analyzed to evaluate if big/flattened macrophages and small/round macrophages show M1-like and M2-like gene expression, respectively. Strikingly, activated macrophages expressing IL1B showed a significant bigger and more elliptic shape (higher eccentricity) compared to cells expressing anti-inflammatory marker genes (Figure 23D and E). No significant differences were found if IL1B cells were compared to cells expressing GAPDH (Figure 23E). Although not computationally evaluated, images from macrophages treated with LPS for up to two days indicated that these differences between both morphological states manifest over time (compare Figure 23A, Figure 23C and Figure 23F). Live-cell imaging revealed that some macrophages (untreated) change between morphological states while others remain in one morphological state over time (Figure 24). Similarly, this was observed for primary human macrophages (not shown).

Together, these results suggest that macrophage morphology is a proxy for a cell's transcriptional M1-like or M2-like identity. Consequently, M1-like or M2-like states are to some extend transient and conferable to resting macrophages. However, a more sophisticated computational analysis is required to investigate this aspect of macrophage dynamics over time in more depth.

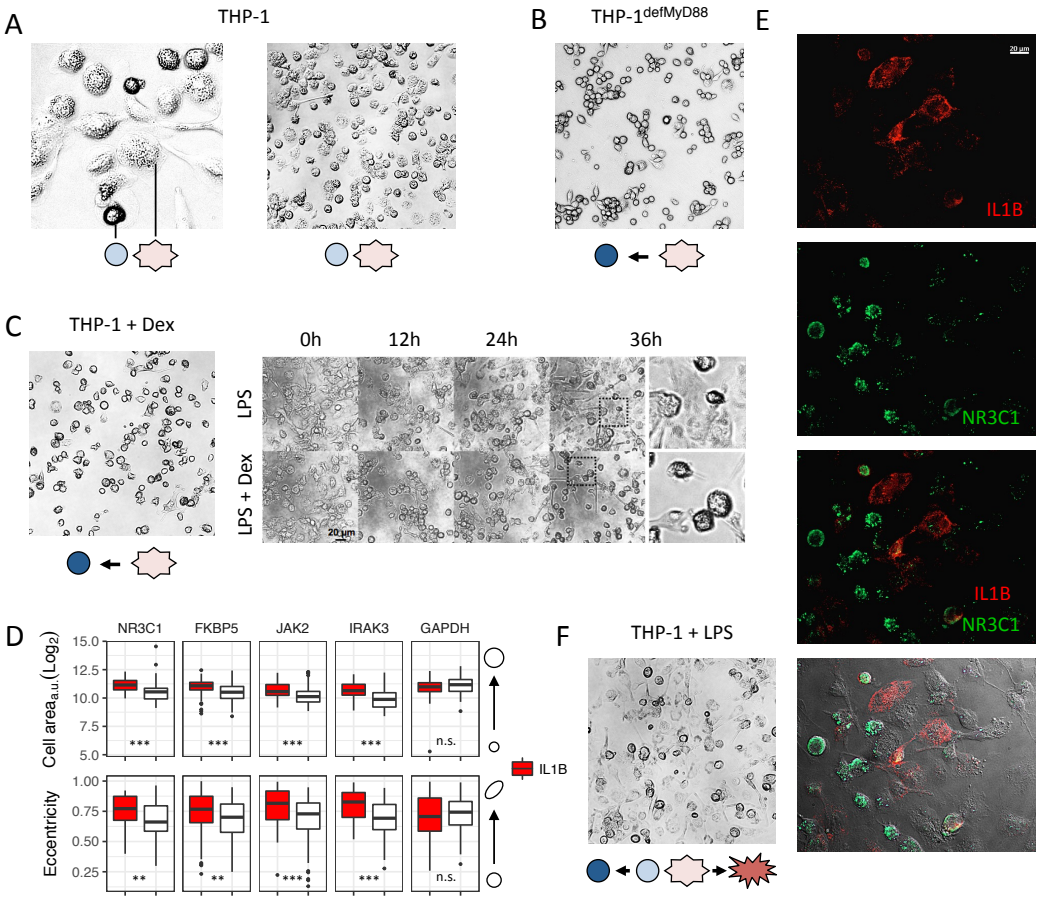

Figure 23: Macrophage morphology as a proxy for state identity. **A**: 72 hours differentiated THP-1 macrophages. **B**: Differentiated THP1-XBlue-defMyD cells. **C**: Bright field microscopy images were acquired in one hour intervals at constant positions. Macrophages were treated with 100ng/ml LPS or with addition of 1µM Dexamethason. Left image shows cells stimulated for 48 hours. **D**: Quantification of cell size (arbitrary units) and eccentricity (0 = circle, 1 = ellipse) for cells with high expression for indicated genes. The red box plots represent data from IL1B positive cells. White box plots represent data from cells with high expression of genes indicated at the top. Statistical analysis was done with one-way ANOVA followed by Dunn's multiple comparison test (n.s. p-value > 0.05; ** p-value < 0.01; *** p-value < 0.001). **E**: FISH analysis example picture recorded for IL1B (red) and NR3C1 transcripts (green). Bottom image shows merged image of fluorescence channels and differential interference contrast images. 20 Z-stacks were recorded and images were deconvoluted. **F**: Bright field images from THP-1 cells 48 hours after stimulation with 100ng/ml LPS. Light blue and dark blue circles indicate unstimulated and stimulated M2-like cells, respectively. Light red and dark red circles indicate unstimulated and stimulated M1-like cells, respectively.

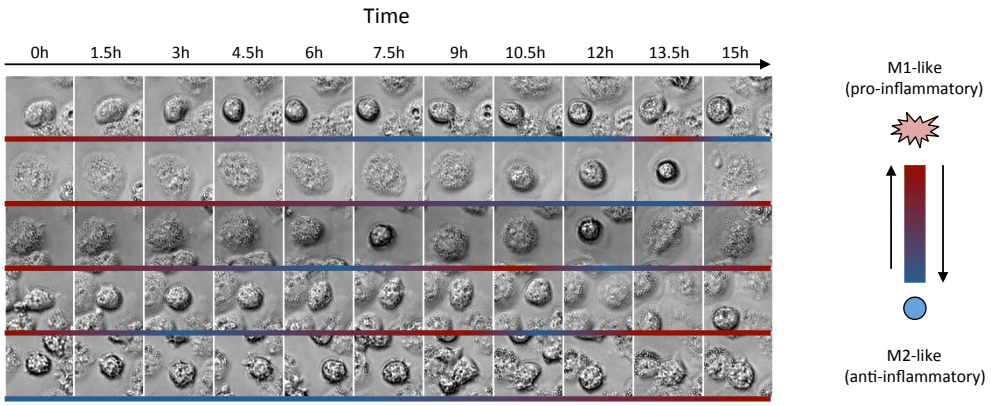

Figure 24: Macrophages show dynamic morphology transitions. Representative bright field live-cell tracking results for resting cells with changing morphological properties. Image acquisition was done every 2 minutes in Z-stack mode for a time period of 16 hours. Individual images shown were derived manually and by using EBimage (Pau et al. 2010). Red gradients highlight M1-like morphology and blue gradients highlight M2-like morphology.

Chapter 4

Discussion

Heterogeneity between individual cells is a common feature of dynamic cellular processes, including signaling, transcription, and cell fate (Elowitz et al. 2002). Even simple visual observations of the diverse morphologies of macrophages suggest that heterogeneity is an intrinsic property of those cells. How macrophages integrate signals from bacterial pathogen-associated molecular patterns (PAMPs) to determine cell fate is fundamental to understanding infection biology and finding novel treatment options for acute and chronic inflammatory disease.

Various diseases, such as atherosclerosis, allergy, autoimmune disorders and cancer, are associated with or caused by M1- or M2-like macrophage responses (Mills 2012). Changing the M1/M2 balance promise therapeutic potential. In case of atherosclerosis, research suggests that M2 macrophages are athero-protective by promoting efficient clearance of apoptotic cells within atherosclerotic plaques and resolution of inflammation (Chinetti-Gbaguidi et al. 2015). However, the simplified view of pro-inflammatory M1 macrophage as "Fight" (bad) versus anti-inflammatory M2 macrophage "Fix" (good) seems too short-sighted. For example in cancer, intratumor macrophages show primarily M2-like characteristics and promote tumor progression and the presence of intratumor M1 macrophages is very favorable for survival (Yamaguchi et al., Ohri et al. 2009, Williams et al. 2016). Because of health implications in various settings, a sustainable knowledge of macrophage heterogeneity may help to understand macrophage-associated diseases and to develop diverse therapeutic strategies.

The here established generation and in-depth analysis of transcriptomic data sets of single human macrophages, provides a step forward to characterize how macrophages integrate signals from their local microenvironment under inflammatory and non-inflammatory conditions. Traditionally, macrophage phenotypes were studied with polarization model systems. Macrophage phenotypes can be induced by stimulation with IFNγ/LPS into pro-inflammatory M1 state macrophages or by stimulation with i.e. IL4 and IL13 into anti-inflammatory M2 state macrophages that promote healing processes (Nathan et al. 1983, Stein et al. 1992). Macrophages usually derive these signals from T helper cells. Whether M1 and M2 macrophages are discrete subtypes opposed to ends of a continuum of functional states is incompletely evaluated. For example, whether the M1 cells are directly repolarized to M2 rather than cleared to make way for new monocyte-derived M2 cells remained unknown. We are only beginning to gather evidence that supports, that M1/M2 state dichotomy exists in the absence of adaptive immune signals.

4.1 Macrophages feature three transcriptional states

Computational analysis of single-cell transcriptome profiles of resting and activated macrophages, suggested the presence of three functionally related macrophage states. These states were initially characterized according to pathway annotations. Two of these states showed overall M1-like (pro-inflammatory) or M2-like (anti-inflammatory) transcriptional profiles. In contrast, a third state showed transcriptional profiles similar to unpolarized M0-like macrophages (homeostasis-preserving).

Based on previous research, the presence of macrophage states with M1-like and M2-like transcriptome signatures in isogenic THP-1 macrophages, represents a rather unexpected finding. Evidence for distinct transcriptional states was supported by clustering analyses of cell-to-cell correlations matrices. This analysis suggested three sub-clusters for both resting and activated macrophages, respectively (Figure 7C, Figure 8E and Figure 9A). Clustering of gene expression vectors illustrated distinct transcriptional signatures for the different states (Figure 10A).

ICA-projection of state-specific gene expression data revealed spatially distinct densities of local over-expression areas, co-occurring with defined macrophage states (Figure 10C).

Several observations supported that macrophage states for resting and activated macrophages are associated with each other. Overlap of state specific-genes and pathways showed significant relations and similar gene expression distributions (Figure 10E, Figure 11 and Figure 12). Single-cell transcriptomes analyzed with multivariate approaches applying ICA and t-SNE, also indicated these relationships by the close distance or similar behavior of cells from associated states (Figure 9C and D). More general measurements showed similar *trends* of distributions, underlining state associations, including data from shrinkage t-score statistics, state-stability, intra-cluster correlation and pathway entropy (Figure 11C and D, Figure 15A and C and Figure 16C).

In summary, functional annotations of genes and pathways and different multivariate distance measures indicate distinct transcriptional profiles inherent to macrophage heterogeneity. These profiles are related to the known macrophage M1/M2 dichotomy and were used as a conceptual framework to aid further characterization of macrophage dynamics (Figure 25). Especially, the term 'M1-like state' for a group of resting macrophages seems counterintuitive. However, this terminology was used based on the following observations. The M1-like state in resting macrophages showed state-restricted expression of genes related to inflammatory pathways (i.e. Toll-like receptor pathway, Figure 12). The genes matching these pathways represent factors involved in general control and limiting of inflammation (i.e. TNFAIP3, IKBKB and PIK3). Expression of classical pro-inflammatory effector genes was absent (i.e. IL1B, IL8 and CCL4). Moreover, differential pathway analysis revealed additional M2-like pathway terms in resting macrophages for this particular state (i.e. IL4-signaling, Figure 13A). Thus, this state was classified as M1-like state with pro-inflammatory potential.

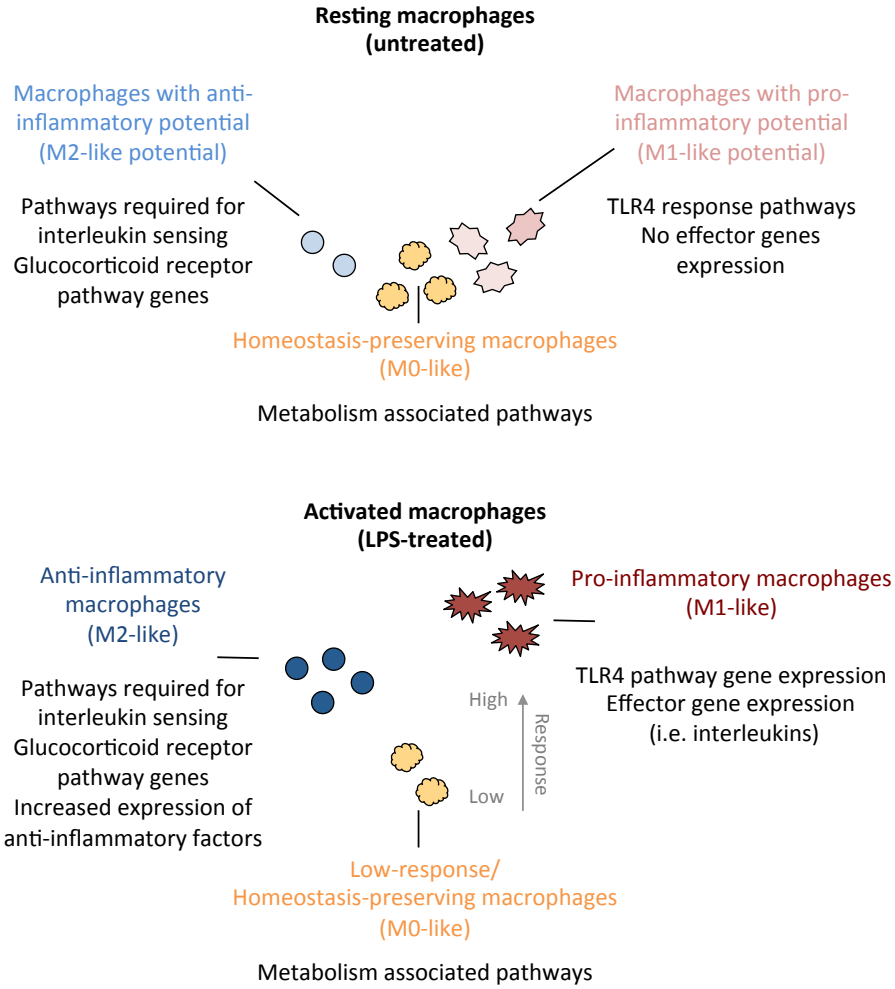

Figure 25: Model of macrophage states for resting and activated macrophages. Macrophages exist in three transcriptional states with M0-like, M1-like and M2-like gene expression for resting and activated macrophages. Stimulation with LPS leads to pro-inflammatory effector gene expression in M1-like macrophages (high response) and increased expression of anti-inflammatory factors in M2-like macrophages (medium response). M0-like macrophages show low response upon stimulation.

4.2 Increasing evidence supports the model of intrinsic M1/M2 dichotomy

The work presented here and recent single-cell transcriptomics studies in dendritic cells (DCs), mouse macrophages and primary human macrophages, similarly suggested the presence of M1-like and M2-like macrophage states independent of signals from other immune cells (Shalek et al. 2014, Saliba et al. 2016, Gierahn et al. 2017).

On the basis of functional and phenotypical characteristics, DCs and macrophages are closely related. Shalek et al. found substantial variation between identically stimulated DCs and identified co-expression modules with antiviral gene expression in addition to pro-inflammatory modules (Shalek et al. 2014). These modules contributed to separation of distinct states for DCs upon LPS-stimulation. Using functional experiments, Shalek et al. showed that found cellular heterogeneity depends to a large extend on paracrine cell-to-cell communication.

Using single-cell mRNA-seq, to analyze mouse bone-marrow-derived macrophages, exposed to *Salmonella typhimurium,* Saliba et al. explained the observed macrophage heterogeneity by pathogen grow rates. Infected macrophages with non-growing *Salmonella* showed markers of pro-inflammatory M1-like macrophages and macrophages containing growing bacteria showed anti-inflammatory, M2-like state expression signatures. The authors did not observe M1/M2 polarization in non-infected macrophages analyzed (n=15). Saliba et al. speculated that intracellular *Salmonella* drive those macrophages unable to clear the infection away from the hostile M1 to the more permissive M2 polarization state (Saliba et al. 2016).

A recent study from Gierahn et al. matched most closely to the model system studied in this work. These authors found three macrophage clusters by analyzing ∼2.500 $CD14^+$ PBMC-derived primary human macrophages that were left unexposed or were exposed to *Mycobacterium tuberculosis*. Found macrophage states were not excessively analyzed and only a small number of expressed genes was defined as cluster-specific (growth, hypoxia and metabolism). Clusters from exposed and non-exposed macrophages were highly overlapping and, especially two

of the clusters, did not show strong stimulation-dependent separation (Gierahn et al. 2017).

Together, the work presented here, and studies of Saliba et al. and Gierahn et al. represent initial evidence that M1-like and M2-like transcriptional profiles are inherent parts of macrophage heterogeneity. Although not specifically emphasized by Gierahn et. al., observations of overlapping states from untreated and treated macrophages suggest that macrophages might intrinsically separate towards M1/M2 phenotypes with pro- and anti-inflammatory potential. For the *ex vivo* model system used by Saliba et al. and Gierahn et al., a predetermination of monocytes cannot be ruled out. The *in vivo* collected macrophages may have experienced signals from other immune cells at the monocytic state before blood collection. However, predetermination by other immune cells can be secluded in case of here applied THP-1 macrophages, supporting that M1/M2 dichotomy is a common principle to explain macrophage heterogeneity.

4.3 External cues shape macrophage state dynamics towards segregate populations

Although functionally related, associated states of activated and resting macrophages showed differential responsiveness in gene expression profiles and annotated pathways (Figure 13). Upon LPS-induced activation, pro-inflammatory state macrophages showed around hundred differentially expressed genes, including known pro-inflammatory effector genes (Figure 14C-F). Contrary, anti-inflammatory state macrophages were characterized by lower responsiveness and expression of anti-inflammatory factors. In contrast, homeostasis-preserving cells showed low responsiveness comparable to resting macrophages.

In concordance with the observed transcriptional response, macrophage heterogeneity was markedly shaped upon stimulation. Synchronization of cells from each of the responsive states increased and signaling entropy decreased suggesting more deterministic signal transduction (Figure 15C and G). Together, these results suggest that states of resting macrophage transit from uncorrelated variation (unstable) towards highly correlated intra-state variability (stable) in activated

macrophages, assumingly to shapen functionally distinct cellular states (Figure 26A).

Analysis of state-specific macrophage gene expression indicated mutually exclusive expression of competing gene-regulatory factors. Gained knowledge in cell biology research often relies on analyses of population assays, based on the assumption of homogenous cells populations. Thus, fundamental regulatory features such as competitive inhibition of transcriptional regulation within a cell have been postulated for numerous phenomena, thereby reinforcing the viewpoint that individual cells might be able to supply intracellularly all required functionalities. This perception is in part challenged by the partly mutually exclusive segregation of functional macrophage state signatures and targeted experiments observed here (Figure 18). Instead, cellular heterogeneity with more or less distinct subpopulations with different functional capacities may act synergistically together to generate higher-level population functions. Mutual expression under increasing doses of LPS stimulation, as shown for NR3C1/IRAK3 vs. IL1B/HIF1A, underline a stimulus-depended shift towards an increasing number of both M1-like and M2-like macrophages, possibly accompanied by a decreased number of low-response macrophages (Figure 20A and Figure 26B). Together, gene expression dynamics were observed as all-or-none (digital) activation outcomes as previously observed in 3T3 mouse fibroblasts and mouse macrophages (Tay et al. 2010, Liu et al. 2014).

Analysis of state-specific gene modules allowed to define central molecular hubs that operate in several macrophage states or classify dominant molecular switches for both opposing sides of the macrophage spectrum. Thereby, glucocorticoid receptor (GR, NR3C1) was identified as a major molecular switch, which once induced by dexamethason, can shift the macrophage population towards an M2-like transcriptional and morphological status (Figure 22B and Figure 23C). Similarly, macrophage population transition towards an M2-like status was observed if TLR4 pathway activity was impaired by MYD88 knock down (Figure 22A, Figure 23B and Figure 26C). These observations helped to link single-cell transcriptome signatures to observable morphological phenotypes of macrophage cells using FISH analysis (Figure 23D and E). Having learned how macrophage morphology is linked to macrophage states, finally will allow to interpret macrophage shape transitions

over time, suggesting that macrophage states are transient transition events . This shows that macrophages not terminally differentiate to fixed M1-like or M2-like polarization states but are highly flexible in reacting towards signaling events in micro-environments to maintain a balanced and robust cell population. However, more work is required to validate these observations with independent methods i.e. by detecting marker gene expression with long-term live cell imaging (Skylaki et al. 2016). Thus, efficient inhibitory gene regulation mechanisms seem to exist that either keep macrophages in a pro-inflammatory or in an anti-inflammatory state. Digital signaling with mutual exclusive expression characteristics may enhance robustness of cellular decisions in noisy environments.

4.4 Concluding remarks

The results presented in this work, along with other single-cell studies published, highlight the value of high-throughput transcriptome-wide quantitative measurements with single-cell resolution to shed some light on consequences of cellular heterogeneity. It is crucial to anticipate that single-cell sequencing measurements only represent a snapshot in time. In addition to the loss of temporal information, the spatial context of cell ensembles in micro-environments is obscured, once cells are collected for sequencing analysis. Responses to receptor stimulation is encoded by the spatial and temporal dynamics of downstream signaling networks. Therefor, processes that are actually spatially separated in different cell populations are hard or impossible to be deconvoluted (Achim et al. 2015). But for understanding immune cell dynamics, time and space constitute major determinators that need to be addressed to guide understanding of regulation of heterogeneity (Kholodenko 2006). Interestinlgy, novel strategies are being developed to integrate these important aspects with single-cell omics datasets:

To measure temporal dynamics, a combination of single-cell omics derived candidate factors may be investigated by sophisticated live-cell imaging strategies (Junkin et al. 2016). New methods are being developed that combine live-cell imaging, dynamic stimulation and subsequent single-cell sequencing preparation with microfluidics technologies (Wills et al. 2017). Approaches to temporally

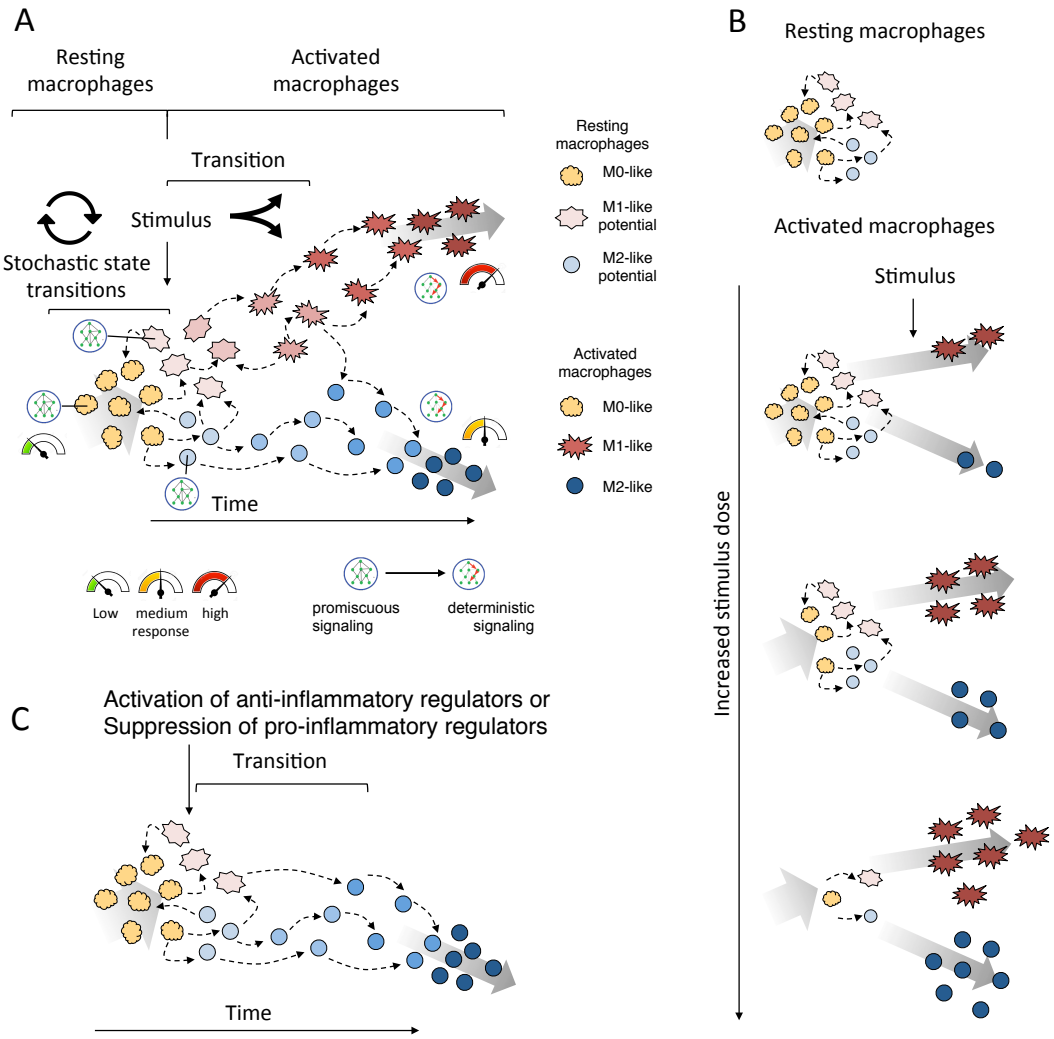

Figure 26: Proposed models of macrophage state dynamics. A: Unstimulated (resting) macrophages exhibit states with promiscuous signaling dynamics (stochastic state transition). Upon stimulation M1-like and M2-like macrophages show high gene expression response and deterministic signaling (transition). M0-like macrophages remain low in gene expression response. **B**: Increased stimulus doses lead to increased number of macrophages that show characteristic M1-like or M2-like gene expression and morphology. **C**: Activation of anti-inflammatory regulators or suppression of pro-inflammatory regulators promotes the transition towards M2-like macrophages.

resolve single-cell dynamics often depend on sophisticated equipment. Contrary, integration of spatial information may be accomplished by computational methods. Analysis strategies for spatial "back-mapping" of cells locations in complex tissues or even in more artificial micro-environments have been developed. For example, Satija and co-workers developed a computational strategy to infer cellular localization by integrating single-cell mRNA-seq data with *in situ* RNA patterns in zebrafish embryos (Satija et al. 2015).

In this work, the dynamic response of macrophages towards external signals was initially investigated descriptively by the use of guilty-by-association approaches. While, these approaches are helpful to predict functional factors that control cellular processes, they do not not imply causation. Although, some aspects of spatial, temporal and functional dynamics were tackled in this work, it is important to consider possible limitations and pitfalls of data interpretation. Several aspects need further evaluation to guide a better understanding. These include for example the following aspects: i) Experimental evaluation of factors that control defined homeostasis-preserving cells. ii) Revealing the vectors that define macrophage states in the absence of stimulation. iii) Identification of fundamental cues that initiate macrophage dichotomy. Instead of suggesting definite regulators that drive macrophage population behavior, this work shall rather depict basic properties of macrophage heterogeneity in an simplified *in vitro* framework to guide interpretation of heterogeneity *in vivo*. Thus, this work, provides insights into basic modes of macrophage dynamics to optimal strategies of a population adapting to a changing, i.e. pathogenic environment.

Chapter 5

Summary

Phenotypic and functional flexibility is a key feature of immune cells such as macrophages, instrumental to their functions in pathogen defense and to maintain homeostasis. Traditional population average measurements have been widely applied to characterize macrophage diversity. But population average measurements obscure the underlying single-cell heterogeneity, and thus hinder an unbiased characterization of cellular response to external stimulation. Analyzing isogenic human THP-1 macrophages and primary human macrophages by single-cell RNA sequencing, we investigated cellular heterogeneity in the context of early innate activation, using lipopolysaccharide (LPS) as a defined stimulus. For resting and in particular for activated macrophages, significant differences in expression of central immune genes was observed in three macrophage states with pro-inflammatory (M1-like), anti-inflammatory (M2-like) and low-response homeostasis-preserving (M0-like) characteristics. Results from RNA-fluorescence *in situ* hybridization assays for selected transcripts suggest different morphological phenotypes for pro-inflammatory and anti-inflammatory macrophages. Macrophages flexibly switch between these phenotypes over time or shift towards one phenotype upon stimulations. Moreover, identified state-specific hub genes for pro- and anti-inflammatory cells, including hypoxia-inducible factor 1 (HIF-1) and glucocorticoid receptor (GR), respectively, revealed digital all-or-none gene expression response to potentially govern macrophage state balance. Notably, observed cellular states featured differential responsiveness and signaling dynamics after stimulation. While low-

response cells showed promiscuous signaling, the pro- and the anti-inflammatory cells showed high response and lower signaling entropy. Titration experiments suggest, that low-response macrophages act as a reservoir to allow transitions into pro- or anti-inflammatory cells under increasing doses of applied stimuli. In summary, the here shown analyses indicate cellular mechanisms to respond efficiently to external stimulation, by inducing cell state specific expression of genes. Holistic, single-cell based characterization of macrophage states might serve as a new framework to advance our understanding of cellular heterogeneity in general and for future research to explore mechanisms of physiological resilience in health and disease.

Kapitel 6

Zusammenfassung

Funktionelle Flexibilität ist eine entscheidende Eigenschaft von Makrophagen, um Krankheitserreger bekämpfen zu können und gleichzeitig Homöostase aufrechtzuerhalten. Um die damit einhergehende Diversität von Makrophagen mittels Transkriptom-Analysen zu messen, wurden bisher überwiegend Methoden eingesetzt, die keinen Rückschluss auf die Identität einzelner Zellen zulassen. Dies erschwert die unverfälschte Charakterisierung der tatsächlichen, heterogenen Makrophagenantwort. In dieser Arbeit wurden Sequenzierungsverfahren eingesetzt, welche die genomweite Analyse von Transkriptomen einzelner Zellen ermöglichen. Hierbei wurden humane THP-1 Makrophagen sowie primäre humane Makrophagen, die mit Lipopolysacchariden (LPS) behandelt wurden, als Modellsystem genutzt. Die Behandlung mit LPS dient als Stimulus, um die angeborene Immunantwort bei Makrophagen auszulösen und schließlich zu untersuchen. Bei stimulierten Makrophagen, und im schwächeren Ausmaß bei unbehandelten Zellen, wurden drei unterscheidbare Makrophagenpopulationen ermittelt. Diese Subpopulationen wiesen divergente Genaktivitäten auf, die sich mit der etablierten Einteilung von Makrophagen vergleichen ließen: Proinflammatorische M1-Makrophagen, antiinflammatorische M2-Makrophagen und kaum reagierende, homöostatische, M0-Makrophagen. Mittels Fluoreszenz-in-situ-Hybridisierung (FISH) konnte anhand ausgewählter Gene gezeigt werde, dass proinflammatorische und antiinflammatorische Makrophagen distinkte morphologische Phänotypen haben, zwischen denen sie, im zeitlichen Verlauf, flexibel wechseln können. Durch integrative Analysen

konnten zentrale, regulatorische Gene ermittelt werden, die für proinflammatorische oder antiinflammatorische Makrophagen spezifisch sind. Die Expression dieser Gene und deren Proteine (z.B. Hypoxie-induzierter Faktor 1 (HIF1) und Glukokortikoid-Rezeptor (GR)) hatten binären Charakter und trat im wechselseitigen Ausschluss in unterschiedlichen Zellen auf. Die Fähigkeit der Makrophagenpopulationen auf Signale zu reagieren war stark unterschiedlich. Proinflammatorische und antiinflammatorische Makrophagen zeigten starke Reaktionen gegenüber externen Signalen. Homöostatische Makrophagen wiesen hingegen eine sehr schwache Immunantwort auf. Experimente unter Applikation erhöhter Stimulierung, deuteten darauf hin, dass homöostatische Makrophagen als Reservoir für eine Umwandelung in Proinflammatorische oder antiinflammatorische Zellen dienen. Die hier durchgeführten Analysen weisen auf Mechanismen hin, welche die effektive Immunantwort von Makrophagen, durch ihre inhärente Heterogenität ermöglichen.

Chapter 7

Supplementary data

7.1 Supplementary figures

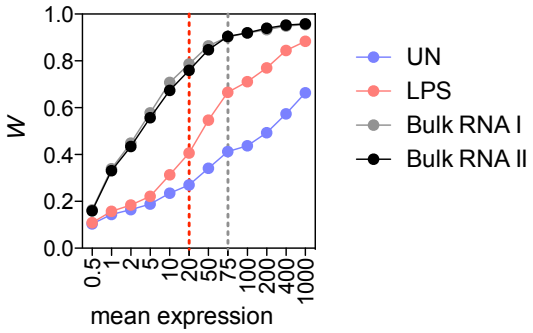

Figure 27: Estimation of gene expression cut-offs to select genes with high biological variability. Testing normality of gene expression distributions from single-cell RNA-seq data (UN: resting macrophages; LPS: activated macrophages) and population spike-in RNA data (Bulk RNA I and II). Shapiro–Wilk test (W) for normality for 12 bins of 100 genes ranging from low (left), middle (center) to high (right) expression values. W was obtained by averaging W of each gene within bins. $W \sim 1$ indicates expression values that are normally (Gaussian) distributed (Piras and Selvarajoo 2015). See Materials and methods for details (2.2.3). Dashed red line at mean count 20 indicates cut-off used for most analysis. Dashed grey line at mean count 75 indicates cut-off used for entropy analysis (Material and Methods 2.2.10).

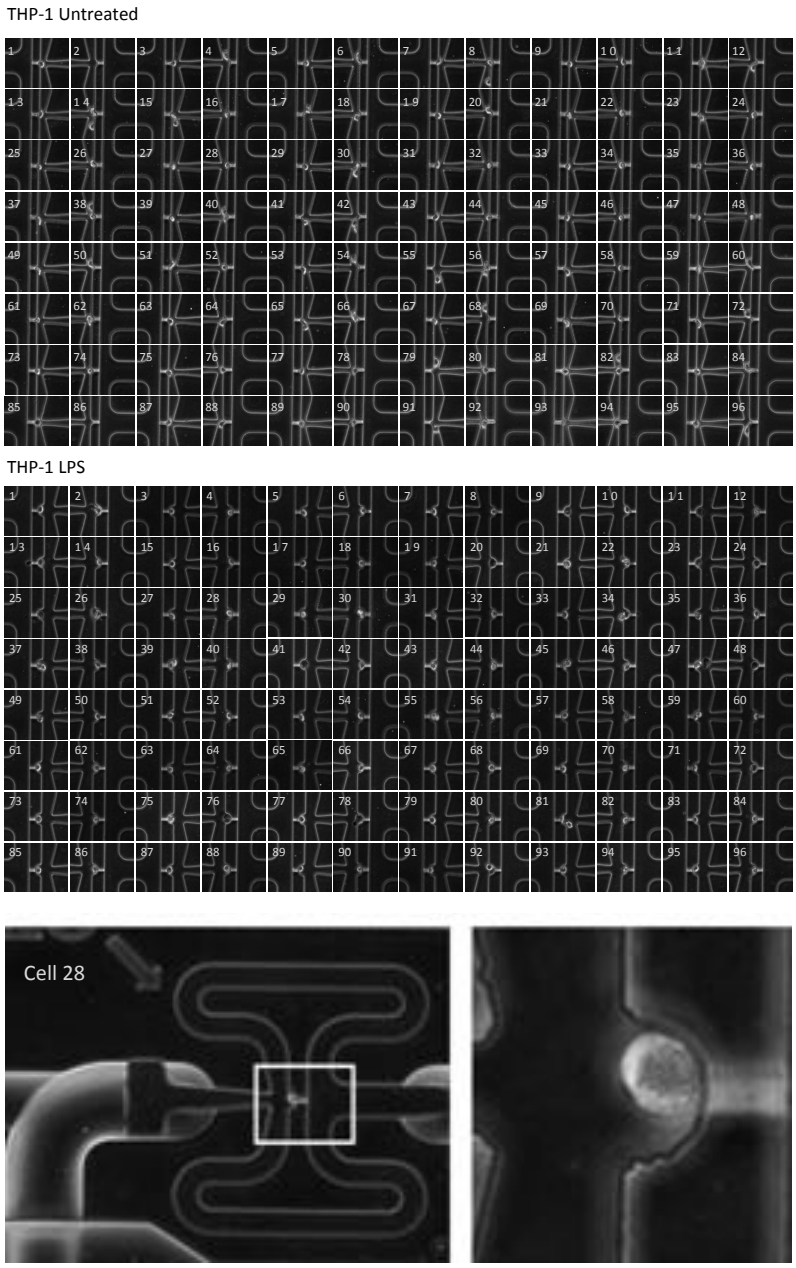

Figure 28: Microfluidic integrated fluidic circuit (IFC) micro-chamber screening. Images of cell-loaded microfluidic integrated fluidic circuit (IFC) micro-chambers used to evaluate cell integrity and successful loading of single cells.

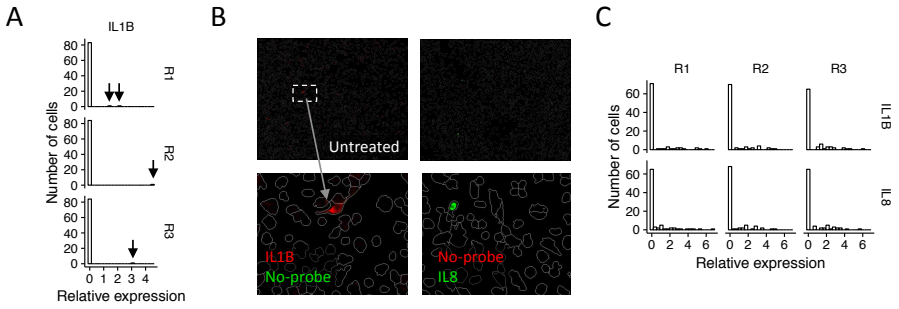

Figure 29: IL1B/IL8 expression in resting THP-1 macrophages and clonal expanded THP-1 macrophages. A: Rare events of IL1B/IL8 expression in resting macrophages. Single-cell qPCR results from detection of IL1B in resting macrophages (R1-3: replicated measurement from ∼88 cells). **B**: RNA-FISH analysis of resting macrophages. Spontaneous bursting of inflammatory gene expression in immune cells under untreated condition as observed by i.e. Diercks et al. 2009 linked to pervasive transcription (Wade and Grainger 2014). **C**: Single-cell qPCR results from detection of IL1B and IL8 in clonal expanded THP-1 cells.

.

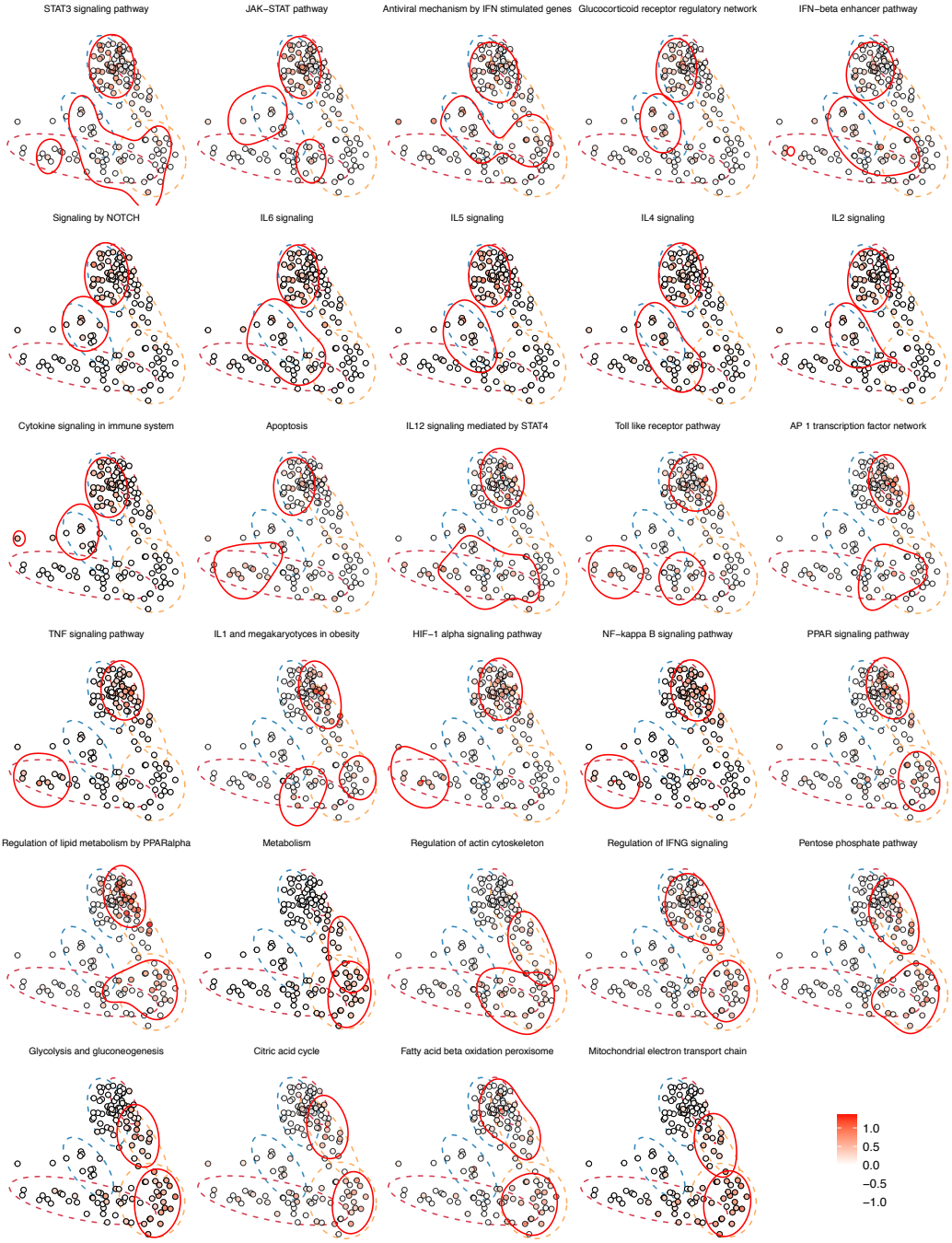

Figure 30: ICA projection of common pathways. ICA projection of gene expression from common pathways for activated and resting macrophages. Color gradient indicates mean expression levels of pathway-specific genes. White indicates low expression and red indicates high expression per cell.

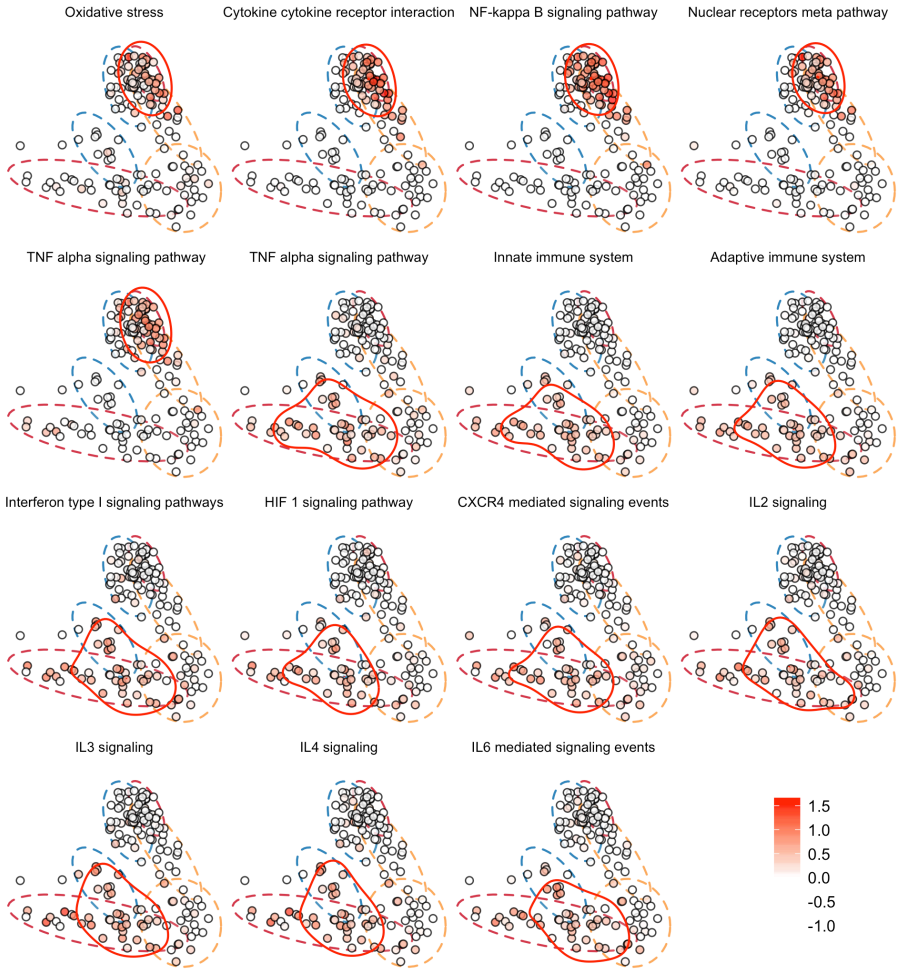

Figure 31: ICA projection of distinct pathways. ICA projection of gene expression from differential pathways of pro-inflammatory (activated) macrophages and macrophages with pro-inflammatory potential (resting macrophages). Color gradient indicates mean expression levels of pathway-specific genes. White indicates low expression and red indicates high expression per cell.

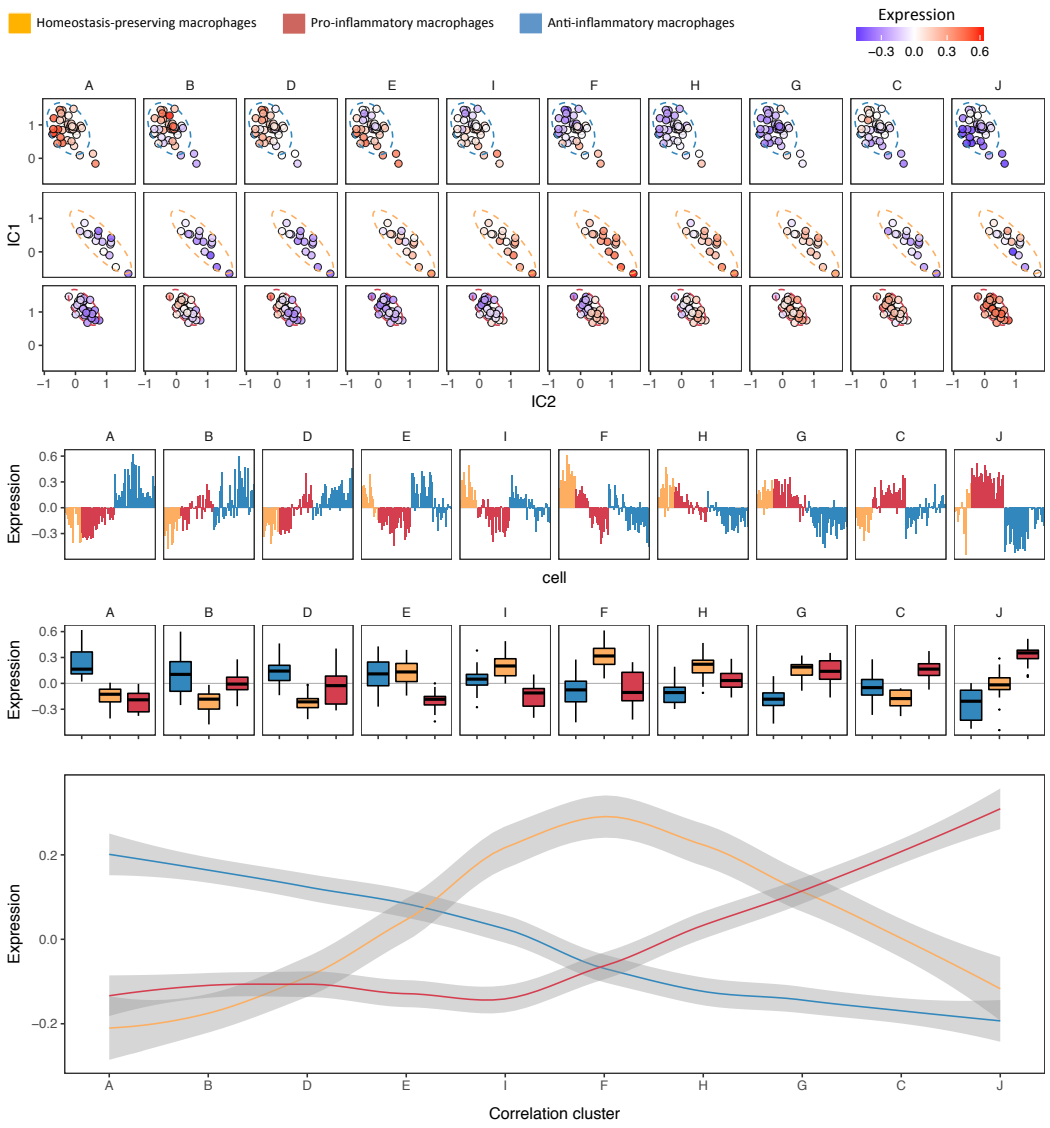

Figure 32: Gene regulatory modules of activated macrophages. Association of correlation cluster-defined gene regulatory modules to states of activated macrophages. First row: ICA projection of mean correlation cluster expression. Second row: Bar plot representation of mean correlation cluster expression per cell. Third row. Summarized expression for macrophage states. Fourth row: Alternative line graph visualization.

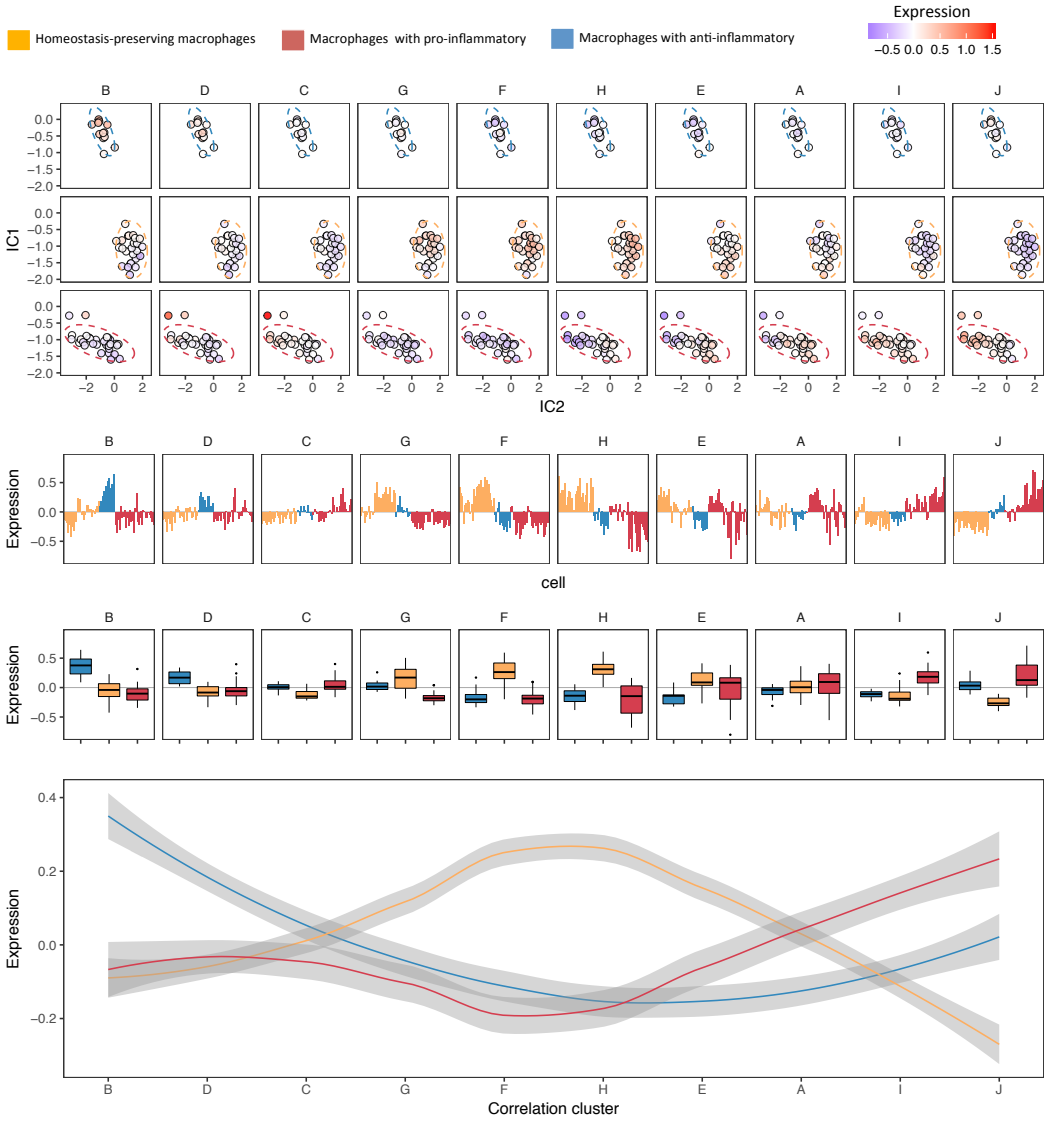

Figure 33: Gene regulatory modules of resting macrophages. Association of correlation cluster-defined gene regulatory modules to states of activated macrophages. First row: ICA projection of mean correlation cluster expression. Second row: Bar plot representation of mean correlation cluster expression per cell. Third row. Summarized expression for macrophage states. Fourth row: Alternative line graph visualization.

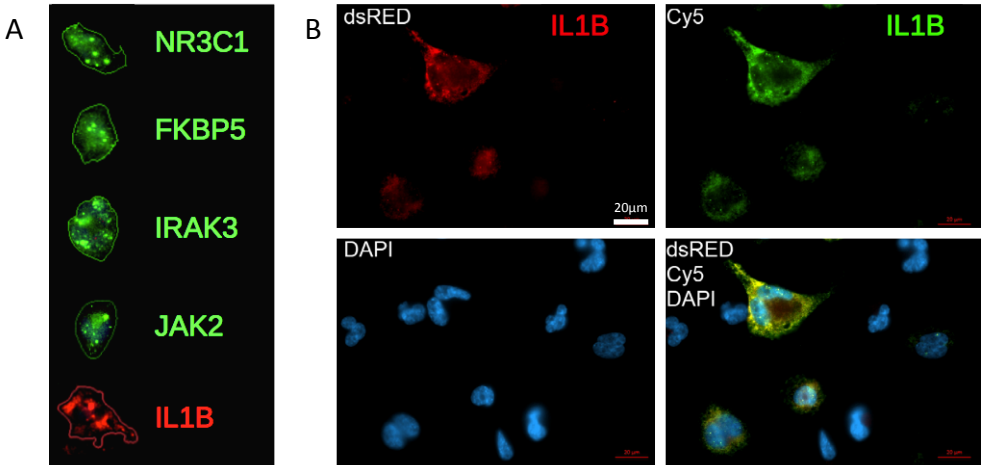

Figure 34: FISH double staining. A: Example cells, single-molecule detection. **B:** Double staining for the detection of IL1B. Images were taken with a Zeiss Z1 Observer wide-field fluorescence microscope with a 60x oil immersion objective (Materials and methods 2.1.14).

7.2 Supplementary tables

ID	UN	LPS	ID	UN	LPS	ID	UN	LPS	ID	UN	LPS
1	+	+	25	+	+	49	+	+	73	+	+
2	q	+	26	+	+	50	q	+	74	+	+
3	+	+	27	+	+	51	-	+	75	q	+
4	-	+	28	+	+	52	+	+	76	+	+
5	+	+	29	+	+	53	q	+	77	+	+
6	+	+	30	v	+	54	+	+	78	+	+
7	+	+	31	+	+	55	+	+	79	+	+
8	v	+	32	+	+	56	v	+	80	+	+
9	+	+	33	+	+	57	q	+	81	+	v
10	+	+	34	+	v	58	+	+	82	v	+
11	+	+	35	q	+	59	+	v	83	+	+
12	+	+	36	+	+	60	+	+	84	+	+
13	+	+	37	q	q	61	+	+	85	+	+
14	v	+	38	v	+	62	+	+	86	-	+
15	q	+	39	q	v	63	q	+	87	+	+
16	+	+	40	v	+	64	+	+	88	q	+
17	+	+	41	+	q	65	+	+	89	+	+
18	+	+	42	v	+	66	+	+	90	+	+
19	+	+	43	+	+	67	+	+	91	+	+
20	+	+	44	+	v	68	+	q	92	+	v
21	+	+	45	q	v	69	+	q	93	+	+
23	+	+	47	+	+	71	+	+	95	+	+
24	+	+	48	+	q	72	+	+	96	+	q

Table 2: Cell discrimination - Fluidigm IFC screening. Cells loaded in micro-chambers of Fluidigm C1 IFCs were microscopically observed (see Supplementary Figure 28 on page 107). Data from micro-chambers without cells (**-**), deformed cells, cell doublets or damaged cells was removed from further analysis (**v**). Data from micro-chambers with cells with low sequencing quality or low mean expression per cell was not considered for further analysis (**q**). Data from all remaining cells were used for further analysis (+). **ID** indicates the identifier of the micro-wells. **LPS** indicates activated macrophages. **UN** indicates resting macrophages (untreated).

Nr. of genes	q-value	Pathway	Source
122	6.12E-19	Signal Transduction	Reactome
109	4.24E-17	Immune System	Reactome
49	7.74E-13	Signaling by Interleukins	Reactome
44	1.86E-11	Metabolism	Reactome
42	5.95E-11	Adaptive Immune System	Reactome
38	7.26E-10	GPCR downstream signaling	Reactome
62	7.26E-10	Innate Immune System	Reactome
37	9.52E-10	Pathways in cancer - Homo sapiens (human)	KEGG
37	9.52E-10	Nuclear Receptors Meta-Pathway	Wikipathways
37	9.52E-10	Hemostasis	Reactome
60	9.94E-10	Cytokine Signaling in Immune system	Reactome
59	1.34E-09	Signaling by GPCR	Reactome
58	1.81E-09	Cytokine-cytokine receptor interaction - Homo sapiens (human)	KEGG
35	2.54E-09	JAK STAT pathway and regulation	INOH
35	2.54E-09	GPCR ligand binding	Reactome
34	4.76E-09	TNF signaling pathway - Homo sapiens (human)	KEGG
33	8.46E-09	Class A/1 (Rhodopsin-like receptors)	Reactome
33	8.46E-09	PI3K-Akt signaling pathway - Homo sapiens (human)	KEGG
32	1.60E-08	GPCR signaling-G alpha s PKA and ERK	INOH
31	2.65E-08	Developmental Biology	Reactome
31	2.65E-08	GPCR signaling-G alpha s Epac and ERK	INOH
31	2.65E-08	Metabolism of proteins	Reactome
31	2.65E-08	VEGFA-VEGFR2 Signaling Pathway	Wikipathways
30	4.51E-08	GPCR signaling-G alpha i	INOH
30	4.51E-08	GPCR signaling-pertussis toxin	INOH
30	4.51E-08	GPCR signaling-cholera toxin	INOH
30	4.51E-08	GPCR signaling-G alpha q	INOH
29	8.12E-08	Signalling by NGF	Reactome
29	8.12E-08	Gastrin-CREB signalling pathway via PKC and MAPK	Reactome
29	8.12E-08	Gene Expression	Reactome
28	1.52E-07	HTLV-I infection - Homo sapiens (human)	KEGG
28	1.52E-07	Signaling by PDGF	Reactome
27	2.95E-07	Axon guidance	Reactome
26	5.00E-07	miR-targeted genes in lymphocytes - TarBase	Wikipathways
26	5.00E-07	Fc epsilon receptor (FCERI) signaling	Reactome
26	5.00E-07	Signaling by SCF-KIT	Reactome
26	5.00E-07	Downstream signal transduction	Reactome
26	5.00E-07	Signaling by EGFR	Reactome
26	5.00E-07	Focal Adhesion-PI3K-Akt-mTOR-signaling pathway	Wikipathways
25	9.28E-07	NGF signalling via TRKA from the plasma membrane	Reactome
25	9.28E-07	Signaling by VEGF	Reactome
25	9.28E-07	DAP12 interactions	Reactome
24	1.69E-06	NF-kappa B signaling pathway - Homo sapiens (human)	KEGG
24	1.69E-06	Post-translational protein modification	Reactome
24	1.69E-06	Jak-STAT signaling pathway - Homo sapiens (human)	KEGG
24	1.69E-06	DAP12 signaling	Reactome
23	3.00E-06	Disease	Reactome
23	3.00E-06	Generic Transcription Pathway	Reactome
21	9.90E-06	Transcriptional misregulation in cancer - Homo sapiens (human)	KEGG
21	9.90E-06	TNFalpha	NetPath
21	9.90E-06	miR-targeted genes in muscle cell - TarBase	Wikipathways
21	9.90E-06	G alpha (i) signalling events	Reactome
21	9.90E-06	Signaling by Leptin	Reactome
20	1.66E-05	Metabolism of lipids and lipoproteins	Reactome
20	1.66E-05	Diseases of signal transduction	Reactome
20	1.66E-05	Photodynamic therapy-induced NF-kB survival signaling	Wikipathways
20	1.66E-05	Focal Adhesion	Wikipathways
20	1.66E-05	Transmembrane transport of small molecules	Reactome
20	1.66E-05	Peptide ligand-binding receptors	Reactome

Table 3: Pathway analysis for up-regulated genes. Genes from differential pathway analysis activated vs. resting macrophages (Log_2-Fold-change>2, p-value<0.001).

Nr. of genes	q-value	Pathway
31	6.80E-08	Signal Transduction
25	2.18E-06	Immune System
20	4.64E-05	Signaling by GPCR
18	0.000139236	Innate Immune System
17	0.000222778	Metabolism
15	0.000742594	GPCR downstream signaling
12	0.005092076	GPCR ligand binding
11	0.008911133	Metabolism of proteins
10	0.014257813	GPCRs, Class A Rhodopsin-like
10	0.014257813	Class A/1 (Rhodopsin-like receptors)
8	0.035644531	Transcriptional misregulation in cancer - Homo sapiens (human)
8	0.035644531	Adaptive Immune System
8	0.035644531	G alpha (i) signalling events
8	0.035644531	Developmental Biology
8	0.035644531	Rho GTPase cycle
8	0.035644531	Signaling by Rho GTPases

Table 4: Pathway analysis for down-regulated genes. Genes from differential pathway analysis activated vs. resting macrophages (Log_2-Fold-change<-2, p-value<0.001).

	LPS					UN				
Cluster	**Symbol**	**T.Score**	**p-value**	**Fdr**	**Mean expr.**	**Symbol**	**T.Score**	**p-value**	**Fdr**	**Mean expr.**
Cluster I	ACTB	3.57	8.3E-03	3.1E-02	1745	FTL	5.34	9.3E-05	6.9E-05	12055
	CD63	4.15	2.1E-03	1.6E-02	581	EEF1A1	6.32	3.8E-06	1.9E-06	5231
	HSPA8	5.38	6.9E-05	1.9E-03	536	B2M	6.72	8.5E-07	1.9E-06	4318
	ALDOA	4.3	1.5E-03	1.3E-02	432	CAPZA1	6.45	2.4E-06	1.9E-06	2488
	PLAUR	4.35	1.3E-03	1.2E-02	425	SH3BGRL3	5.75	2.6E-05	4.0E-05	1579
	PRDX1	3.78	5.2E-03	2.5E-02	387	UBXN11	4.84	4.0E-04	1.2E-04	870
	RP11-386G11.10	4.75	4.5E-04	6.4E-03	313	*HSPA8*	4.22	2.0E-03	3.8E-04	855
	TFRC	4.2	1.9E-03	1.5E-02	301	FCER1G	5.55	4.8E-05	4.0E-05	759
	SLC20A1	5.56	4.0E-05	1.6E-03	194	*RP11-386G11.10*	3.9	4.3E-03	9.6E-04	746
	SRP14	3.62	7.5E-03	2.9E-02	172	ANXA2	4.29	1.7E-03	3.8E-04	667
	SSR1	4	3.1E-03	1.9E-02	158	*ALDOA*	6.32	3.7E-06	1.9E-06	667
	BZW1	4.75	4.4E-04	6.4E-03	138	C6orf62	4.94	3.0E-04	1.2E-04	626
	CALM1	3.64	7.1E-03	2.9E-02	125	TMBIM6	4.3	1.6E-03	3.8E-04	611
	PRDX3	10.36	1.9E-14	2.4E-12	124	RHOA	4.58	8.1E-04	3.8E-04	536
	EIF3I	3.67	6.6E-03	2.8E-02	118	SRSF6	3.94	4.0E-03	9.6E-04	535
	PAPSS1	5.35	7.6E-05	1.9E-03	111	PPIA	6.92	4.1E-07	1.7E-06	499
	CYCS	3.49	9.8E-03	3.4E-02	107	CD164	4.07	2.9E-03	3.8E-04	468
	PSMB3	3.78	5.2E-03	2.5E-02	100	TSPYL1	8.58	3.4E-10	3.6E-08	467
	TAGLN2	3.82	4.7E-03	2.4E-02	93	ARPC4	5.55	4.9E-05	4.0E-05	461
	ERGIC3	5.54	4.2E-05	1.6E-03	82	S100A11	6.99	3.1E-07	4.6E-07	458
Cluster II	SOD2	5.48	4.2E-06	3.7E-07	4932	MT-ND3	4.56	8.4E-05	1.8E-03	854
	SPP1	6.16	2.4E-07	3.3E-08	4133	MTATP6P1	3.16	6.5E-03	1.9E-02	799
	TNFAIP2	5.34	7.3E-06	6.0E-07	4122	CTSD	3.41	3.3E-03	1.9E-02	228
	SAT1	7.83	5.1E-11	2.0E-11	2050	NUCKS1	3.29	4.6E-03	1.9E-02	169
	IL8	3.56	2.8E-03	9.1E-05	1959	MT-ATP8	3.48	2.7E-03	7.8E-03	96
	GREP	9.6	6.7E-16	7.0E-16	1617	GUK1	3.55	2.2E-03	7.8E-03	94
	CCL3	7.78	6.6E-11	2.3E-11	1412	NFE2L1	3.11	7.4E-03	1.9E-02	91
	Lnc-CCL18	7.68	1.1E-10	3.6E-11	1302	HDAC7	3.43	3.1E-03	7.8E-03	73
	MARCKS	7.3	8.8E-10	2.2E-10	982	DHRS9	3.11	7.3E-03	1.9E-02	67
	IL1B	5.66	2.0E-06	1.9E-07	956	ERP29	3.04	8.9E-03	2.0E-02	55
	ALCAM	6.94	5.9E-09	1.2E-09	878	MTND4P12	4.35	1.8E-04	2.3E-03	55
	FMNL2	7.49	3.3E-10	9.5E-11	585	MTRNR2L12	4.94	2.1E-05	1.8E-03	53
	CCL20	4.78	6.0E-05	3.7E-06	575	MTCO2P2	5.37	3.8E-06	6.0E-04	53
	HIF1A	3.42	4.1E-03	1.2E-04	554	RN7SK	3.67	1.6E-03	7.8E-03	52
	ITGB8	9	4.4E-14	2.7E-14	529	PTBP1	3.3	4.4E-03	1.9E-02	48
	PINLYP	5.08	2.0E-05	1.5E-06	467	RNASET2	3.48	2.7E-03	7.8E-03	47
	MMP9	6.11	3.0E-07	4.1E-08	461	LPAR2	3.75	1.2E-03	7.8E-03	44
	RIN2	5.22	1.2E-05	9.3E-07	455	CTD-2540B15.11	3.43	3.2E-03	7.8E-03	44
	TNFAIP6	9.09	2.4E-14	1.8E-14	451	HNRNPL	3.84	9.5E-04	7.3E-03	39
	NAMPT	6.02	4.3E-07	5.5E-08	449	MAN2B2	3.14	6.8E-03	1.9E-02	36
Cluster III	ARID2	4.17	1.3E-03	3.9E-04	1297	PNISR	3.66	3.0E-03	2.1E-02	519
	MYCBP2	5.07	9.5E-05	6.4E-05	500	RBM39	3.25	8.4E-03	2.9E-02	507
	ZNF117	5.07	9.4E-05	6.4E-05	334	N4BP2L2	3.89	1.6E-03	1.6E-02	462
	OGT	4	2.1E-03	4.9E-04	279	STAT2	4.4	3.6E-04	1.0E-02	420
	ANKRD36B	7.49	7.9E-09	3.7E-08	251	LUC7L3	3.25	8.3E-03	2.9E-02	325
	DAPP1	5.86	6.4E-06	9.7E-06	246	MARCH6	3.38	6.1E-03	2.9E-02	257
	ZNF292	4.21	1.2E-03	3.7E-04	221	INSR	3.2	9.5E-03	2.9E-02	199
	BMP2K	5.48	2.5E-05	2.3E-05	212	ANKRD36C	5.43	1.1E-05	4.2E-04	186
	RASA1	4	2.1E-03	4.9E-04	198	DOCK5	3.82	1.9E-03	1.6E-02	170
	INSL6	3.84	3.1E-03	6.2E-04	190	ASH1L	4.75	1.2E-04	3.9E-03	164
	JAK2	3.45	7.9E-03	1.2E-03	176	NEMF	3.61	3.4E-03	2.1E-02	135
	ANKRD36	5.75	9.7E-06	1.1E-05	163	ANKRD28	3.39	6.0E-03	2.9E-02	134
	PAQR3	4.74	2.7E-04	1.5E-04	162	*CCDC14*	4.24	5.9E-04	1.6E-02	120
	CCDC14	4.38	7.4E-04	2.9E-04	157	RC3H1	3.79	2.1E-03	1.6E-02	116
	FKBP5	4.47	5.7E-04	2.5E-04	138	*RASA1*	3.57	3.8E-03	2.9E-02	114
	TNRC6B	4.05	1.8E-03	4.6E-04	134	VPS13B	5.28	1.8E-05	3.9E-03	110
	ERP27	4.53	4.9E-04	2.3E-04	118	CRLF3	3.24	8.6E-03	2.9E-02	87
	PTK2B	6.14	2.3E-06	5.3E-06	115	ZDHHC17	3.22	9.0E-03	2.9E-02	81
	ARHGAP15	3.55	6.3E-03	1.0E-03	111	SUZ12P1	3.75	2.4E-03	2.1E-02	68
	IRAK3	3.85	3.0E-03	6.0E-04	107	KIAA2026	4.44	3.2E-04	3.9E-03	63

Table 5: Top 20 state-specific genes. Top 20 lists of most significantly restricted state-specific genes for every defined clusters for activated (LPS) and resting (UN) macrophages.

	Pathway	p-value	q-value	Source	Number of genes	Pathway size	Genes
Cluster I	Metabolism	6.24E-12	1.45E-10	Reactome	41	1481	AK2, NDUFAB1, SLC25A5, UQCRC1, ELOVL5, MDH1, NDUFS1, SLC2A3, MPC1, CTSA, ELOVL1, PFKP, IDI1, PKM, PTPLAD1, ENO1, FDFT1, GSTP1, HADHA, B4GALT1, DLD, COMT, ACO2, PYGL, GSS, IDH3B, PGK1, ASAH1, OAZ1, GPI, PLD3, PNPO, ENO3, PRKAR1A, NDUFC1, UGDH, OSBP, ATP5B, PTGES3, GAPDH, ...
	Mitochondrial Electron Transport Chain	5.43E-11	1.17E-09	SMPDB	13	20	UQCRC1, ATP5B, GAPDH, ATP5F1, SDHB, ATP5E, NDUFA1, ATP5G2, ATP5A1, ATP5C1, CYCS, MT-ATP6, SDHD
	Glycolysis and Gluconeogenesis	3.20E-10	6.56E-09	Wikipathways	19	49	MDH1, SLC2A3, MPC1, PFKP, PKM, ENO1, DLD, PGK1, GPI, ENO3, GAPDH, TPI1, LDHB, PDHA1, MPC2, MDH2, ALDOA, PDHB, PGAM1
	Citric Acid Cycle	4.11E-08	6.25E-07	SMPDB	11	21	MPC1, DLD, ACO2, IDH3B, SDHB, PDHA1, MDH2, SUCLG1, IDH3A, PDHB, SDHD
	Fatty acid beta oxidation peroxisome	6.32E-05	9.53E-04	HumanCyc	7	19	SCP2, ACSL3, HSD17B4, HADHB, HADH, ACOX1, ACAA2
	Regulation of IFNG signaling	8.03E-05	1.14E-03	Reactome	6	14	IFNGR1, PTPN6, SUMO1, IFNGR2, PTPN2, PTPN11
	Regulation of actin cytoskeleton - Homo sapiens (human)	6.03E-04	3.58E-03	KEGG	29	215	RHOA, CDC42, ACTN1, ACTB, PXN, MYL12A, PFN1, ARPC3, MYL12B, GNA13, RAC2, ACTN4, ARPC1B, RAC1, PIK3R1, MSN, GSN, ITGB1, ITGB2, ITGA5, ARPC5, ITGAM, CFL1, ACTG1, TMSB4X, NRAS, MYL5, ARPC4, BRK1
	Pentose Phosphate Pathway	2.12E-03	1.08E-02	SMPDB	5	14	GPI, ALDOA, TKT, TALDO1, RPE
Cluster II	IL1 and megakaryotyces in obesity	3.99E-05	2.32E-03	Wikipathways	8	24	TIMP2, ICAM1, MMP9, TIMP1, IL1B, TLR2, IL18, S100A9
	TNF signaling pathway - Homo sapiens (human)	5.53E-05	2.56E-03	KEGG	44	110	MAPK9, PIK3CB, CASP8, TNFRSF1A, **NFKBIA, IKBKB,** MAP2K6, BIRC2, AKT3, **TNFAIP3, ATF4,** MAP3K7, RIPK1, MMP14, **FOS,** PIK3CD, CHUK, EIF3A, RAC1, RPS6, CALM2, PIK3R1, CALM3, GRB2, CALM1, TNFRSF1B, TRAF1, ITCH, CXCL2, DNM1L, ICAM1, NFKBIA, MMP9, JAG1, IKBKB, MAPK8, CCL20, TNFAIP3, IL1B, ATF4, PIK3R5, CXCL1, CASP3, FOS
	HIF-1 signaling pathway - Homo sapiens (human)	1.24E-04	4.52E-03	PID	25	23	**HIF1AN, ELOB,** HIF1A, EIF4E2, TFRC, RPS6, CUL2, IL6R, ENO3, PDHA1, PDHA1ENO1, PIK3R1, PGK1, ENO1, **EGLN1,** PDHB, RBX1, ELOC, OS9, LTBR, MKNK2, PFKL, PIK3CB, PIK3CD, PIK3CG
	Apoptosis - Homo sapiens (human)	1.40E-04	4.85E-03	KEGG	24	86	TOMM22, ACO2, ATP5B, TIMM17A, HSPD1, ATP5A1, TOMM70A, ATP5G1, TOMM20, VDAC1, BID, PIK3CB, CASP8, TNFRSF1A, IRAK3, CSF2RB, NFKBIA, XIAP, IKBKB, BIRC2, AKT3, RIPK1, PIK3CD, CHUK
	PPAR signaling pathway - Homo sapiens (human)	1.96E-03	1.95E-02	KEGG	11	69	ACSL4, PLTP, ACSBG1, PPARG, CD36, CYP27A1, ACSL1, FABP5, OLR1, ACSL5, GK
	NF kappa B signaling pathway - Homo sapiens (human)	2.51E-03	2.92E-02	KEGG	22	91	TNFRSF1A, ERC1, **NFKBIA, XIAP, IKBKB,** BIRC2, LTBR, **TNFAIP3,** TRIM25, MAP3K7, RIPK1, CHUK, TRAF1, CXCL2, ICAM1, CD40, IL1B, BCL2A1, BCL10, IL8, BCL2, LYN
	IL12 signaling mediated by STAT4	6.74E-03	4.33E-02	PID	6	33	CREBBP, MAPK8, IRF1, STAT4, IL18, FOS
	AP 1 transcription factor network	6.90E-03	4.35E-02	PID	10	70	CBFB, FOSL2, HIF1A, MMP9, TIMP1, BAG1, DUSP1, ETS1, IL8, FOS
	Toll like receptor pathway	8.98E-03	5.46E-02	BioCarta	12	35	SOAT1, SQLE, LIPA, HMGCS1, ACAT2, LSS, NFKBIA, IKBKB, MAP2K6, MAP3K7, FOS, CHUK
	Regulation of lipid metabolism by Peroxisome proliferator activated receptor alpha PPARalpha	9.87E-03	5.44E-02	Wikipathways	7	42	HMGCS1, G0S2, CD36, PLIN2, ACSL1, ABCA1, TXNRD1
Cluster III	IL2	1.35E-05	1.59E-03	NetPath	12	76	MKNK1, PIK3CG, NFKB1, CBL, MAPK14, NR3C1, STAT1, CREB1, PTK2B, PIK3CA, RAF1, VAV1
	STAT3 signaling pathway	4.69E-05	1.72E-03	BioCarta	5	8	JAK2, TYK2, JAK3, JAK1, STAT3
	IL5	2.56E-04	5.54E-03	NetPath	25	48	PIK3CB, MKNK1, JAK2, JAK3, PIK3CG, NFKB1, CBL, MAPK14, MAPK14, NR3C1, STAM2, STAT1, ATF2, CREB1, PTK2B, PTK2B, PIK3CA, STAT5A, MAP2K2, RAF1, VAV1, JAK1, STAT3, GSK3B, HCLS1
	Antiviral mechanism by IFN stimulated genes	6.69E-04	8.03E-03	Reactome	14	31	PIK3CB, TAB2, JAK2, PIK3CA, WWP1, STAT5A, NCOR1, ADAM17, STAT1, EIF4E2, FLNB, PPM1B, ARIH1, UBA7
	Cytokine Signaling in Immune system	7.33E-04	1.20E-02	Reactome	64	376	**PIAS1, CUL3,** PIK3CB, TAB2, EIF4G3, **RASAL2,** APBB1IP, IRAK3, **JAK2,** RELB, TYK2, JAK3, DDX58, **RAPGEF2,** SPTBN1, SOCS2, **PTK2B, PIK3CA,** STAT5A, MAP2K2, IL6ST, **PPM1B, VAV1, RASA1,** ADAM17, RASGRP3, RASA2, JAK1, PAQR3, STAT3, INPP5D, **NRG4, STAT2,** RASGRP1, TRAF6, PTPN2, TNFSF15, **UBA7, IRAK4,** SPRED2, PIAS1, CUL3, RASAL2, JAK2, NFKB1, RAPGEF2, CBL, STAT1, PTK2B, PIK3CA, RAF1, EIF4E2, FLNB, PPM1B, VAV1, RASA1, BRAF, FRS2, ARIH1, NRG4, STAT2, UBA7, NF1, IRAK4
	Glucocorticoid receptor regulatory network	2.05E-03	1.38E-02	PID	9	80	NFKB1, SUV420H1, MAPK14, NR3C1, STAT1, CREB1, NFATC1, SMARCC2, NCOA2
	Signaling by NOTCH	2.58E-03	2.11E-02	Reactome	21	107	HDAC9, ST3GAL6, TNRC6B, MIB1, TLE4, FBXW7, CCNC, CREB1, AGO3, CDK8, AGO4, NCOR1, ADAM17, MOV10, POGLUT1, CREB1, AGO3, AGO4, NCOR1, MOV10, POGLUT1
	JAK-STAT pathway	3.63E-03	2.73E-02	INOH	9	50	JAK2, TYK2, JAK3, CSF3R, STAT5A, IL6ST, JAK1, STAT3, STAT2
	IL6	4.59E-03	2.24E-02	NetPath	13	74	JAK2, NFKB1, CBL, MAPK14, STAT1, PTK2B, VAV1, AR, JAK3, STAT5A, MAP2K2, JAK1, STAT3
	IL4	5.69E-03	3.28E-02	NetPath	10	63	JAK2, ADRBK2, TYK2, JAK3, MAPK14, ATF2, PIK3CA, JAK1, STAT3, INPP5D
	The information processing pathway at the ifn beta enhancer	8.38E-03	3.99E-02	BioCarta	6	29	NR3C1, ATF2, ARID1A, GTF2F1, SMARCC2, HMGB1

Table 6: Pathway analysis for state-specific gene expression. Pathway annotation analysis for state-specific gene expression. For pathway terms "TNF signaling pathway - Homo sapiens (human)", "HIF-1 signaling pathway - Homo sapiens (human)", "NF kappa B signaling pathway - Homo sapiens (human)" and "Cytokine Signaling in Immune system" gene names were highlighted if genes were only found for activated macrophages (blue) or only found for resting macrophages (black). Remaining genes for these pathways were found for both treatment models.

Macrophage state	Regulation	Gene	Cells	Fold-change
Homeostasis-preserving macrophages (Cluster I)	up-regulated	BIRC3	7	2.89
		IL23A	5	2.45
		DUSP2	6	1.76
		SDC4	6	1.37
		GPR84	7	1.22
		PLAUR	8	0.95
		SHISA2	7	0.88
		CTD-2636A23.2	6	0.85
		TM4SF19-AS1	7	0.71
		MAP1B	6	0.64
		FLNA	8	0.63
		SNHG16	7	0.48
		HSPA8	7	0.48
		SLC20A1	8	0.46
		ST6GALNAC2	6	0.43
		TAF13	8	0.41
		CYCS	7	0.41
		AP1S2	8	0.41
		BZW1	5	0.38
		ACTG1	6	0.38
		RAPH1	5	0.37
		CLIC1	6	0.37
		CALU	8	0.36
		ACTN1	6	0.35
		POLR2D	7	0.35
		ITGB1BP1	7	0.34
		GOLT1B	5	0.33
	down-regulated	DAB2	5	-0.55
		ECH1	9	-0.31
		SNX2	5	-0.28
Pro-inflammatory macrophages (Cluster II)	up-regulated	CCL4	24	11.63
		CCL4L1	20	10.60
		CCL3	20	10.52
		AC069363.1	20	10.45
		TNFAIP6	12	10.27
		IL1B	20	9.87
		IL8	14	9.74
		CCL20	20	9.61
		CCL3L1	20	9.23
		CXCL1	14	9.22
		CCR7	10	9.13
		CXCL2	11	9.07
		CCL3L3	19	8.98
		RP1-68D18.2	15	6.36
		RNF144B	20	6.22
		IL7R	5	6.06
		EHD1	7	5.76
		ITGB8	21	5.67
		DLL4	15	5.56
		ELOVL7	15	5.52
		KLF5	11	5.41
		HS3ST3B1	18	5.31
		NAMPT	22	5.24
		TNFAIP2	6	5.01
		MSC	14	5.01
		RP1-68D18.4	10	4.90
		ZC3H12C	9	4.90
		RASGEF1B	5	4.84
		ATP2B1	23	4.75
		LEPREL1	12	4.69
		F3	16	4.49

Macrophage state	Regulation	Gene	Cells	Fold-change
Pro-inflammatory macrophages (Cluster II)	up-regulated	ACSL1	14	4.43
		INSIG1	20	4.40
		BCL2A1	18	4.38
		DRAM1	14	4.28
		CHST2	15	4.26
		EBI3	6	4.22
		KANK1	18	4.11
		G0S2	17	4.11
		USP12	14	4.07
		SERPINE2	17	3.84
		TNFAIP8	8	3.67
		TNFRSF9	17	3.52
		CRIM1	14	3.49
		LRP12	20	3.47
		PELI1	17	3.38
		LUCAT1	22	3.38
		BCL11A	6	3.35
		MARCKS	8	3.24
		HIVEP2	16	3.24
	down-regulated	GCLC	11	-1.06
		CLEC7A	19	-1.06
		ADAM28	18	-1.03
		RNF149	14	-0.96
		FABP5	6	-0.76
Anti-inflammatory macrophages (Cluster III)	up-regulated	GCH1	6	5.70
		RASGRP1	8	5.25
		MST4	6	3.71
		ZBTB10	6	3.70
		MCOLN2	7	3.62
		GBP2	8	3.60
		DENND5A	7	3.50
		RP11-212I21.2	7	3.49
		RAP2C	5	3.43
		TFAP2A	6	3.05
		PDSS1	7	2.78
		SPRED2	5	2.55
		NAV3	8	2.51
		PIK3AP1	5	2.48
		GBP5	6	2.38
		DENND4A	6	2.33
		WT1	5	2.27
		RP3-325F22.3	7	2.15
		LL21NC02-1C16.2	7	2.10
		FKBP5	11	2.09
		MCTP1	7	1.96
		STX12	5	1.91
		RP11-37B2.1	8	1.79
		MAP3K5	5	1.75
		LCOR	5	1.71
		KCNN2	6	1.68
		HDAC9	6	1.64
		CTD-2031P19.5	5	1.63
		EYA3	5	1.57
		C21orf91	6	1.57
		CCDC82	9	1.53
		PLAGL2	5	1.46
		FAM65C	5	1.44
		CEP85L	6	1.43
		NET1	12	1.41
		SLC5A6	7	1.36
		SLC12A6	5	1.35

Macrophage state	Regulation	Gene	Cells	Fold-change
Anti-inflammatory macrophages (Cluster III)	up-regulated	SIK3	6	1.29
		FAM49A	6	1.28
		CD38	5	1.27
		LYRM4	6	1.25
		CPM	6	1.18
		EMILIN2	6	1.17
		RP11-611O2.5	6	1.17
		TPRG1	5	1.16
		SNX11	6	1.12
		ABCA6	5	1.08
		LRRC8B	10	1.08
		TMEM194A	11	1.04
	down-regulated	FAM46A	13	-1.78
		CCSAP	8	-1.64
		CASP2	12	-1.53
		PSIP1	10	-1.41
		KIAA1009	7	-1.37
		METTL7A	7	-1.31
		PARP9	9	-1.30
		SSH2	6	-1.22
		MMS22L	8	-1.22
		MEIS1	6	-1.19
		NAA16	8	-1.18
		SESN1	5	-1.18
		CYTH4	6	-1.16
		MS4A14	5	-1.09
		SUZ12P	6	-1.03
		IRF2BP2	8	-1.02
		FLT3	7	-0.95
		SOCS2	6	-0.94
		DCLRE1C	9	-0.94
		HMGB2	7	-0.94
		NCOA7	9	-0.93
		LRRC8C	8	-0.93
		TNRC6B	8	-0.93
		RCOR3	9	-0.93
		PCMTD2	5	-0.90
		GIT2	9	-0.90
		RP11-295P9.3	5	-0.89
		C2orf68	5	-0.88
		ELF2	6	-0.87
		JMJD1C	5	-0.86
		S100PBP	10	-0.86
		PHF21A	10	-0.86
		FAM178A	7	-0.85
		FANCM	7	-0.84
		ZNF292	8	-0.83
		BRD8	11	-0.83
		CSF3R	7	-0.83
		RAD52	8	-0.82
		TBC1D8	5	-0.81
		C4orf29	9	-0.81
		CHKA	5	-0.80
		CMYA5	7	-0.80
		ARID4A	11	-0.78
		USP37	9	-0.78
		ADRBK2	5	-0.77
		METTL17	6	-0.76
		TRIM38	5	-0.75
		NR2C1	7	-0.75
		ERMARD	6	-0.74
		INSR	6	-0.74

Table 7: Top differentially expressed genes from responsiveness analysis. List is derived from state-specific differential gene expression induced upon LPS-stimulation (for visualization see Figure 14F).

Bibliography

A

Kaia Achim, Jean-Baptiste Pettit, Luis R. Saraiva, Daria Gavriouchkina, Tomas Larsson, Detlev Arendt, and John C. Marioni. High-throughput spatial mapping of single-cell RNA-seq data to tissue of origin. *Nature Biotechnology*, 33(5):503–509, 2015. ISSN 1087-0156. doi: 10.1038/nbt.3209.

Sony Agrawal, Steven Cifelli, Richard Johnstone, David Pechter, Deborah A. Barbey, Karen Lin, Tim Allison, Shree Agrawal, Aida Rivera-Gines, James A. Milligan, Jonathan Schneeweis, Kevin Houle, Alice J. Struck, Richard Visconti, Matthew Sills, and Mary Jo Wildey. Utilizing Low-Volume Aqueous Acoustic Transfer with the Echo 525 to Enable Miniaturization of qRT-PCR Assay. *Journal of Laboratory Automation*, 21(1):57–63, February 2016. ISSN 2211-0690. doi: 10.1177/2211068215609315.

Shizuo Akira, Satoshi Uematsu, and Osamu Takeuchi. Pathogen recognition and innate immunity. *Cell*, 124(4): 783–801, February 2006. ISSN 0092-8674. doi: 10.1016/j.cell.2006.02.015.

Simon Anders, Paul Theodor Pyl, and Wolfgang Huber. HTSeq–a Python framework to work with high-throughput sequencing data. *Bioinformatics (Oxford, England)*, 31(2):166–169, January 2015. ISSN 1367-4811. doi: 10.1093/bioinformatics/btu638.

U. Andersson and H. Rauvala. Introduction: HMGB1 in inflammation and innate immunity. *Journal of Internal Medicine*, 270(4):296–300, October 2011. ISSN 1365-2796. doi: 10.1111/j.1365-2796.2011.02430.x.

Henry Andrews. FastQC: a quality control tool for high throughput sequence data, 2010.

Cedric Auffray, Darin Fogg, Meriem Garfa, Gaelle Elain, Olivier Join-Lambert, Samer Kayal, Sabine Sarnacki, Ana Cumano, Gregoire Lauvau, and Frederic Geissmann. Monitoring of blood vessels and tissues by a population of monocytes with patrolling behavior. *Science (New York, N.Y.)*, 317(5838):666–670, August 2007. ISSN 1095-9203. doi: 10.1126/science.1142883.

J. Auwerx. The human leukemia cell line, THP-1: a multifacetted model for the study of monocyte-macrophage differentiation. *Experientia*, 47(1):22–31, January 1991. ISSN 0014-4754.

B

Rhonda Bacher and Christina Kendziorski. Design and computational analysis of single-cell RNA-sequencing experiments. *Genome Biology*, 17:63, April 2016. ISSN 1474-760X. doi: 10.1186/s13059-016-0927-y.

Youssef Bakri, Sandrine Sarrazin, Ulrich P. Mayer, Silke Tillmanns, Claus Nerlov, Annie Boned, and Michael H. Sieweke. Balance of MafB and PU.1 specifies alternative macrophage or dendritic cell fate. *Blood*, 105(7): 2707–2716, April 2005. ISSN 0006-4971. doi: 10.1182/blood-2004-04-1448.

BIBLIOGRAPHY

Megan N. Ballinger, Michael W. Newstead, Xianying Zeng, Urvashi Bhan, Xiaokui M. Mo, Steven L. Kunkel, Bethany B. Moore, Richard Flavell, John W. Christman, and Theodore J. Standiford. IRAK-M promotes alternative macrophage activation and fibroproliferation in bleomycin-induced lung injury. *Journal of Immunology (Baltimore, Md.: 1950)*, 194(4):1894–1904, February 2015. ISSN 1550-6606. doi: 10.4049/jimmunol.1402377.

Jacques Behmoaras, Gurjeet Bhangal, Jennifer Smith, Kylie McDonald, Brenda Mutch, Ping Chin Lai, Jan Domin, Laurence Game, Alan Salama, Brian M. Foxwell, Charles D. Pusey, H. Terence Cook, and Timothy J. Aitman. Jund is a determinant of macrophage activation and is associated with glomerulonephritis susceptibility. *Nature Genetics*, 40(5):553–559, May 2008. ISSN 1546-1718. doi: 10.1038/ng.137.

Martin Bengtsson, Anders Ståhlberg, Patrik Rorsman, and Mikael Kubista. Gene expression profiling in single cells from the pancreatic islets of Langerhans reveals lognormal distribution of mRNA levels. *Genome Research*, 15(10):1388–1392, October 2005. ISSN 1088-9051. doi: 10.1101/gr.3820805.

Vipul Bhargava, Pang Ko, Erik Willems, Mark Mercola, and Shankar Subramaniam. Quantitative transcriptomics using designed primer-based amplification. *Scientific Reports*, 3:1740, 2013. ISSN 2045-2322. doi: 10.1038/srep01740.

Ashish Bhattacharjee, Srabani Pal, Gerald M. Feldman, and Martha K. Cathcart. Hck Is a Key Regulator of Gene Expression in Alternatively Activated Human Monocytes. *Journal of Biological Chemistry*, 286(42):36709–36723, October 2011. ISSN 0021-9258, 1083-351X. doi: 10.1074/jbc.M111.291492.

Pengpeng Bi and Shihuan Kuang. Notch signaling as a novel regulator of metabolism. *Trends in endocrinology and metabolism: TEM*, 26(5):248–255, May 2015. ISSN 1043-2760. doi: 10.1016/j.tem.2015.02.006.

Hans Binder, Henry Wirth, Arsen Arakelyan, Kathrin Lembcke, Evgeny S. Tiys, Vladimir A. Ivanisenko, Nikolay A. Kolchanov, Alexey Kononikhin, Igor Popov, Evgeny N. Nikolaev, Lyudmila Kh Pastushkova, and Irina M. Larina. Time-course human urine proteomics in space-flight simulation experiments. *BMC Genomics*, 15(12):S2, 2014. ISSN 1471-2164. doi: 10.1186/1471-2164-15-S12-S2.

Åsa K. Björklund, Marianne Forkel, Simone Picelli, Viktoria Konya, Jakob Theorell, Danielle Friberg, Rickard Sandberg, and Jenny Mjösberg. The heterogeneity of human CD127(+) innate lymphoid cells revealed by single-cell RNA sequencing. *Nature Immunology*, 17(4):451–460, April 2016. ISSN 1529-2916. doi: 10.1038/ni.3368.

Wah Chin Boon, Karolina Petkovic-Duran, Yonggang Zhu, Richard Manasseh, Malcolm K. Horne, and Tim D. Aumann. Increasing cDNA yields from single-cell quantities of mRNA in standard laboratory reverse transcriptase reactions using acoustic microstreaming. *Journal of Visualized Experiments: JoVE*, (53):e3144, July 2011. ISSN 1940-087X. doi: 10.3791/3144.

Dimitra Bourboulia and William G. Stetler-Stevenson. Matrix MetalloProteinases (MMPs) andTissue Inhibitors of MetalloProteinases (TIMPs): positive and negative regulators intumor cell adhesion. *Seminars in cancer biology*, 20(3):161–168, June 2010. ISSN 1044-579X. doi: 10.1016/j.semcancer.2010.05.002.

Philip Brennecke, Simon Anders, Jong Kyoung Kim, Aleksandra A. Kołodziejczyk, Xiuwei Zhang, Valentina Proserpio, Bianka Baying, Vladimir Benes, Sarah A. Teichmann, John C. Marioni, and Marcus G. Heisler. Accounting for technical noise in single-cell RNA-seq experiments. *Nature Methods*, 10(11):1093–1095, November 2013. ISSN 1548-7105. doi: 10.1038/nmeth.2645.

H. D. Brightbill, S. E. Plevy, R. L. Modlin, and S. T. Smale. A prominent role for Sp1 during lipopolysaccharide-mediated induction of the IL-10 promoter in macrophages. *Journal of Immunology (Baltimore, Md.: 1950)*, 164(4):1940–1951, February 2000. ISSN 0022-1767.

Jonathan R. Brody, Eric S. Calhoun, Eike Gallmeier, Talisa D. Creavalle, and Scott E. Kern. Ultra-fast high-resolution agarose electrophoresis of DNA and RNA using low-molarity conductive media. *BioTechniques*, 37(4):598, 600, 602, October 2004. ISSN 0736-6205.

Tanja Buchacher, Anna Ohradanova-Repic, Hannes Stockinger, Michael B. Fischer, and Viktoria Weber. M2 Polarization of Human Macrophages Favors Survival of the Intracellular Pathogen Chlamydia pneumoniae. *PLOS ONE*, 10(11):e0143593, November 2015. ISSN 1932-6203. doi: 10.1371/journal.pone.0143593.

Darren J. Burgess. Technology: A drop in single-cell challenges. *Nature Reviews Genetics*, 16(7):376–377, July 2015. ISSN 1471-0064. doi: 10.1038/nrg3972.

John M. Busillo and John A. Cidlowski. The five Rs of glucocorticoid action during inflammation: ready, reinforce, repress, resolve, and restore. *Trends in Endocrinology and Metabolism*, 24(3):109–119, March 2013. ISSN 1879-3061. doi: 10.1016/j.tem.2012.11.005.

S. A. Bustin. Absolute quantification of mRNA using real-time reverse transcription polymerase chain reaction assays. *Journal of Molecular Endocrinology*, 25(2):169–193, October 2000. ISSN 0952-5041.

R. S. Bystry, V. Aluvihare, K. A. Welch, M. Kallikourdis, and A. G. Betz. B cells and professional APCs recruit regulatory T cells via CCL4. *Nature Immunology*, 2(12):1126–1132, December 2001. ISSN 1529-2908. doi: 10.1038/ni735.

C

Mark G. Carter, Alexei A. Sharov, Vincent VanBuren, Dawood B. Dudekula, Condie E. Carmack, Charlie Nelson, and Minoru S. H. Ko. Transcript copy number estimation using a mouse whole-genome oligonucleotide microarray. *Genome Biology*, 6(7):R61, 2005. ISSN 1474-760X. doi: 10.1186/gb-2005-6-7-r61.

Caroline Cheng, Dennie Tempel, Wijnand K. Den Dekker, Remco Haasdijk, Ihsan Chrifi, Frank L. Bos, Kim Wagtmans, Esther H. van de Kamp, Lau Blonden, Erik A. L. Biessen, Frans Moll, Gerard Pasterkamp, Patrick W. Serruys, Stefan Schulte-Merker, and Henricus J. Duckers. Ets2 determines the inflammatory state of endothelial cells in advanced atherosclerotic lesions. *Circulation Research*, 109(4):382–395, August 2011. ISSN 1524-4571. doi: 10.1161/CIRCRESAHA.111.243444.

Yurii Chinenov, Maddalena Coppo, Rebecca Gupte, Maria A. Sacta, and Inez Rogatsky. Glucocorticoid receptor coordinates transcription factor-dominated regulatory network in macrophages. *BMC genomics*, 15:656, August 2014. ISSN 1471-2164. doi: 10.1186/1471-2164-15-656.

Giulia Chinetti-Gbaguidi, Sophie Colin, and Bart Staels. Macrophage subsets in atherosclerosis. *Nature Reviews. Cardiology*, 12(1):10–17, January 2015. ISSN 1759-5010. doi: 10.1038/nrcardio.2014.173.

Anthony Covarrubias, Vanessa Byles, and Tiffany Horng. ROS sets the stage for macrophage differentiation. *Cell Research*, 23(8):984–985, August 2013. ISSN 1001-0602. doi: 10.1038/cr.2013.88.

Gabor Csardi and Tamas Nepusz. The igraph software package for complex network research. *InterJournal*, Complex Systems(1695), 2006.

D

Luke C. Davies, Stephen J. Jenkins, Judith E. Allen, and Philip R. Taylor. Tissue-resident macrophages. *Nature Immunology*, 14(10):986–995, October 2013. ISSN 1529-2916. doi: 10.1038/ni.2705.

Emilie Debien, Katia Mayol, Vincent Biajoux, Cécile Daussy, Mercedes Gomez De Aguero, Morgan Taillardet, Nicolas Dagany, Lilia Brinza, Thomas Henry, Bertrand Dubois, Dominique Kaiserlian, Jacqueline Marvel, Karl Balabanian, and Thierry Walzer. S1pr5 is pivotal for the homeostasis of patrolling monocytes. *European Journal of Immunology*, 43(6):1667–1675, June 2013. ISSN 1521-4141. doi: 10.1002/eji.201343312.

Alan Diercks, Heather Kostner, and Adrian Ozinsky. Resolving Cell Population Heterogeneity: Real-Time PCR for Simultaneous Multiplexed Gene Detection in Multiple Single-Cell Samples. *PLOS ONE*, 4(7):e6326, July 2009. ISSN 1932-6203. doi: 10.1371/journal.pone.0006326.

J. Ding, O. Ghali, P. Lencel, O. Broux, C. Chauveau, J. C. Devedjian, P. Hardouin, and D. Magne. TNF-alpha and IL-1beta inhibit RUNX2 and collagen expression but increase alkaline phosphatase activity and mineralization in human mesenchymal stem cells. *Life Sciences*, 84(15-16):499–504, April 2009. ISSN 1879-0631. doi: 10.1016/j.lfs.2009.01.013.

L. A. DiPietro, M. Burdick, Q. E. Low, S. L. Kunkel, and R. M. Strieter. MIP-1alpha as a critical macrophage chemoattractant in murine wound repair. *The Journal of Clinical Investigation*, 101(8):1693–1698, April 1998. ISSN 0021-9738. doi: 10.1172/JCI1020.

Alexander Dobin, Carrie A. Davis, Felix Schlesinger, Jorg Drenkow, Chris Zaleski, Sonali Jha, Philippe Batut, Mark Chaisson, and Thomas R. Gingeras. STAR: ultrafast universal RNA-seq aligner. *Bioinformatics*, 29(1): 15–21, January 2013. ISSN 1367-4803. doi: 10.1093/bioinformatics/bts635.

Hannah Dueck, James Eberwine, and Junhyong Kim. Variation is function: Are single cell differences functionally important?: Testing the hypothesis that single cell variation is required for aggregate function. *BioEssays: News and Reviews in Molecular, Cellular and Developmental Biology*, 38(2):172–180, February 2016. ISSN 1521-1878. doi: 10.1002/bies.201500124.

H. F. Dvorak. Tumors: wounds that do not heal. Similarities between tumor stroma generation and wound healing. *The New England Journal of Medicine*, 315(26):1650–1659, December 1986. ISSN 0028-4793. doi: 10.1056/NEJM198612253152606.

Douglas P. Dyer, Catherina L. Salanga, Scott C. Johns, Elena Valdambrini, Mark M. Fuster, Caroline M. Milner, Anthony J. Day, and Tracy M. Handel. The Anti-inflammatory Protein TSG-6 Regulates Chemokine Function by Inhibiting Chemokine/Glycosaminoglycan Interactions. *The Journal of Biological Chemistry*, 291(24): 12627–12640, June 2016. ISSN 1083-351X. doi: 10.1074/jbc.M116.720953.

Jolanta M. Dzik. The ancestry and cumulative evolution of immune reactions. *Acta Biochimica Polonica*, 57(4): 443–466, 2010. ISSN 1734-154X.

E

Karim C. El Kasmi, Joseph E. Qualls, John T. Pesce, Amber M. Smith, Robert W. Thompson, Marcela Henao-Tamayo, Randall J. Basaraba, Till König, Ulrike Schleicher, Mi-Sun Koo, Gilla Kaplan, Katherine A. Fitzgerald, Elaine I. Tuomanen, Ian M. Orme, Thirumala-Devi Kanneganti, Christian Bogdan, Thomas A. Wynn, and Peter J. Murray. Toll-like receptor-induced arginase 1 in macrophages thwarts effective immunity against intracellular pathogens. *Nature Immunology*, 9(12):1399–1406, December 2008. ISSN 1529-2916. doi: 10.1038/ni.1671.

Michael B. Elowitz, Arnold J. Levine, Eric D. Siggia, and Peter S. Swain. Stochastic gene expression in a single cell. *Science (New York, N.Y.)*, 297(5584):1183–1186, August 2002. ISSN 1095-9203. doi: 10.1126/science.1070919.

F

H. Christina Fan, Glenn K. Fu, and Stephen P. A. Fodor. Expression profiling. Combinatorial labeling of single cells for gene expression cytometry. *Science (New York, N.Y.)*, 347(6222):1258367, February 2015. ISSN 1095-9203. doi: 10.1126/science.1258367.

Dulce Frausto-Del-Río, Isabel Soto-Cruz, Claudia Garay-Canales, Xochitl Ambriz, Gloria Soldevila, Jorge Carretero-Ortega, José Vázquez-Prado, and Enrique Ortega. Interferon gamma induces actin polymerization, Rac1 activation and down regulates phagocytosis in human monocytic cells. *Cytokine*, 57(1):158–168, January 2012. ISSN 1096-0023. doi: 10.1016/j.cyto.2011.11.008.

Keisuke Fujita, Mitsuhiro Iwaki, and Toshio Yanagida. Transcriptional bursting is intrinsically caused by interplay between RNA polymerases on DNA. *Nature Communications*, 7:13788, December 2016. ISSN 2041-1723. doi: 10.1038/ncomms13788.

G

Silvia Galván-Peña and Luke A. J. O'Neill. Metabolic Reprograming in Macrophage Polarization. *Frontiers in Immunology*, 5, September 2014. ISSN 1664-3224. doi: 10.3389/fimmu.2014.00420.

Emmanuel L. Gautier, Tal Shay, Jennifer Miller, Melanie Greter, Claudia Jakubzick, Stoyan Ivanov, Julie Helft, Andrew Chow, Kutlu G. Elpek, Simon Gordonov, Amin R. Mazloom, Avi Ma'ayan, Wei-Jen Chua, Ted H. Hansen, Shannon J. Turley, Miriam Merad, Gwendalyn J. Randolph, and Immunological Genome Consortium. Gene-expression profiles and transcriptional regulatory pathways that underlie the identity and diversity of mouse tissue macrophages. *Nature Immunology*, 13(11):1118–1128, November 2012. ISSN 1529-2916. doi: 10.1038/ni.2419.

Todd M. Gierahn, Marc H. Wadsworth, Travis K. Hughes, Bryan D. Bryson, Andrew Butler, Rahul Satija, Sarah Fortune, J. Christopher Love, and Alex K. Shalek. Seq-Well: portable, low-cost RNA sequencing of single cells at high throughput. *Nature Methods*, February 2017. ISSN 1548-7105. doi: 10.1038/nmeth.4179.

Kwang-Il Goh, Michael E. Cusick, David Valle, Barton Childs, Marc Vidal, and Albert-László Barabási. The human disease network. *Proceedings of the National Academy of Sciences of the United States of America*, 104(21):8685–8690, May 2007. ISSN 0027-8424. doi: 10.1073/pnas.0701361104.

Siamon Gordon. Alternative activation of macrophages. *Nature Reviews Immunology*, 3(1):23–35, January 2003. ISSN 1474-1733. doi: 10.1038/nri978.

Siamon Gordon and Philip R. Taylor. Monocyte and macrophage heterogeneity. *Nature Reviews. Immunology*, 5(12):953–964, December 2005. ISSN 1474-1733. doi: 10.1038/nri1733.

Andre Gross, Jonas Schoendube, Stefan Zimmermann, Maximilian Steeb, Roland Zengerle, and Peter Koltay. Technologies for Single-Cell Isolation. *International Journal of Molecular Sciences*, 16(8):16897–16919, July 2015. ISSN 1422-0067. doi: 10.3390/ijms160816897.

Dominic Grün and Alexander van Oudenaarden. Design and Analysis of Single-Cell Sequencing Experiments. *Cell*, 163(4):799–810, November 2015. ISSN 1097-4172. doi: 10.1016/j.cell.2015.10.039.

Mausumee Guha and Nigel Mackman. The phosphatidylinositol 3-kinase-Akt pathway limits lipopolysaccharide activation of signaling pathways and expression of inflammatory mediators in human monocytic cells. *The Journal of Biological Chemistry*, 277(35):32124–32132, August 2002. ISSN 0021-9258. doi: 10.1074/jbc.M203298200.

H

Bente Halvorsen, Martine Z. Espeland, Geir Øystein Andersen, Arne Yndestad, Ellen Lund Sagen, Azita Rashidi, Eva C. Knudsen, Mona Skjelland, Karolina R. Skagen, Kirsten Krohg-Sørensen, Sverre Holm, Vibeke Ritschel, Kirsten B. Holven, Erik A. L. Biessen, Pål Aukrust, and Tuva B. Dahl. Increased expression of NAMPT in PBMC from patients with acute coronary syndrome and in inflammatory M1 macrophages. *Atherosclerosis*, 243(1):204–210, November 2015. ISSN 1879-1484. doi: 10.1016/j.atherosclerosis.2015.09.010.

Kyuho Han, Ariel Jaimovich, Gautam Dey, Davide Ruggero, Oded Meyuhas, Nahum Sonenberg, and Tobias Meyer. Parallel measurement of dynamic changes in translation rates in single cells. *Nature Methods*, 11(1):86–93, January 2014. ISSN 1548-7105. doi: 10.1038/nmeth.2729.

Tamar Hashimshony, Florian Wagner, Noa Sher, and Itai Yanai. CEL-Seq: single-cell RNA-Seq by multiplexed linear amplification. *Cell Reports*, 2(3):666–673, September 2012. ISSN 2211-1247. doi: 10.1016/j.celrep.2012.08.003.

Peter M. Henson and David A. Hume. Apoptotic cell removal in development and tissue homeostasis. *Trends in Immunology*, 27(5):244–250, May 2006. ISSN 1471-4906. doi: 10.1016/j.it.2006.03.005.

Ralf Herwig, Christopher Hardt, Matthias Lienhard, and Atanas Kamburov. Analyzing and interpreting genome data at the network level with ConsensusPathDB. *Nature Protocols*, 11(10):1889–1907, October 2016. ISSN 1750-2799. doi: 10.1038/nprot.2016.117.

Xiaoyu Hu and Lionel B. Ivashkiv. Cross-regulation of signaling pathways by interferon-gamma: implications for immune responses and autoimmune diseases. *Immunity*, 31(4):539–550, October 2009. ISSN 1097-4180. doi: 10.1016/j.immuni.2009.09.002.

I

Saiful Islam, Una Kjällquist, Annalena Moliner, Pawel Zajac, Jian-Bing Fan, Peter Lönnerberg, and Sten Linnarsson. Characterization of the single-cell transcriptional landscape by highly multiplex RNA-seq. *Genome Research*, 21(7):1160–1167, July 2011. ISSN 1549-5469. doi: 10.1101/gr.110882.110.

Saiful Islam, Una Kjällquist, Annalena Moliner, Pawel Zajac, Jian-Bing Fan, Peter Lönnerberg, and Sten Linnarsson. Highly multiplexed and strand-specific single-cell RNA 5' end sequencing. *Nature Protocols*, 7(5): 813–828, April 2012. ISSN 1750-2799. doi: 10.1038/nprot.2012.022.

Paola Italiani and Diana Boraschi. From Monocytes to M1/M2 Macrophages: Phenotypical vs. Functional Differentiation. *Frontiers in Immunology*, 5:514, 2014. doi: 10.3389/fimmu.2014.00514.

Paola Italiani, Emilia M. C. Mazza, Davide Lucchesi, Ingrid Cifola, Claudia Gemelli, Alexis Grande, Cristina Battaglia, Silvio Bicciato, and Diana Boraschi. Transcriptomic profiling of the development of the inflammatory response in human monocytes in vitro. *PloS One*, 9(2):e87680, 2014. ISSN 1932-6203. doi: 10.1371/journal.pone.0087680.

Akiko Iwasaki and Ruslan Medzhitov. Regulation of adaptive immunity by the innate immune system. *Science (New York, N.Y.)*, 327(5963):291–295, January 2010. ISSN 1095-9203. doi: 10.1126/science.1183021.

J

Diego Adhemar Jaitin, Ephraim Kenigsberg, Hadas Keren-Shaul, Naama Elefant, Franziska Paul, Irina Zaretsky, Alexander Mildner, Nadav Cohen, Steffen Jung, Amos Tanay, and Ido Amit. Massively parallel single-cell RNA-seq for marker-free decomposition of tissues into cell types. *Science (New York, N.Y.)*, 343(6172): 776–779, February 2014. ISSN 1095-9203. doi: 10.1126/science.1247651.

C. A. Jr Janeway, Paul Travers, Mark Walport, and Mark J. Shlomchik. *Immunobiology: The Immune System in Health and Disease. 5th edition. New York: Garland Science; 2001. The components of the immune system.* Garland Science, New York, 2001. ISBN 10: 0-8153-3642-X.

Stephen J. Jenkins, Dominik Ruckerl, Peter C. Cook, Lucy H. Jones, Fred D. Finkelman, Nico van Rooijen, Andrew S. MacDonald, and Judith E. Allen. Local macrophage proliferation, rather than recruitment from the blood, is a signature of TH2 inflammation. *Science (New York, N.Y.)*, 332(6035):1284–1288, June 2011. ISSN 1095-9203. doi: 10.1126/science.1204351.

Jason L. Johnson and Andrew C. Newby. Macrophage heterogeneity in atherosclerotic plaques. *Current Opinion in Lipidology*, 20(5):370–378, October 2009. ISSN 0957-9672. doi: 10.1097/MOL.0b013e3283309848.

Helena Jonsson, Paul Allen, and Stanford L. Peng. Inflammatory arthritis requires Foxo3a to prevent Fas ligand-induced neutrophil apoptosis. *Nature Medicine*, 11(6):666–671, June 2005. ISSN 1078-8956. doi: 10.1038/nm1248.

Jeremy B. M. Jowett, Yasunori Okada, Peter J. Leedman, Joanne E. Curran, Matthew P. Johnson, Eric K. Moses, Harald H. H. Goring, Satsuki Mochizuki, John Blangero, Leah Stone, Holly Allen, Chris Mitchell, and Vance B. Matthews. ADAM28 is elevated in humans with the metabolic syndrome and is a novel sheddase of human tumour necrosis factor-α. *Immunology and Cell Biology*, 90(10):966–973, November 2012. ISSN 1440-1711. doi: 10.1038/icb.2012.44.

Jan Philipp Junker and Alexander van Oudenaarden. Every cell is special: genome-wide studies add a new dimension to single-cell biology. *Cell*, 157(1):8–11, March 2014. ISSN 1097-4172. doi: 10.1016/j.cell.2014.02.010.

Michael Junkin, Alicia J. Kaestli, Zhang Cheng, Christian Jordi, Cem Albayrak, Alexander Hoffmann, and Savaş Tay. High-Content Quantification of Single-Cell Immune Dynamics. *Cell Reports*, 15(2):411–422, April 2016. ISSN 2211-1247. doi: 10.1016/j.celrep.2016.03.033.

K

Atanas Kamburov, Ulrich Stelzl, Hans Lehrach, and Ralf Herwig. The ConsensusPathDB interaction database: 2013 update. *Nucleic Acids Research*, 41(Database issue):D793–800, January 2013. ISSN 1362-4962. doi: 10.1093/nar/gks1055.

Jenny E. Kanter, Farah Kramer, Shelley Barnhart, Michelle M. Averill, Anuradha Vivekanandan-Giri, Thad Vickery, Lei O. Li, Lev Becker, Wei Yuan, Alan Chait, Kathleen R. Braun, Susan Potter-Perigo, Srinath Sanda, Thomas N. Wight, Subramaniam Pennathur, Charles N. Serhan, Jay W. Heinecke, Rosalind A. Coleman, and Karin E. Bornfeldt. Diabetes promotes an inflammatory macrophage phenotype and atherosclerosis through acyl-CoA synthetase 1. *Proceedings of the National Academy of Sciences of the United States of America*, 109(12):E715–724, March 2012. ISSN 1091-6490. doi: 10.1073/pnas.1111600109.

Ernest S. Kawasaki. Microarrays and the gene expression profile of a single cell. *Annals of the New York Academy of Sciences*, 1020:92–100, May 2004. ISSN 0077-8923. doi: 10.1196/annals.1310.010.

Boris N. Kholodenko. Cell Signalling Dynamics in Time and Space. *Nature Reviews Molecular Cell Biology*, 7(3):165–176, March 2006. ISSN 1471-0072. doi: 10.1038/nrm1838.

Daniel H. Kim, Georgi K. Marinov, Shirley Pepke, Zakary S. Singer, Peng He, Brian Williams, Gary P. Schroth, Michael B. Elowitz, and Barbara J. Wold. Single-cell transcriptome analysis reveals dynamic changes in lncRNA expression during reprogramming. *Cell Stem Cell*, 16(1):88–101, January 2015. ISSN 1875-9777. doi: 10.1016/j.stem.2014.11.005.

Robert J. Kimmerling, Gregory Lee Szeto, Jennifer W. Li, Alex S. Genshaft, Samuel W. Kazer, Kristofor R. Payer, Jacob de Riba Borrajo, Paul C. Blainey, Darrell J. Irvine, Alex K. Shalek, and Scott R. Manalis. A microfluidic platform enabling single-cell RNA-seq of multigenerational lineages. *Nature Communications*, 7:10220, January 2016. ISSN 2041-1723. doi: 10.1038/ncomms10220.

Allon M. Klein, Linas Mazutis, Ilke Akartuna, Naren Tallapragada, Adrian Veres, Victor Li, Leonid Peshkin, David A. Weitz, and Marc W. Kirschner. Droplet barcoding for single-cell transcriptomics applied to embryonic stem cells. *Cell*, 161(5):1187–1201, May 2015. ISSN 1097-4172. doi: 10.1016/j.cell.2015.04.044.

Koichi Kobayashi, Lorraine D. Hernandez, Jorge E. Galán, Charles A. Janeway Jr., Ruslan Medzhitov, and Richard A. Flavell. IRAK-M Is a Negative Regulator of Toll-like Receptor Signaling. *Cell*, 110(2):191–202, July 2002. ISSN 0092-8674. doi: 10.1016/S0092-8674(02)00827-9.

Teuvo Kohonen. Self-organized formation of topologically correct feature maps. *Biological Cybernetics*, 43(1):59–69, January 1982. ISSN 0340-1200, 1432-0770. doi: 10.1007/BF00337288.

Aleksandra A. Kolodziejczyk, Jong Kyoung Kim, Valentine Svensson, John C. Marioni, and Sarah A. Teichmann. The technology and biology of single-cell RNA sequencing. *Molecular Cell*, 58(4):610–620, May 2015a. ISSN 1097-4164. doi: 10.1016/j.molcel.2015.04.005.

Aleksandra A. Kolodziejczyk, Jong Kyoung Kim, Jason C. H. Tsang, Tomislav Ilicic, Johan Henriksson, Kedar N. Natarajan, Alex C. Tuck, Xuefei Gao, Marc Bühler, Pentao Liu, John C. Marioni, and Sarah A. Teichmann. Single Cell RNA-Sequencing of Pluripotent States Unlocks Modular Transcriptional Variation. *Cell Stem Cell*, 17(4):471–485, October 2015b. ISSN 1875-9777. doi: 10.1016/j.stem.2015.09.011.

Yoshihiro Komohara, Masahisa Jinushi, and Motohiro Takeya. Clinical significance of macrophage heterogeneity in human malignant tumors. *Cancer Science*, 105(1):1–8, January 2014. ISSN 1349-7006. doi: 10.1111/cas.12314.

Magdalena Kozakowska, Katarzyna Pietraszek-Gremplewicz, Alicja Jozkowicz, and Jozef Dulak. The role of oxidative stress in skeletal muscle injury and regeneration: focus on antioxidant enzymes. *Journal of Muscle Research and Cell Motility*, 36:377–393, 2015. ISSN 0142-4319. doi: 10.1007/s10974-015-9438-9.

L

Roland Lang, Michael Hammer, and Jörg Mages. DUSP meet immunology: dual specificity MAPK phosphatases in control of the inflammatory response. *Journal of Immunology (Baltimore, Md.: 1950)*, 177(11):7497–7504, December 2006. ISSN 0022-1767.

Patrice Laquerriere, Alexia Grandjean-Laquerriere, Salima Addadi-Rebbah, Edouard Jallot, Dominique Laurent-Maquin, Patrick Frayssinet, and Moncef Guenounou. MMP-2, MMP-9 and their inhibitors TIMP-2 and TIMP-1 production by human monocytes in vitro in the presence of different forms of hydroxyapatite particles. *Biomaterials*, 25(13):2515–2524, June 2004. ISSN 0142-9612.

Henrik Laurell, Jason S. Iacovoni, Anne Abot, David Svec, Jean-José Maoret, Jean-François Arnal, and Mikael Kubista. Correction of RT-qPCR data for genomic DNA-derived signals with ValidPrime. *Nucleic Acids Research*, 40(7):e51, April 2012. ISSN 1362-4962. doi: 10.1093/nar/gkr1259.

Jürgen Läuter, Friedemann Horn, Maciej Rosołowski, and Ekkehard Glimm. High-dimensional data analysis: selection of variables, data compression and graphics–application to gene expression. *Biometrical Journal. Biometrische Zeitschrift*, 51(2):235–251, April 2009. ISSN 1521-4036. doi: 10.1002/bimj.200800207.

Lise Lefèvre, Amandine Galès, David Olagnier, José Bernad, Laurence Perez, Rémy Burcelin, Alexis Valentin, Johan Auwerx, Bernard Pipy, and Agnès Coste. PPARγ Ligands Switched High Fat Diet-Induced Macrophage M2b Polarization toward M2a Thereby Improving Intestinal Candida Elimination. *PLoS ONE*, 5(9), September 2010. ISSN 1932-6203. doi: 10.1371/journal.pone.0012828.

Yankun Li, Yuan Zhang, Bernhard Dorweiler, Dongying Cui, Tao Wang, Connie W. Woo, Cynthia S. Brunkan, Cynthia Wolberger, Shin-ichiro Imai, and Ira Tabas. Extracellular Nampt Promotes Macrophage Survival via a Nonenzymatic Interleukin-6/STAT3 Signaling Mechanism. *The Journal of Biological Chemistry*, 283(50): 34833–34843, December 2008. ISSN 0021-9258. doi: 10.1074/jbc.M805866200.

Serena Liu and Cole Trapnell. Single-cell transcriptome sequencing: recent advances and remaining challenges. *F1000Research*, 5, 2016. doi: 10.12688/f1000research.7223.1.

Ting Liu, Yoshifumi Yamaguchi, Yoshitaka Shirasaki, Koichi Shikada, Mai Yamagishi, Katsuaki Hoshino, Tsuneyasu Kaisho, Kiwamu Takemoto, Toshihiko Suzuki, Erina Kuranaga, Osamu Ohara, and Masayuki Miura. Single-cell imaging of caspase-1 dynamics reveals an all-or-none inflammasome signaling response. *Cell Reports*, 8(4):974–982, August 2014. ISSN 2211-1247. doi: 10.1016/j.celrep.2014.07.012.

K. J. Livak and T. D. Schmittgen. Analysis of relative gene expression data using real-time quantitative PCR and the 2(-Delta Delta C(T)) Method. *Methods (San Diego, Calif.)*, 25(4):402–408, December 2001. ISSN 1046-2023. doi: 10.1006/meth.2001.1262.

Henry Löffler-Wirth, Martin Kalcher, and Hans Binder. oposSOM: R-package for high-dimensional portraying of genome-wide expression landscapes on bioconductor. *Bioinformatics (Oxford, England)*, 31(19):3225–3227, October 2015. ISSN 1367-4811. doi: 10.1093/bioinformatics/btv342.

Michael I. Love, Wolfgang Huber, and Simon Anders. Moderated estimation of fold change and dispersion for RNA-seq data with DESeq2. *Genome Biology*, 15(12):550, 2014. ISSN 1474-760X. doi: 10.1186/s13059-014-0550-8.

Bing Luan, Young-Sil Yoon, John Le Lay, Klaus H. Kaestner, Susan Hedrick, and Marc Montminy. CREB pathway links PGE2 signaling with macrophage polarization. *Proceedings of the National Academy of Sciences of the United States of America*, 112(51):15642–15647, December 2015. ISSN 0027-8424. doi: 10.1073/pnas.1519644112.

Hans F. Luecke and Keith R. Yamamoto. The glucocorticoid receptor blocks P-TEFb recruitment by NFkappaB to effect promoter-specific transcriptional repression. *Genes & Development*, 19(9):1116–1127, May 2005. ISSN 0890-9369. doi: 10.1101/gad.1297105.

M

Iain C. Macaulay and Thierry Voet. Single cell genomics: advances and future perspectives. *PLoS genetics*, 10 (1):e1004126, January 2014. ISSN 1553-7404. doi: 10.1371/journal.pgen.1004126.

Iain C. Macaulay, Wilfried Haerty, Parveen Kumar, Yang I. Li, Tim Xiaoming Hu, Mabel J. Teng, Mubeen Goolam, Nathalie Saurat, Paul Coupland, Lesley M. Shirley, Miriam Smith, Niels Van der Aa, Ruby Banerjee, Peter D. Ellis, Michael A. Quail, Harold P. Swerdlow, Magdalena Zernicka-Goetz, Frederick J. Livesey, Chris P. Ponting, and Thierry Voet. G&T-seq: parallel sequencing of single-cell genomes and transcriptomes. *Nature Methods*, 12(6):519–522, June 2015. ISSN 1548-7105. doi: 10.1038/nmeth.3370.

G. B. Mackaness. Cellular resistance to infection. *The Journal of Experimental Medicine*, 116:381–406, September 1962. ISSN 0022-1007.

Evan Z. Macosko, Anindita Basu, Rahul Satija, James Nemesh, Karthik Shekhar, Melissa Goldman, Itay Tirosh, Allison R. Bialas, Nolan Kamitaki, Emily M. Martersteck, John J. Trombetta, David A. Weitz, Joshua R. Sanes, Alex K. Shalek, Aviv Regev, and Steven A. McCarroll. Highly Parallel Genome-wide Expression Profiling of Individual Cells Using Nanoliter Droplets. *Cell*, 161(5):1202–1214, May 2015. ISSN 1097-4172. doi: 10.1016/j.cell.2015.05.002.

Marten B. Maeß, Berith Wittig, Andrea Cignarella, and Stefan Lorkowski. Reduced PMA enhances the responsiveness of transfected THP-1 macrophages to polarizing stimuli. *Journal of Immunological Methods*, 402(1-2): 76–81, January 2014. ISSN 1872-7905. doi: 10.1016/j.jim.2013.11.006.

Kevin J. Maloy and Fiona Powrie. Intestinal homeostasis and its breakdown in inflammatory bowel disease. *Nature*, 474(7351):298–306, June 2011. ISSN 1476-4687. doi: 10.1038/nature10208.

Fernando O. Martinez and Siamon Gordon. The M1 and M2 paradigm of macrophage activation: time for reassessment. *F1000prime Reports*, 6:13, 2014. doi: 10.12703/P6-13.

Fernando O. Martinez, Laura Helming, Ronny Milde, Audrey Varin, Barbro N. Melgert, Christina Draijer, Benjamin Thomas, Marco Fabbri, Anjali Crawshaw, Ling Pei Ho, Nick H. Ten Hacken, Viviana Cobos Jiménez, Neeltje A. Kootstra, Jörg Hamann, David R. Greaves, Massimo Locati, Alberto Mantovani, and Siamon Gordon. Genetic programs expressed in resting and IL-4 alternatively activated mouse and human macrophages: similarities and differences. *Blood*, 121(9):e57–e69, February 2013. ISSN 0006-4971, 1528-0020. doi: 10.1182/blood-2012-06-436212.

Fernando Oneissi Martinez, Antonio Sica, Alberto Mantovani, and Massimo Locati. Macrophage activation and polarization. *Frontiers in Bioscience: A Journal and Virtual Library*, 13:453–461, January 2008. ISSN 1093-9946.

Ruslan Medzhitov and Tiffany Horng. Transcriptional control of the inflammatory response. *Nature Reviews. Immunology*, 9(10):692–703, October 2009. ISSN 1474-1741. doi: 10.1038/nri2634.

Sebastiaan H. Meijsing, Cem Elbi, Hans F. Luecke, Gordon L. Hager, and Keith R. Yamamoto. The Ligand Binding Domain Controls Glucocorticoid Receptor Dynamics Independent of Ligand Release. *Molecular and Cellular Biology*, 27(7):2442–2451, April 2007. ISSN 0270-7306. doi: 10.1128/MCB.01570-06.

Jacek Michalkiewicz, Anna Helmin-Basa, Renata Grzywa, Mieczyslawa Czerwionka-Szaflarska, Anna Szaflarska-Poplawska, Grazyna Mierzwa, Andrzej Marszalek, Magdalena Bodnar, Magdalena Nowak, and Katarzyna Dzierzanowska-Fangrat. Innate Immunity Components and Cytokines in Gastric Mucosa in Children with Helicobacter pylori Infection. *Mediators of Inflammation*, 2015:e176726, April 2015. ISSN 0962-9351. doi: 10.1155/2015/176726.

C. D. Mills, K. Kincaid, J. M. Alt, M. J. Heilman, and A. M. Hill. M-1/M-2 macrophages and the Th1/Th2 paradigm. *Journal of Immunology (Baltimore, Md.: 1950)*, 164(12):6166–6173, June 2000. ISSN 0022-1767.

Charles D. Mills. M1 and M2 Macrophages: Oracles of Health and Disease. *Critical Reviews in Immunology*, 32 (6):463–488, 2012. ISSN 1040-8401.

Charles D. Mills and Klaus Ley. M1 and M2 macrophages: the chicken and the egg of immunity. *Journal of Innate Immunity*, 6(6):716–726, 2014. ISSN 1662-8128. doi: 10.1159/000364945.

Masanori Miyata, Ji-Yun Lee, Seiko Susuki-Miyata, Wenzhuo Y. Wang, Haidong Xu, Hirofumi Kai, Koichi S. Kobayashi, Richard A. Flavell, and Jian-Dong Li. Glucocorticoids suppress inflammation via the upregulation of negative regulator IRAK-M. *Nature Communications*, 6:6062, January 2015. ISSN 2041-1723. doi: 10.1038/ncomms7062.

Trine H. Mogensen. Pathogen recognition and inflammatory signaling in innate immune defenses. *Clinical Microbiology Reviews*, 22(2):240–273, Table of Contents, April 2009. ISSN 1098-6618. doi: 10.1128/CMR.00046-08.

David M. Mosser and Justin P. Edwards. Exploring the full spectrum of macrophage activation. *Nature Reviews. Immunology*, 8(12):958–969, December 2008. ISSN 1474-1741. doi: 10.1038/nri2448.

Subhankar Mukhopadhyay, Yunying Chen, Marko Sankala, Leanne Peiser, Timo Pikkarainen, Georg Kraal, Karl Tryggvason, and Siamon Gordon. MARCO, an innate activation marker of macrophages, is a class A scavenger receptor for Neisseria meningitidis. *European Journal of Immunology*, 36(4):940–949, April 2006. ISSN 0014-2980. doi: 10.1002/eji.200535389.

Peter J. Murray, Judith E. Allen, Subhra K. Biswas, Edward A. Fisher, Derek W. Gilroy, Sergij Goerdt, Siamon Gordon, John A. Hamilton, Lionel B. Ivashkiv, Toby Lawrence, Massimo Locati, Alberto Mantovani, Fernando O. Martinez, Jean-Louis Mege, David M. Mosser, Gioacchino Natoli, Jeroen P. Saeij, Joachim L. Schultze, Kari Ann Shirey, Antonio Sica, Jill Suttles, Irina Udalova, Jo A. van Ginderachter, Stefanie N. Vogel, and Thomas A. Wynn. Macrophage activation and polarization: nomenclature and experimental guidelines. *Immunity*, 41(1):14–20, July 2014. ISSN 1097-4180. doi: 10.1016/j.immuni.2014.06.008.

Katie J. Mylonas, Meera G. Nair, Lidia Prieto-Lafuente, Daniel Paape, and Judith E. Allen. Alternatively activated macrophages elicited by helminth infection can be reprogrammed to enable microbial killing. *Journal of Immunology (Baltimore, Md.: 1950)*, 182(5):3084–3094, March 2009. ISSN 1550-6606. doi: 10.4049/jimmunol.0803463.

N

Takashi Nagano, Yaniv Lubling, Tim J. Stevens, Stefan Schoenfelder, Eitan Yaffe, Wendy Dean, Ernest D. Laue, Amos Tanay, and Peter Fraser. Single-cell Hi-C reveals cell-to-cell variability in chromosome structure. *Nature*, 502(7469):59–64, October 2013. ISSN 1476-4687. doi: 10.1038/nature12593.

Matthias Nahrendorf, Filip K. Swirski, Elena Aikawa, Lars Stangenberg, Thomas Wurdinger, Jose-Luiz Figueiredo, Peter Libby, Ralph Weissleder, and Mikael J. Pittet. The healing myocardium sequentially mobilizes two monocyte subsets with divergent and complementary functions. *The Journal of Experimental Medicine*, 204(12):3037–3047, November 2007. ISSN 1540-9538. doi: 10.1084/jem.20070885.

Tomonori Nakamura, Yukihiro Yabuta, Ikuhiro Okamoto, Shinya Aramaki, Shihori Yokobayashi, Kazuki Kurimoto, Kiyotoshi Sekiguchi, Masato Nakagawa, Takuya Yamamoto, and Mitinori Saitou. SC3-seq: a method for highly parallel and quantitative measurement of single-cell gene expression. *Nucleic Acids Research*, 43(9): e60, May 2015. ISSN 1362-4962. doi: 10.1093/nar/gkv134.

C. F. Nathan, H. W. Murray, M. E. Wiebe, and B. Y. Rubin. Identification of interferon-gamma as the lymphokine that activates human macrophage oxidative metabolism and antimicrobial activity. *The Journal of Experimental Medicine*, 158(3):670–689, September 1983. ISSN 0022-1007.

Michael J. Nemeth, Martha R. Kirby, and David M. Bodine. Hmgb3 regulates the balance between hematopoietic stem cell self-renewal and differentiation. *Proceedings of the National Academy of Sciences of the United States of America*, 103(37):13783–13788, September 2006. ISSN 0027-8424. doi: 10.1073/pnas.0604006103.

O

A M O'Farrell, Y Liu, K W Moore, and A L Mui. IL-10 inhibits macrophage activation and proliferation by distinct signaling mechanisms: evidence for Stat3-dependent and -independent pathways. *The EMBO Journal*, 17(4):1006–1018, February 1998. ISSN 0261-4189. doi: 10.1093/emboj/17.4.1006.

C. M. Ohri, A. Shikotra, R. H. Green, D. A. Waller, and P. Bradding. Macrophages within NSCLC tumour islets are predominantly of a cytotoxic M1 phenotype associated with extended survival. *The European Respiratory Journal*, 33(1):118–126, January 2009. ISSN 1399-3003. doi: 10.1183/09031936.00065708.

S. Oliver. Guilt-by-association goes global. *Nature*, 403(6770):601–603, February 2000. ISSN 0028-0836. doi: 10.1038/35001165.

P

Oren Parnas, Marko Jovanovic, Thomas M. Eisenhaure, Rebecca H. Herbst, Atray Dixit, Chun Jimmie Ye, Dariusz Przybylski, Randall J. Platt, Itay Tirosh, Neville E. Sanjana, Ophir Shalem, Rahul Satija, Raktima Raychowdhury, Philipp Mertins, Steven A. Carr, Feng Zhang, Nir Hacohen, and Aviv Regev. A Genome-wide CRISPR Screen in Primary Immune Cells to Dissect Regulatory Networks. *Cell*, 162(3):675–686, July 2015. ISSN 1097-4172. doi: 10.1016/j.cell.2015.06.059.

Grégoire Pau, Florian Fuchs, Oleg Sklyar, Michael Boutros, and Wolfgang Huber. EBImage–an R package for image processing with applications to cellular phenotypes. *Bioinformatics (Oxford, England)*, 26(7):979–981, April 2010. ISSN 1367-4811. doi: 10.1093/bioinformatics/btq046.

Geber Peña, Bolin Cai, Edwin A. Deitch, and Luis Ulloa. JAK2 inhibition prevents innate immune responses and rescues animals from sepsis. *Journal of Molecular Medicine (Berlin, Germany)*, 88(8):851–859, August 2010. ISSN 0946-2716. doi: 10.1007/s00109-010-0628-z.

Geethanjali Pickert, Hee-Young Lim, Andreas Weigert, Annett Häussler, Thekla Myrczek, Maximilian Waldner, Sandra Labocha, Nerea Ferreirós, Gerd Geisslinger, Jörn Lötsch, Christoph Becker, Bernhard Brüne, and Irmgard Tegeder. Inhibition of GTP cyclohydrolase attenuates tumor growth by reducing angiogenesis and M2-like polarization of tumor associated macrophages. *International Journal of Cancer*, 132(3):591–604, February 2013. ISSN 1097-0215. doi: 10.1002/ijc.27706.

Vincent Piras and Kumar Selvarajoo. The reduction of gene expression variability from single cells to populations follows simple statistical laws. *Genomics*, 105(3):137–144, March 2015. ISSN 1089-8646. doi: 10.1016/j.ygeno.2014.12.007.

Olivier B. Poirion, Xun Zhu, Travers Ching, and Lana Garmire. Single-Cell Transcriptomics Bioinformatics and Computational Challenges. *Frontiers in Genetics*, 7:163, 2016. doi: 10.3389/fgene.2016.00163.

Alex A. Pollen, Tomasz J. Nowakowski, Joe Shuga, Xiaohui Wang, Anne A. Leyrat, Jan H. Lui, Nianzhen Li, Lukasz Szpankowski, Brian Fowler, Peilin Chen, Naveen Ramalingam, Gang Sun, Myo Thu, Michael Norris, Ronald Lebofsky, Dominique Toppani, Darnell W. Kemp, Michael Wong, Barry Clerkson, Brittnee N. Jones, Shiquan Wu, Lawrence Knutsson, Beatriz Alvarado, Jing Wang, Lesley S. Weaver, Andrew P. May, Robert C. Jones, Marc A. Unger, Arnold R. Kriegstein, and Jay A. A. West. Low-coverage single-cell mRNA sequencing reveals cellular heterogeneity and activated signaling pathways in developing cerebral cortex. *Nature Biotechnology*, 32(10):1053–1058, October 2014. ISSN 1546-1696. doi: 10.1038/nbt.2967.

Jean-Francois Poulin, Bosiljka Tasic, Jens Hjerling-Leffler, Jeffrey M. Trimarchi, and Rajeshwar Awatramani. Disentangling neural cell diversity using single-cell transcriptomics. *Nature Neuroscience*, 19(9):1131–1141, August 2016. ISSN 1546-1726. doi: 10.1038/nn.4366.

B. Pulendran, J. L. Smith, G. Caspary, K. Brasel, D. Pettit, E. Maraskovsky, and C. R. Maliszewski. Distinct dendritic cell subsets differentially regulate the class of immune response in vivo. *Proceedings of the National Academy of Sciences of the United States of America*, 96(3):1036–1041, February 1999. ISSN 0027-8424.

R

Arjun Raj, Charles S. Peskin, Daniel Tranchina, Diana Y. Vargas, and Sanjay Tyagi. Stochastic mRNA synthesis in mammalian cells. *PLoS biology*, 4(10):e309, October 2006. ISSN 1545-7885. doi: 10.1371/journal.pbio.0040309.

Arjun Raj, Patrick van den Bogaard, Scott A. Rifkin, Alexander van Oudenaarden, and Sanjay Tyagi. Imaging individual mRNA molecules using multiple singly labeled probes. *Nature Methods*, 5(10):877–879, October 2008. ISSN 1548-7105. doi: 10.1038/nmeth.1253.

Vladimir R. Ramirez-Carrozzi, Daniel Braas, Dev M. Bhatt, Christine S. Cheng, Christine Hong, Kevin R. Doty, Joshua C. Black, Alexander Hoffmann, Michael Carey, and Stephen T. Smale. A unifying model for the selective regulation of inducible transcription by CpG islands and nucleosome remodeling. *Cell*, 138(1):114–128, July 2009. ISSN 1097-4172. doi: 10.1016/j.cell.2009.04.020.

Daniel Ramsköld, Shujun Luo, Yu-Chieh Wang, Robin Li, Qiaolin Deng, Omid R. Faridani, Gregory A. Daniels, Irina Khrebtukova, Jeanne F. Loring, Louise C. Laurent, Gary P. Schroth, and Rickard Sandberg. Full-length mRNA-Seq from single-cell levels of RNA and individual circulating tumor cells. *Nature Biotechnology*, 30(8):777–782, August 2012. ISSN 1546-1696. doi: 10.1038/nbt.2282.

Peter J. Rousseeuw. Silhouettes: A graphical aid to the interpretation and validation of cluster analysis. *Journal of Computational and Applied Mathematics*, 20:53–65, November 1987. ISSN 0377-0427. doi: 10.1016/0377-0427(87)90125-7.

S

Eric K. Sackmann, Lars Majlof, Annett Hahn-Windgassen, Brent Eaton, Temo Bandzava, Jay Daulton, Arne Vandenbroucke, Matthew Mock, Richard G. Stearns, Stephen Hinkson, and Sammy S. Datwani. Technologies That Enable Accurate and Precise Nano- to Milliliter-Scale Liquid Dispensing of Aqueous Reagents Using Acoustic Droplet Ejection. *Journal of Laboratory Automation*, 21(1):166–177, February 2016. ISSN 2211-0690. doi: 10.1177/2211068215602191.

Antoine-Emmanuel Saliba, Lei Li, Alexander J. Westermann, Silke Appenzeller, Daphne A. C. Stapels, Leon N. Schulte, Sophie Helaine, and Jörg Vogel. Single-cell RNA-seq ties macrophage polarization to growth rate of intracellular Salmonella. *Nature Microbiology*, 2:16206, November 2016. ISSN 2058-5276. doi: 10.1038/nmicrobiol.2016.206.

Yohei Sasagawa, Itoshi Nikaido, Tetsutaro Hayashi, Hiroki Danno, Kenichiro D. Uno, Takeshi Imai, and Hiroki R. Ueda. Quartz-Seq: a highly reproducible and sensitive single-cell RNA sequencing method, reveals non-genetic gene-expression heterogeneity. *Genome Biology*, 14(4):R31, April 2013. ISSN 1474-760X. doi: 10.1186/gb-2013-14-4-r31.

Rahul Satija, Jeffrey A. Farrell, David Gennert, Alexander F. Schier, and Aviv Regev. Spatial reconstruction of single-cell gene expression data. *Nature Biotechnology*, 33(5):495–502, 2015. ISSN 1087-0156. doi: 10.1038/nbt.3192.

Kate Schroder, Katharine M. Irvine, Martin S. Taylor, Nilesh J. Bokil, Kim-Anh Le Cao, Kelly-Anne Masterman, Larisa I. Labzin, Colin A. Semple, Ronan Kapetanovic, Lynsey Fairbairn, Altuna Akalin, Geoffrey J. Faulkner, John Kenneth Baillie, Milena Gongora, Carsten O. Daub, Hideya Kawaji, Geoffrey J. McLachlan, Nick Goldman, Sean M. Grimmond, Piero Carninci, Harukazu Suzuki, Yoshihide Hayashizaki, Boris Lenhard, David A. Hume, and Matthew J. Sweet. Conservation and divergence in Toll-like receptor 4-regulated gene expression in primary human versus mouse macrophages. *Proceedings of the National Academy of Sciences of the United States of America*, 109(16):E944–953, April 2012. ISSN 1091-6490. doi: 10.1073/pnas.1110156109.

Jessica Severin, Andrew M. Waterhouse, Hideya Kawaji, Timo Lassmann, Erik van Nimwegen, Piotr J. Balwierz, Michiel Jl de Hoon, David A. Hume, Piero Carninci, Yoshihide Hayashizaki, Harukazu Suzuki, Carsten O. Daub, and Alistair Rr Forrest. FANTOM4 EdgeExpressDB: an integrated database of promoters, genes, microRNAs, expression dynamics and regulatory interactions. *Genome Biology*, 10(4):R39, 2009. ISSN 1474-760X. doi: 10.1186/gb-2009-10-4-r39.

Alex K. Shalek, Rahul Satija, Xian Adiconis, Rona S. Gertner, Jellert T. Gaublomme, Raktima Raychowdhury, Schraga Schwartz, Nir Yosef, Christine Malboeuf, Diana Lu, John J. Trombetta, Dave Gennert, Andreas Gnirke, Alon Goren, Nir Hacohen, Joshua Z. Levin, Hongkun Park, and Aviv Regev. Single-cell transcriptomics reveals bimodality in expression and splicing in immune cells. *Nature*, 498(7453):236–240, June 2013. ISSN 1476-4687. doi: 10.1038/nature12172.

Alex K. Shalek, Rahul Satija, Joe Shuga, John J. Trombetta, Dave Gennert, Diana Lu, Peilin Chen, Rona S. Gertner, Jellert T. Gaublomme, Nir Yosef, Schraga Schwartz, Brian Fowler, Suzanne Weaver, Jing Wang, Xiaohui Wang, Ruihua Ding, Raktima Raychowdhury, Nir Friedman, Nir Hacohen, Hongkun Park, Andrew P. May, and Aviv Regev. Single-cell RNA-seq reveals dynamic paracrine control of cellular variation. *Nature*, 510(7505):363–369, June 2014. ISSN 1476-4687. doi: 10.1038/nature13437.

Stavroula Skylaki, Oliver Hilsenbeck, and Timm Schroeder. Challenges in long-term imaging and quantification of single-cell dynamics. *Nature Biotechnology*, 34(11):1137–1144, November 2016. ISSN 1546-1696. doi: 10.1038/nbt.3713.

Berend Snijder and Lucas Pelkmans. Origins of regulated cell-to-cell variability. *Nature Reviews Molecular Cell Biology*, 12(2):119–125, 2011. ISSN 1471-0080. doi: 10.1038/nrm3044.

Anders Ståhlberg and Mikael Kubista. The workflow of single-cell expression profiling using quantitative real-time PCR. *Expert Review of Molecular Diagnostics*, 14(3):323–331, April 2014. ISSN 1744-8352. doi: 10.1586/14737159.2014.901154.

Oliver Stegle, Sarah A. Teichmann, and John C. Marioni. Computational and analytical challenges in single-cell transcriptomics. *Nature Reviews Genetics*, 16(3):133–145, March 2015. ISSN 1471-0064. doi: 10.1038/nrg3833.

M. Stein, S. Keshav, N. Harris, and S. Gordon. Interleukin 4 potently enhances murine macrophage mannose receptor activity: a marker of alternative immunologic macrophage activation. *The Journal of Experimental Medicine*, 176(1):287–292, July 1992. ISSN 0022-1007.

Robert D. Stout and Jill Suttles. Functional plasticity of macrophages: reversible adaptation to changing microenvironments. *Journal of Leukocyte Biology*, 76(3):509–513, September 2004. ISSN 0741-5400. doi: 10.1189/jlb.0504272.

Robert D. Stout, Chuancang Jiang, Bharati Matta, Illya Tietzel, Stephanie K. Watkins, and Jill Suttles. Macrophages sequentially change their functional phenotype in response to changes in microenvironmental influences. *Journal of Immunology (Baltimore, Md.: 1950)*, 175(1):342–349, July 2005. ISSN 0022-1767.

N. Stoy. Macrophage biology and pathobiology in the evolution of immune responses: a functional analysis. *Pathobiology: Journal of Immunopathology, Molecular and Cellular Biology*, 69(4):179–211, 2001. ISSN 1015-2008. doi: 55944.

Ryota Suzuki and Hidetoshi Shimodaira. Pvclust: an R package for assessing the uncertainty in hierarchical clustering. *Bioinformatics (Oxford, England)*, 22(12):1540–1542, June 2006. ISSN 1367-4803. doi: 10.1093/bioinformatics/btl117.

T

Fuchou Tang, Catalin Barbacioru, Yangzhou Wang, Ellen Nordman, Clarence Lee, Nanlan Xu, Xiaohui Wang, John Bodeau, Brian B. Tuch, Asim Siddiqui, Kaiqin Lao, and M. Azim Surani. mRNA-Seq whole-transcriptome analysis of a single cell. *Nature Methods*, 6(5):377–382, May 2009. ISSN 1548-7105. doi: 10.1038/nmeth.1315.

Songqing Tang, Taoyong Chen, Zhou Yu, Xuhui Zhu, Mingjin Yang, Bin Xie, Nan Li, Xuetao Cao, and Jianli Wang. RasGRP3 limits Toll-like receptor-triggered inflammatory response in macrophages by activating Rap1 small GTPase. *Nature Communications*, 5:4657, August 2014. ISSN 2041-1723. doi: 10.1038/ncomms5657.

Savaş Tay, Jacob J. Hughey, Timothy K. Lee, Tomasz Lipniacki, Stephen R. Quake, and Markus W. Covert. Single-cell NF-kappaB dynamics reveal digital activation and analogue information processing. *Nature*, 466 (7303):267–271, July 2010. ISSN 1476-4687. doi: 10.1038/nature09145.

Andrew Teschendorff. Signalling Entropy: an introductory tutorial. URL: www.picb.ac.cn/compsysg/Software/SignalEntropy/intro.pdf. 2014.

Andrew E. Teschendorff. Single-cell entropy for quantification of differentiation potency from a cell's transcriptome. *bioRxiv*, page 084202, October 2016. doi: 10.1101/084202.

Andrew E. Teschendorff, Peter Sollich, and Reimer Kuehn. Signalling entropy: A novel network-theoretical framework for systems analysis and interpretation of functional omic data. *Methods (San Diego, Calif.)*, 67 (3):282–293, June 2014. ISSN 1095-9130. doi: 10.1016/j.ymeth.2014.03.013.

Fu-Ju Tian, Li-Na An, Guo-Kun Wang, Jia-Qi Zhu, Qing Li, Ying-Ying Zhang, An Zeng, Jun Zou, Rong-Fang Zhu, Xiao-Shuai Han, Nan Shen, Huang-Tian Yang, Xian-Xian Zhao, Shuang Huang, Yong-Wen Qin, and Qing Jing. Elevated microRNA-155 promotes foam cell formation by targeting HBP1 in atherogenesis. *Cardiovascular Research*, 103(1):100–110, July 2014. ISSN 1755-3245. doi: 10.1093/cvr/cvu070.

Barbara Treutlein, Doug G. Brownfield, Angela R. Wu, Norma F. Neff, Gary L. Mantalas, F. Hernan Espinoza, Tushar J. Desai, Mark A. Krasnow, and Stephen R. Quake. Reconstructing lineage hierarchies of the distal lung epithelium using single-cell RNA-seq. *Nature*, 509(7500):371–375, May 2014. ISSN 1476-4687. doi: 10.1038/nature13173.

V

R. van Furth, Z. A. Cohn, J. G. Hirsch, J. H. Humphrey, W. G. Spector, and H. L. Langevoort. The mononuclear phagocyte system: a new classification of macrophages, monocytes, and their precursor cells. *Bulletin of the World Health Organization*, 46(6):845–852, 1972. ISSN 0042-9686.

M. A. Vega and A. L. Corbi. Human macrophage activation: Too many functions and phenotypes for a single cell type. *Inmunología*, 25(4):248–272, 2006.

Daphne Y. S. Vogel, Judith E. Glim, Andrea W. D. Stavenuiter, Marjolein Breur, Priscilla Heijnen, Sandra Amor, Christine D. Dijkstra, and Robert H. J. Beelen. Human macrophage polarization in vitro: maturation and activation methods compared. *Immunobiology*, 219(9):695–703, September 2014. ISSN 1878-3279. doi: 10.1016/j.imbio.2014.05.002.

W

Joseph T. Wade and David C. Grainger. Pervasive transcription: illuminating the dark matter of bacterial transcriptomes. *Nature Reviews Microbiology*, 12(9):647–653, September 2014. ISSN 1740-1526. doi: 10.1038/nrmicro3316.

Allon Wagner, Aviv Regev, and Nir Yosef. Revealing the vectors of cellular identity with single-cell genomics. *Nature Biotechnology*, 34(11):1145–1160, November 2016. ISSN 1546-1696. doi: 10.1038/nbt.3711.

Liguo Wang, Shengqin Wang, and Wei Li. RSeQC: quality control of RNA-seq experiments. *Bioinformatics (Oxford, England)*, 28(16):2184–2185, August 2012a. ISSN 1367-4811. doi: 10.1093/bioinformatics/bts356.

Nan Wang, Hongwei Liang, and Ke Zen. Molecular mechanisms that influence the macrophage m1-m2 polarization balance. *Frontiers in Immunology*, 5:614, 2014. doi: 10.3389/fimmu.2014.00614.

Yongjun Wang, Xin Tang, Bin Yu, Yun Gu, Ying Yuan, Dengbing Yao, Fei Ding, and Xiaosong Gu. Gene network revealed involvements of Birc2, Birc3 and Tnfrsf1a in anti-apoptosis of injured peripheral nerves. *PloS One*, 7(9):e43436, 2012b. ISSN 1932-6203. doi: 10.1371/journal.pone.0043436.

Christine A. Wells, Timothy Ravasi, Geoffrey J. Faulkner, Piero Carninci, Yasushi Okazaki, Yoshihide Hayashizaki, Matthew Sweet, Brandon J. Wainwright, and David A. Hume. Genetic control of the innate immune response. *BMC Immunology*, 4:5, June 2003. ISSN 1471-2172. doi: 10.1186/1471-2172-4-5.

Carly Bess Williams, Elizabeth S Yeh, and Adam C Soloff. Tumor-associated macrophages: unwitting accomplices in breast cancer malignancy. *NPJ Breast Cancer*, 2, 2016. ISSN 2374-4677. doi: 10.1038/npjbcancer.2015.25.

Quin F. Wills, Esther Mellado-Gomez, Rory Nolan, Damien Warner, Eshita Sharma, John Broxholme, Benjamin Wright, Helen Lockstone, William James, Mark Lynch, Michael Gonzales, Jay West, Anne Leyrat, Sergi Padilla-Parra, Sarah Filippi, Chris Holmes, Michael D. Moore, and Rory Bowden. The nature and nurture of cell heterogeneity: accounting for macrophage gene-environment interactions with single-cell RNA-Seq. *BMC Genomics*, 18:53, 2017. ISSN 1471-2164. doi: 10.1186/s12864-016-3445-0.

M. Wills-Karp, A. Nathan, K. Page, and C. L. Karp. New insights into innate immune mechanisms underlying allergenicity. *Mucosal Immunology*, 3(2):104–110, March 2010. ISSN 1935-3456. doi: 10.1038/mi.2009.138.

Gavin W. Wilson and Lincoln D. Stein. RNASequel: accurate and repeat tolerant realignment of RNA-seq reads. *Nucleic Acids Research*, 43(18):e122–e122, October 2015. ISSN 0305-1048. doi: 10.1093/nar/gkv594.

Heather M. Wilson. SOCS Proteins in Macrophage Polarization and Function. *Frontiers in Immunology*, 5, July 2014. ISSN 1664-3224. doi: 10.3389/fimmu.2014.00357.

Henry Wirth, Markus Löffler, Martin von Bergen, and Hans Binder. Expression cartography of human tissues using self organizing maps. *BMC Bioinformatics*, 12:306, July 2011. ISSN 1471-2105. doi: 10.1186/1471-2105-12-306.

Henry Wirth, Martin von Bergen, and Hans Binder. Mining SOM expression portraits: feature selection and integrating concepts of molecular function. *BioData Mining*, 5(1):18, October 2012. ISSN 1756-0381. doi: 10.1186/1756-0381-5-18.

Cecily J. Wolfe, Isaac S. Kohane, and Atul J. Butte. Systematic survey reveals general applicability of "guilt-by-association" within gene coexpression networks. *BMC Bioinformatics*, 6:227, September 2005. ISSN 1471-2105. doi: 10.1186/1471-2105-6-227.

Yong Wu, Xiaoxue Zhang, Fawzia Bardag-Gorce, Rose C. V. Robel, Jonathan Aguilo, Lixin Chen, Ying Zeng, Kelly Hwang, Samuel W. French, Shelly C. Lu, and Yu-Jui Y. Wan. Retinoid X receptor alpha regulates glutathione homeostasis and xenobiotic detoxification processes in mouse liver. *Molecular Pharmacology*, 65 (3):550–557, March 2004. ISSN 0026-895X. doi: 10.1124/mol.65.3.550.

X

Feiyu Xiong, Moshe Kam, Leonid Hrebien, and Yanjun Qi. Ranking with Distance Metric Learning for Biomedical Severity Detection, 2014.

Jia Xue, Susanne V. Schmidt, Jil Sander, Astrid Draffehn, Wolfgang Krebs, Inga Quester, Dominic De Nardo, Trupti D. Gohel, Martina Emde, Lisa Schmidleithner, Hariharasudan Ganesan, Andrea Nino-Castro, Michael R. Mallmann, Larisa Labzin, Heidi Theis, Michael Kraut, Marc Beyer, Eicke Latz, Tom C. Freeman, Thomas Ulas, and Joachim L. Schultze. Transcriptome-based network analysis reveals a spectrum model of human macrophage activation. *Immunity*, 40(2):274–288, February 2014. ISSN 1097-4180. doi: 10.1016/j.immuni.2014.01.006.

Y

Takahisa Yamaguchi, Sachio Fushida, Yasuhiko Yamamoto, Tomoya Tsukada, Jun Kinoshita, Katsunobu Oyama, Tomoharu Miyashita, Hidehiro Tajima, Itasu Ninomiya, Seiichi Munesue, Ai Harashima, Shinichi Harada, Hiroshi Yamamoto, and Tetsuo Ohta. Tumor-associated macrophages of the M2 phenotype contribute to progression in gastric cancer with peritoneal dissemination. *Gastric Cancer: Official Journal of the International Gastric Cancer Association and the Japanese Gastric Cancer Association*, 19(4):1052–1065, October 2016. ISSN 1436-3305. doi: 10.1007/s10120-015-0579-8.

Liying Yan, Mingyu Yang, Hongshan Guo, Lu Yang, Jun Wu, Rong Li, Ping Liu, Ying Lian, Xiaoying Zheng, Jie Yan, Jin Huang, Ming Li, Xinglong Wu, Lu Wen, Kaiqin Lao, Ruiqiang Li, Jie Qiao, and Fuchou Tang. Single-cell RNA-Seq profiling of human preimplantation embryos and embryonic stem cells. *Nature Structural & Molecular Biology*, 20(9):1131–1139, September 2013. ISSN 1545-9985. doi: 10.1038/nsmb.2660.

Fengjiao Yuan, Xiao Fu, Hengfei Shi, Guopu Chen, Ping Dong, and Weiyun Zhang. Induction of Murine Macrophage M2 Polarization by Cigarette Smoke Extract via the JAK2/STAT3 Pathway. *PLOS ONE*, 9(9): e107063, September 2014. ISSN 1932-6203. doi: 10.1371/journal.pone.0107063.

Z

Amit Zeisel, Ana B. Muñoz-Manchado, Simone Codeluppi, Peter Lönnerberg, Gioele La Manno, Anna Juréus, Sueli Marques, Hermany Munguba, Liqun He, Christer Betsholtz, Charlotte Rolny, Gonçalo Castelo-Branco, Jens Hjerling-Leffler, and Sten Linnarsson. Brain structure. Cell types in the mouse cortex and hippocampus revealed by single-cell RNA-seq. *Science (New York, N.Y.)*, 347(6226):1138–1142, March 2015. ISSN 1095-9203. doi: 10.1126/science.aaa1934.

Ji Zhang and Hai Fang. *Using Self-Organizing Maps to Visualize, Filter and Cluster Multidimensional Bio-Omics Data, Applications of Self-Organizing Maps*. DOI: 10.5772/51702, 2012.

Grace X. Y. Zheng, Jessica M. Terry, Phillip Belgrader, Paul Ryvkin, Zachary W. Bent, Ryan Wilson, Solongo B. Ziraldo, Tobias D. Wheeler, Geoff P. McDermott, Junjie Zhu, Mark T. Gregory, Joe Shuga, Luz Montesclaros, Jason G. Underwood, Donald A. Masquelier, Stefanie Y. Nishimura, Michael Schnall-Levin, Paul W. Wyatt, Christopher M. Hindson, Rajiv Bharadwaj, Alexander Wong, Kevin D. Ness, Lan W. Beppu, H. Joachim Deeg, Christopher McFarland, Keith R. Loeb, William J. Valente, Nolan G. Ericson, Emily A. Stevens, Jerald P. Radich, Tarjei S. Mikkelsen, Benjamin J. Hindson, and Jason H. Bielas. Massively parallel digital transcriptional profiling of single cells. *Nature Communications*, 8:14049, January 2017. ISSN 2041-1723. doi: 10.1038/ncomms14049.

Qing Zhou, Hongying Wang, Daniella M. Schwartz, Monique Stoffels, Yong Hwan Park, Yuan Zhang, Dan Yang, Erkan Demirkaya, Masaki Takeuchi, Wanxia Li Tsai, Jonathan J. Lyons, Xiaomin Yu, Claudia Ouyang, Celeste Chen, David T. Chin, Kristien Zaal, Settara C. Chandrasekharappa, Eric P Hanson, Zhen Yu, James C. Mullikin, Sarfaraz A. Hasni, Ingrid E. Wertz, Amanda K. Ombrello, Deborah L. Stone, Patrycja Hoffmann, Anne Jones, Beverly K. Barham, Helen L. Leavis, Annet van Royen-Kerkof, Cailin Sibley, Ezgi D. Batu, Ahmet Gül, Richard M. Siegel, Manfred Boehm, Joshua D. Milner, Seza Ozen, Massimo Gadina, JaeJin Chae, Ronald M. Laxer, Daniel L. Kastner, and Ivona Aksentijevich. Loss-of-function mutations in TNFAIP3 leading to A20 haploinsufficiency cause an early-onset autoinflammatory disease. *Nature Genetics*, 48(1): 67–73, January 2016. ISSN 1546-1718. doi: 10.1038/ng.3459.

Chapter 8

List of publications

- Feldmann, Radmila, **Cornelius Fischer**, Vitam Kodelja, Sarah Behrens, Stefan Haas, Martin Vingron, Bernd Timmermann, Anne Geikowski, and Sascha Sauer. *Genome-Wide Analysis of LXRα Activation Reveals New Transcriptional Networks in Human Atherosclerotic Foam Cells*. Nucleic Acids Research, 41(6):3518–31, April 2013. ISSN 1362-4962. doi:10.1093/nar/gkt034.

- Weidner, Christopher*, **Cornelius Fischer***, and Sascha Sauer. *PHOXTRACK - a Tool for Interpreting Comprehensive Datasets of Post-Translational Modifications of Proteins*. Bioinformatics, 30(23):3410–11, December 2014. ISSN 1367-4811. doi:10.1093/bioinformatics/btu572.

- Weidner, Christopher, Morten Rousseau, Annabell Plauth, Sylvia J. Wowro, **Cornelius Fischer**, Heba Abdel-Aziz, and Sascha Sauer. *Melissa Officinalis Extract Induces Apoptosis and Inhibits Proliferation in Colon Cancer Cells through Formation of Reactive Oxygen Species*. Phytomedicine: International Journal of Phytotherapy and Phytopharmacology, 22(2):262–70, February 2015. ISSN 1618-095X. doi:10.1016/j.phymed.2014.12.008.

- Weidner, Christopher, Morten Rousseau, Robert J. Micikas, **Cornelius Fischer**, Annabell Plauth, Sylvia J. Wowro, Karsten Siems, Gregor Hetterling, Magdalena Kliem, Frank C. Schroeder, and Sascha Sauer. *Amorfrutin C Induces Apoptosis and Inhibits Proliferation in Colon Cancer Cells through Targeting Mitochondria*. Journal of Natural Products, 79(1):2–12, January 2016. ISSN 1520-6025. doi:10.1021/acs.jnatprod.5b00072.

- Weidner, Christopher, Morten Rousseau, Annabell Plauth, Sylvia J. Wowro, **Cornelius Fischer**, Heba Abdel-Aziz, and Sascha Sauer. *Iberis Amara Extract Induces Intracellular Formation of Reactive Oxygen Species and Inhibits Colon Cancer*. PLoS ONE, 11(4), April 2016. ISSN 1932-6203. doi:10.1371/journal.pone.0152398.

- Luge, Toni*, **Cornelius Fischer***, and Sascha Sauer. *Efficient Application of De Novo RNA Assemblers for Proteomics Informed by Transcriptomics*. Journal of Proteome Research 15, 10(15):3938–43, October 2016. ISSN 1535-3907. doi:10.1021/acs.jproteome.6b00301.

- Hernáez, Bruno, Graciela Alonso, Juan Manuel Alonso-Lobo, Alberto Rastrojo, **Cornelius Fischer**, Sascha Sauer, Begoña Aguado, and Antonio Alcamí. *RNA-Seq Based Transcriptome Analysis of the Type I Interferon Host Response upon Vaccinia Virus Infection of Mouse Cells*. Journal of Immunology Research, 2017:5157626, January 2017. ISSN 2314-7156. doi:10.1155/2017/5157626.

* These authors contributed equally to this work